

# QCD Radiation Effects on Collider Observables

Ayan Mukhopadhyay

A Thesis Submitted to  
Indian Institute of Technology Hyderabad  
In Partial Fulfillment of the Requirements for  
The Degree of Doctor of Philosophy



भारतीय प्रौद्योगिकी संस्थान हैदराबाद  
Indian Institute of Technology Hyderabad

Department of Physics

September 2022

## Declaration

I declare that this written submission represents my ideas in my own words, and where ideas or words of others have been included, I have adequately cited and referenced the original sources. I also declare that I have adhered to all principles of academic honesty and integrity and have not misrepresented or fabricated or falsified any idea/data/fact/source in my submission. I understand that any violation of the above will be a cause for disciplinary action by the Institute and can also evoke penal action from the sources that have thus not been properly cited, or from whom proper permission has not been taken when needed.

*Ayan Mukhopadhyay*

---

(Signature)

---

(Ayan Mukhopadhyay)

---

(Roll No. PH16RESCH11001)

## Approval Sheet

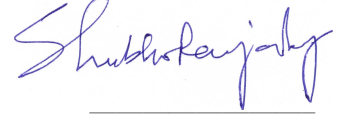
This Thesis entitled QCD Radiation Effects on Collider Observables by Ayan Mukhopadhyay is approved for the degree of Doctor of Philosophy from IIT Hyderabad



(Prof. Pankaj Agarwal) Examiner  
Institute of Physics, Bhubaneswar



(Prof. Anuradha Misra) Examiner  
University of Mumbai



(Dr. Shubho Ranjan Roy) Internal Examiner  
Dept. of Physics  
IITH



(Dr. Anurag Tripathi) Adviser  
Dept. of Physics  
IITH



(Dr. Kaushik Nayak) Chairman  
Dept. of Electrical Engineering  
IITH

## Acknowledgements

To be honest, I have been looking forward to this moment for years to thank those individuals who shaped me into the person I am today. Throughout my research adventure, I have been fortunate to get significant assistance from many people, without which I would not have been able to finish my research.

Foremost, I express my sincere gratitude to my supervisor Dr. Anurag Tripathi. During my Ph.D. period, he genuinely became my friend, philosopher, and guide. He assisted me in every way he could, both academically and non-academically. I can not thank him enough for his patience and guidance without which this would not have been possible for me. I am very thankful to my collaborator Neelima for collaborating on several projects and enormous support. I spent some quality time with Anurag, Neelima, and their son Aarush at their house, and enjoyed the delicious home-cooked meals, which were both appealing and necessary for a research scholar staying away from home.

Further, I would like to express my sincere gratitude to my Ph.D. doctoral committee members: Dr. Shubho R. Roy, Dr. Priyotosh Bandyopadhyay, and Dr. Kaushik Nayak, for their insightful remarks and suggestions. I am very thankful to Priyotosh for his thorough and in-depth discussions during my course work at IIT Hyderabad (IITH). Life at IITH became beautiful because of a few people, and Dr. Shubho will undoubtedly be one of them. I will never forget how much physics I learned from him while attending his lectures and discussions over a cup of tea. Both Anurag and Shubho are excellent teachers, and I consider myself fortunate to have had the opportunity to attend their live classes.

I am very much grateful to my collaborators Dr. Goutam, Dr. Pulak and Dr. Prasanna. I would like to thank Prof. Ravindran for his insightful suggestions and advice. I use this opportunity to express my sincere thanks to all my teachers. I thank all the faculty members of the physics department, IITH.

Being the first Ph.D. student of Anurag, I am the senior-most in our QCD group at IITH. It gives me great pleasure to express my gratitude to all the students in our group, I cannot forget their help and suggestions, which helped me in every step in my research work. I would like to thank Sourav Pal, Abhinava Danish, Shubham Mishra, and Aditya Srivastav. Special thanks to Tanmay, Shubham, Sourav, Abhinava, and Aditya for carefully reading my thesis and giving useful suggestions.

A special thanks to the Ministry of Human Resource Development (MHRD), Govt. of India and IIT Hyderabad, for the financial support during my Ph.D.

I would like to express my heartfelt gratitude to my dear friend Bhramar for her unconditional support, love, and motivation.

Finally, my deep respect goes to my parents, Mrs. Bandana Mukhopadhyay and Mr. Dhananjay Mukhopadhyay and my younger brother Mr. Subham Mukhopadhyay for their love, support, and faith in me. I am grateful to all of my family members for their encouragement and trust in me during my Ph.D. journey. A special thanks to my uncle Partha Sarathi Mukhopadhyay, my aunt Suvra Mukhopadhyay and my sister Disha. With huge pleasure, I express my heartfelt gratitude to my grandpa, Late. Pareshnath Mukhopadhyay and my grandma Late. Siddheshwari Mukhopadhyay.

# Dedication

To my  
**Parents**

and

to my  
dear friend **Bhramar**

# Abstract

Precision calculations in Quantum field theory has been a field of active research for several years, as they act as a reference to experimentalists to test numerous hypothesis of the Standard Model and also to obtain the signatures of new physics. This thesis is based on both the study of standard Model and beyond standard Model precision studies from the theoretical point of view.

The discovery of the Higgs boson discovery at the LHC completes the last missing piece in the Standard Model, and the next step toward precision measurement is to look for a signature from BSM. Pseudo-scalar Higgs is one of the BSM candidates we are interested in due to the similarities with the Higgs boson as long as production procedure is concerned. The small  $p_T$  region that supplies most of the cross-section is inaccessible to fixed-order perturbation theory due to the presence of large logarithms in the perturbative series. We present the calculation of the combined  $O(\alpha_s^4)$  fixed order result for the transverse momentum distribution of a pseudo-scalar Higgs boson, with a resummation of large logarithms in the small  $p_T$  limit to NNLL. We have observed a significant reduction going from NLO + NLL to NNLO<sub>A</sub> + NNLL for  $p_T$  distribution. The calculation is performed assuming the top quark is infinitely heavy. Thus, the phenomenological relevance depends to a large extent on whether a pseudo-scalar Higgs boson of mass below twice the top mass will be found or not. The calculation builds on well-known methods and results but fills a noticeable gap in the theoretical landscape of higher-order Higgs predictions. We present a complete phenomenological assessment in the setting of 14 TeV and 13 TeV center-of-mass energy of the LHC, considering various masses, scales, and parton distribution functions, which will be beneficial in the future hunt for such particles at the LHC.

In the context of  $e^+e^-$  collider, we have used well-studied event shape variables to study hadronization effects. Power corrections, a non-perturbative effect, can be recovered from the perturbative ambiguity of Borel-resummed distributions and can be studied efficiently using Dressed gluon exponentiation (DGE). We offer a simplified version of the DGE approach that finds all dominant power corrections to event shapes using straightforward computations. We named our method Eikonal Dressed Gluon Exponentiation (EDGE). Using this method, we computed the Characteristic and Borel functions for three widely used event shapes in literature: thrust,  $C$  parameter, and angularities. We have also shown how to calculate the Sudakov exponent in the case of thrust.

# List of Publications Based on this Thesis

- **Journal Publications:**

1. N. Agarwal, P. Banerjee, P.K. Dhani, G. Das, **A. Mukhopadhyay**, V. Ravindran and A. Tripathi, “Resummed transverse momentum distribution of pseudo-scalar Higgs boson at NNLO<sub>A</sub> + NNLL,” in *Journal of High Energy Physics*, Article number: 105 (2018), December 2018.
2. N. Agarwal, **A. Mukhopadhyay**, S. Pal and A. Tripathi, “Power corrections to event shapes using Eikonal dressed gluon exponentiation,” in *Journal of High Energy Physics*, Article number: 155 (2021), March 2021.

# List of Figures

1.1	Emission of one soft photon from a hard matrix element . . . . .	5
1.2	Real emission diagram . . . . .	6
1.3	Virtual correction diagram . . . . .	7
1.4	Born diagram . . . . .	8
1.5	Soft photon emission from an outgoing electron line with momentum $k$ . . . . .	8
1.6	Two soft photon emissions in QED . . . . .	9
1.7	$n$ soft photons attached to an external electron line . . . . .	10
1.8	Factorization of soft and hard process . . . . .	10
1.9	1 <sup>st</sup> order correction with only one photon . . . . .	11
1.10	2 <sup>nd</sup> order correction with two photons . . . . .	12
1.11	Born process . . . . .	14
1.12	Feynman diagrams for real emission of one gluon . . . . .	15
1.13	The phase space for $q\bar{q}g$ , where all particles are massless. The lines AC, BC, AB correspond to $x_1 = 1$ , $x_2 = 1$ and $x_3 = 1$ respectively. At point D $x_1, x_2, x_3$ all equal to value $2/3$ . It is easy to check that any point in the plane identically satisfies the constraint $x_1 + x_2 + x_3 = 2$ . . . . .	17
2.1	Resummation scale variation for (a) NLO+NLL and (b) NNLO <sub>A</sub> +NNLL at 14 TeV	32
2.2	Resummation scale variation for (a) NLO+NLL and (b) NNLO <sub>A</sub> +NNLL at 13 TeV	32
2.3	$\mu_R$ and $\mu_F$ variation at NLO+NLL and NNLO <sub>A</sub> +NNLL for (a) 14 TeV and (b) 13 TeV	33
2.4	Variation of $\mu_R$ at NLO+NLL and NNLO <sub>A</sub> +NNLL keeping $\mu_F$ fixed at $m_A$ for (a) 14 TeV and (b) 13 TeV . . . . .	34
2.5	Variation of $\mu_F$ at NLO+NLL and NNLO <sub>A</sub> +NNLL keeping $\mu_R$ fixed at $m_A$ for (a) 14 TeV and (b) 13 TeV . . . . .	34
2.6	$Q$ , $\mu_R$ and $\mu_F$ variation at NLO+NLL and NNLO <sub>A</sub> +NNLL for (a) 14 TeV and (b) 13 TeV . . . . .	35
2.7	PDF variation at NNLO <sub>A</sub> +NNLL for (a) 14 TeV and (b) 13 TeV using various sets. The y-axis represents the ratio of extremum variation over the central PDF set. . . . .	35
2.8	Pseudo-scalar Higgs mass variation at NNLO <sub>A</sub> +NNLL for (a) 14 TeV and (b) 13 TeV	36



3.1	Dalitz plot showing phase space for $\gamma \rightarrow q\bar{q}g$ with off-shell gluon. The energy momentum conservation condition $x_1 + x_2 + x_3 = 2$ is satisfied throughout this $x_1 - x_2$ plane and the actual length along $x_3$ axis is $\sqrt{2}$ times the measured length. The collinear limit (when the gluon is collinear to the quark) corresponds to $x_1 = 1 - \xi$ , $x_2 = 0$ , while the soft limit (when the gluon is soft to the quark) corresponds to $x_1 = x_2 = 1 - \sqrt{\xi}$ . The soft boundary of the phase space $1 - x_2 = \xi/(1 - x_1)$ is denoted by the red curve. . . . .	42
A.1	QCD Feynman rules . . . . .	56
B.1	Bubble chain diagram where we can see fermion loop insertion into a single gluon line which leads to renormalon . . . . .	62

# List of Tables

2.1	$q_T$ distributions at NNLO <sub>A</sub> +NNLL using different PDF sets along with percentage uncertainties for $q_T = 7.0, 13.0, 19.0, 25.0, 31.0$ for $\sqrt{s} = 14$ TeV. . . . .	36
2.2	$q_T$ distributions at NNLO <sub>A</sub> +NNLL using different PDF sets along with percentage uncertainties for $q_T = 7.0, 13.0, 19.0, 26.0, 32.0$ for $\sqrt{s} = 13$ TeV. . . . .	36
3.1	The size of the residues of renormalon singularities for soft power corrections. The numbers quoted are $\pi$ times the residue and $\bar{\Lambda} = \Lambda e^{5/6}$ . We ignore here the $\mathcal{O}(1)$ factor $C_F/2\beta_0$ in Eq. (3.9). . . . .	52

# List of Abbreviations

<b>QED</b>	Quantum Electro Dynamics
<b>pQCD</b>	Perturbative Quantum Chromo Dynamics
<b>BSM</b>	Beyond Standard Model
<b>MSSM</b>	Minimal Super Symmetric Standard Model
<b>LO</b>	Leading order
<b>NLO</b>	Next to Leading order
<b>NNLO</b>	Next to Next to Leading Order
<b>NLL</b>	Next to Leading Log
<b>NNLL</b>	Next to Next to Leading Log
<b>DGE</b>	Dressed Gluon Exponentiation
<b>EDGE</b>	Eikonal Dressed Gluon Exponentiation
<b>COM</b>	Centre of Mass

# Contents

Declaration . . . . .	ii
Approval Sheet . . . . .	iii
Acknowledgements . . . . .	iv
Abstract . . . . .	vi
List of Publications Based on this Thesis . . . . .	vii
List of Figures . . . . .	viii
List of Tables . . . . .	ix
List of Abbreviations . . . . .	x
<b>1 Introduction</b>	<b>1</b>
1.1 QCD Lagrangian . . . . .	3
1.2 Asymptotic freedom in QCD . . . . .	3
1.3 IR divergence . . . . .	5
1.4 Exponentiation . . . . .	8
1.5 Factorization and resummation . . . . .	13
1.5.1 A demonstration of how large logarithms arise: The case of thrust distribution	14
<b>2 Resummed <math>p_T</math> distribution of Pseudo-scalar Higgs</b>	<b>20</b>
2.1 Introduction . . . . .	20
2.2 Theoretical Framework . . . . .	23
2.2.1 Matching the cross section across the large and small $p_T$ regions . . . . .	27
2.2.2 Resummation coefficients and determination of $H_g^{A,(2)}$ . . . . .	28
2.3 The results: Hard coefficients and matched distributions . . . . .	29
2.3.1 Evaluation of hard coefficient . . . . .	29
2.3.2 Fixed order distribution at NNLO . . . . .	31
2.3.3 Matched distributions . . . . .	31
2.4 Conclusions . . . . .	36
<b>3 Power corrections to event shapes</b>	<b>38</b>
3.1 Introduction . . . . .	38
3.2 Dressed Gluon Exponentiation . . . . .	40
3.3 Borel function using Eikonal Dressed Gluon Exponentiation . . . . .	41
3.3.1 Thrust . . . . .	42
3.3.2 $C$ -parameter . . . . .	44
3.3.3 Angularities . . . . .	46

3.4	Borel function using Eikonal Dressed Gluon Exponentiation in the light-cone variables	47
3.4.1	Thrust . . . . .	48
3.4.2	$C$ -parameter . . . . .	49
3.4.3	Angularities . . . . .	49
3.5	The Sudakov exponent . . . . .	50
3.6	Conclusions . . . . .	52
<b>4</b>	<b>Conclusions and Future directions</b>	<b>53</b>
	<b>Appendix</b>	<b>54</b>
<b>A</b>	<b>Useful Relations needed for this thesis</b>	<b>55</b>
A.1	Feynman Rules . . . . .	55
A.2	Relations between Gamma Matrices . . . . .	57
A.3	Trace Technology . . . . .	57
A.4	Casimir Invariants of $SU(N)$ . . . . .	57
<b>B</b>	<b>Proof of some relations used in the main section</b>	<b>59</b>
B.1	Proof of the eikonal identity regarding soft photon emissions . . . . .	59
B.2	Borel Summation and Renormalons . . . . .	60
	<b>References</b>	<b>63</b>

# Chapter 1

## Introduction

The Standard Model (SM) of particle physics, which describes the physics at the subatomic levels, is a very successful theory to date. With the discovery of Higgs Boson at the Large Hadron Collider (LHC) [1, 2] the Standard Model is complete. New physics could manifest as minor deviations from the precise SM predictions. The primary objectives of the theoretical studies are: SM verification with extraordinary precision and the search for physics beyond the SM (BSM). To this end, reliable theoretical predictions are necessary to fulfil these essential tasks. As the theory is not solvable exactly, perturbation theory is the most practical and accepted method, in which an observable  $\widehat{O}$  has the following form:

$$\widehat{O} = \widehat{O}_0 + \alpha_s \widehat{O}_1 + \alpha_s^2 \widehat{O}_2 + \dots , \quad (1.1)$$

where,  $\alpha_s$  is the coupling constant.  $\widehat{O}_0$  is the leading order (LO) term,  $\widehat{O}_1$  is the next-to-leading order (NLO) term and so on. At leading order SM has been tested for a wide range of phenomena and found to be exceptionally successful. However, we witnessed a revolution in technology in the past three decades [3–7], as a result we have more powerful colliders, from which we are getting enormous amount of data. To match the experimental data, one needs to perform precision calculations.

In general, the observables beyond the leading order contain large logarithms, and a well motivated strategy to handle these logarithms is resummation. In the resummation method, Eq. (1.1) is reorganized in such a way that the potentially large logs are combined into an exponent to obtain a finite result.

A crucial property in performing resummation is the factorization of Infrared singularities from the non-singular parts. This factorization introduces a factorization scale, denoted by  $\mu_F$  in general. Also, renormalization of UV singularities in a theory introduces a renormalization scale  $\mu_R$ . Fixed order results in general depend on both the renormalization ( $\mu_R$ ) and factorization ( $\mu_F$ ) scale. This scale dependency becomes weaker as we go higher-order in perturbation theory. Thus, theoretical predictions will be improved as we calculate the observables at higher-orders in  $\alpha_s$ .

This thesis has been divided into two parts: the first deals with pseudo-scalar Higgs  $p_T$  resummation, and the second with power corrections to event shapes. A brief discussions of these two works are as follows:

**(I)  $p_T$  resummation:** Several beyond the standard model (BSM) scenarios predict the existence of pseudo-scalar Higgs particles. Among the several BSM models, the minimal supersymmetric standard model (MSSM) is the most popular one. In this model, we have five Higgs bosons rather

than one as in the standard model: two scalars ( $h, H$ ), one pseudo-scalar ( $A$ ), and two charged Higgs Bosons ( $H^\pm$ ). One of the important differences between pseudo-scalar Higgs and scalar Higgs is that the former is CP-odd, whereas the latter is CP-even. They have many similarities; for example, the most dominant channel of production for both is gluon fusion. The typical feature of the perturbation theory is that the observable depends on the renormalization ( $\mu_R$ ) and factorization ( $\mu_F$ ) scale. This scale dependency becomes weaker as we go higher-order in perturbation theory. Consequently, theoretical predictions will be improved. Pseudo-scalar Higgs  $p_T$  spectrum upto NLO+NLL accuracy [8] has been known for long. It shows scale uncertainty as high as 25%. We obtained the various components required for the  $p_T$  resummation of a pseudo-scalar Higgs boson to NNLL precision. The resummed contribution has to be matched with the fixed order result to get a realistic distribution valid in the full  $p_T$  spectrum. We apply the ansatz prescribed in [9] to extract the NNLO piece to an excellent approximation. We modified publicly available code HqT [10–12] to get the full  $p_T$  spectrum. At NNLO+NNLL scale uncertainty reduces to 11%. At the LHC, we are looking beyond SM signatures, and we need accurate prediction from the theory side to cross-check the results from the experiment. In the literature, we already have pseudo-scalar Higgs  $p_T$  distribution up to NLO + NLL accuracy. So, the next step towards precision physics calculation should be the result of  $p_T$  distribution, which is one order higher than the previous one, i.e., NNLO + NNLL. We have done extensive phenomenological studies on pseudo-scalar Higgs  $p_T$  which will be tested in the upcoming run at the LHC.

**(II) Power Corrections:** Shape variables are among the most commonly used observables for validating QCD and better understanding its dynamics. The study of event shapes began in the late 1970s as a tool to verify whether gluons were vector particles or scalar. Event shape variables are computed in perturbative QCD as they are IR-safe observables. The precision event shapes study are also be used to determine the strong coupling [13–17]. The most accurate global event shape result for  $\alpha_s$  determination shows discrepancies compare to even more precise lattice result. Some commonly used event shapes are, namely thrust [18–21],  $C$  parameter [22–25] and angularity [26–28]. Event shapes are also addressed in experiments and the study of event shapes in  $e^+e^-$  collider points toward significant non-perturbative effects, which are of comparable size to next-to-leading-order perturbative predictions. The state-of-the-art for fixed orders is next-to-next-to-leading order (NNLO) accuracy [29–33], whereas next-to-leading log (NLL) resummation has been known for some time [34–37]. The NNLL resummation architecture has also been developed in recent years [13, 38–48]. We combine an eikonal version of the matrix element and a soft version of the event shapes in the EDGE technique. This merger is accomplished [49] through the dressed gluon exponentiation approach (DGE), which was already applied in a wide range of event shapes [50–52] and other key QCD observables [53–55]. DGE, in addition to including the NLL resummation of Sudakov logarithms on such a consistent basis, gives a renormalon-based assessment of both soft and collinear power corrections. One of the important points about the event shapes is that no other observable class except shape variables show non-perturbative effects such as power corrections which generally vary as significant as  $1/Q$ , where  $Q$  is the hard scale. The complete calculation of these shape variables is complicated, and we have developed a method where we can calculate the leading power corrections to these shape variables easily.

The thesis is structured as follows. In the rest of this chapter, we discuss the basics of Infrared singularities and exponentiation which are crucial for resummation. In chapter 2, we describe  $p_T$

resummation for pseudo scalar Higgs boson. Further in chapter 3, we describe power corrections to event shape variables using a new method, which we call EDGE. In chapter 4, we conclude our findings and give a flavour of future directions.

## 1.1 QCD Lagrangian

Quantum Chromodynamics (QCD) is based on the  $SU(3)$  group of the Standard Model. The theoretical predictions and experimental verification have established QCD as a theory of strong interaction among the quarks and gluons. The Lagrangian for QCD is given by,

$$\mathcal{L}_{QCD} = \mathcal{L}_{\text{classical}} + \mathcal{L}_{\text{gauge-fix}} + \mathcal{L}_{\text{ghost}} , \quad (1.2)$$

Here the classical part is the Lagrangian of a system that is invariant under  $SU(3)$  group, and is given by,

$$\mathcal{L}_{\text{classical}} = \bar{\Psi}(i\gamma^\mu\partial_\mu - m)\Psi - \frac{1}{4}(F_{\mu\nu}^a)^2 + \hat{g}_s\bar{\Psi}\gamma^\mu T^a\Psi A_\mu^a , \quad (1.3)$$

where  $\psi$  are the fermion fields,  $A_\mu$  are the gauge boson fields, and the field tensor  $F_{\mu\nu}^a$  is given by,

$$F_{\mu\nu}^a = \partial_\mu A_\nu^a - \partial_\nu A_\mu^a + \hat{g}_s f^{abc} A_\mu^b A_\nu^c , \quad (1.4)$$

Here  $\hat{g}_s$  is the strong coupling constant. To remove the unphysical degrees of freedom of the massless gauge bosons, one needs to perform Gauge fixing by adding a gauge-fixing term to the Lagrangian in Eq. (1.3), which has the following form,

$$\mathcal{L}_{\text{gauge-fix}} = -\frac{1}{2\xi} (\partial^\mu A_\mu^a)^2 . \quad (1.5)$$

Note that the gauge fixing parameter  $\xi$  can take any value, and throughout the thesis we have considered  $\xi = 1$ , which is known as Feynman gauge. The addition of gauge-fixing term brings in ghosts which are scalar fields anti-commuting among each other and the Lagrangian for this term is given by,

$$\mathcal{L}_{\text{ghost}} = \partial^\mu \chi^{a*} (\delta_{ab}\partial_\mu - \hat{g}_s f_{abc} A_\mu^c) \chi^b , \quad (1.6)$$

The appearance of Gell-Mann matrices  $T^a$  which are generators of the Lie group  $SU(3)$  form a Lie algebra and the algebra is defined as

$$[T^a, T^b] = i f^{abc} T^c , \quad (1.7)$$

where,  $f^{abc}$  are known as structure constants. The Feynman rules corresponding to QCD Lagrangian are shown in Appendix A.

## 1.2 Asymptotic freedom in QCD

The Lagrangian and the corresponding Feynman rules enable us to calculate the Green functions in a given QFT. At higher order in the perturbation theory, these Green functions, and the associated physical quantities involve loop integrals and suffer from singularities. In a theory involving massless



gauge bosons, such as QED and QCD suffer from two kinds of singularities: UV and IR singularities. We start our discussion on UV singularities and the process of removing them from a theory.

The UV singularities appear in a theory when the momentum of the particle flowing in the loop becomes infinite. A well-known method of renormalization removes the UV singularities from the Green functions of a given quantum field theory. Renormalization involves following two steps: introduction of a regulator that regulates non-physical quantities, and absorption of the divergences into the redefinition of fields and parameters. There are many ways to regularize a theory, and all of them are equivalent to each other. The most common methods of renormalizations are: cut-off, Pauli-Villiers, on-shell, dimensional regularization, etc. Throughout the thesis, we use dimensional regularization [56] method due to its Lorentz invariant nature and wide applications in perturbative QCD. In this method, instead of working in 4 dimensions, one works in  $4 - \epsilon$  dimensions; then the singularities in the Green functions show up as poles in  $\epsilon$ .

The first step of renormalization is to define the bare fields and parameters in terms of renormalized fields. For our discussion on asymptotic freedom, it is sufficient to consider only the renormalized coupling, which is given by,

$$\hat{g}_s = Z_g^2(\mu_R^2, \epsilon) (\mu_R^2)^{-\epsilon/2} g_s(\mu_R^2). \quad (1.8)$$

Here  $\hat{g}_s$  and  $g_s$  are known as the bare coupling and the renormalized coupling respectively; and  $\mu_R$  is called renormalization scale. The renormalization scale has been introduced to make the renormalized coupling dimensionless while performing the renormalization. The equations that control the behaviour of all the parameters in a Lagrangian on the renormalization scale are called renormalization group equations. To study the asymptotic freedom, it is sufficient to calculate only the variation of coupling constant with the renormalization scale. In literature this is commonly known as  $\beta$ -function, and is given by,

$$\beta(a_s(\mu_R^2)) = \mu_R^2 \frac{da_s(\mu_R^2)}{d\mu_R^2} \quad (1.9)$$

where  $a_s = g_s^2/4\pi$ . Now, using Eq. (1.8), the  $\beta$  function is given by,

$$\beta(a_s(\mu_R^2)) = \frac{\epsilon}{2} a_s(\mu_R^2) - a_s(\mu_R^2) \mu_R^2 \frac{d \log Z_g^2}{d\mu_R^2}. \quad (1.10)$$

At one loop, the renormalization constant  $Z_g$  is given by (in  $\overline{MS}$  scheme) [57],

$$Z_g = 1 + \frac{a_s(\mu_R^2)}{\epsilon} \frac{1}{6} (11C_A - 4T_F n_f) + \mathcal{O}(a_s^2(\mu_R^2)). \quad (1.11)$$

using  $Z_g$  and the definition of the beta function we can write,

$$\beta(a_s(\mu_R^2)) = \frac{\epsilon}{2} a_s(\mu_R^2) - \beta_0 a_s^2(\mu_R^2) - \beta_1 a_s^3(\mu_R^2) - \beta_2 a_s^4(\mu_R^2) - \beta_3 a_s^5(\mu_R^2) - \dots \quad (1.12)$$

The beta function has been calculated upto five loops till date [58]. Below we have mentioned few

of them

$$\beta_0 = \frac{11}{3}C_A - \frac{4}{3}n_f T_F, \quad (1.13)$$

$$\beta_1 = \frac{34}{3}C_A^2 - \frac{4}{3}n_f T_F(3C_F + 5C_A), \quad (1.14)$$

$$\begin{aligned} \beta_2 = & \frac{2857}{54}C_A^3 - \frac{1415}{27}C_A^2 n_f T_F + \frac{158}{27}C_A n_f^2 T_F^2 + \frac{44}{9}C_F n_f^2 T_F^2 \\ & - \frac{205}{9}C_A C_F n_f T_F + 2C_F^2 n_f T_F, \end{aligned} \quad (1.15)$$

$$\begin{aligned} \beta_3 = & \left( \frac{17152}{243} + \frac{448}{9}\zeta_3 \right) C_A C_F n_f^2 T_F^2 + \left( -\frac{4204}{27} + \frac{352}{9}\zeta_3 \right) C_A C_F^2 n_f T_F \\ & + \frac{424}{243}C_A n_f^3 T_F^3 + \left( \frac{7073}{243} - \frac{656}{9}\zeta_3 \right) C_A^2 C_F n_f T_F + \left( \frac{7930}{81} + \frac{224}{9}\zeta_3 \right) C_A^2 n_f^2 T_F^2 \\ & + \frac{1232}{243}C_F n_f^3 T_F^3 + \left( -\frac{39143}{81} + \frac{136}{3}\zeta_3 \right) C_A^3 n_f T_F + \left( \frac{150653}{486} - \frac{44}{9}\zeta_3 \right) C_A^4 \\ & + \left( \frac{1352}{27} - \frac{704}{9}\zeta_3 \right) C_F^2 n_f^2 T_F^2 + 46C_F^3 T_F n_f + \left( \frac{512}{9} - \frac{1664}{3}\zeta_3 \right) n_f \frac{N(N^2 + 6)}{48} \\ & + \left( -\frac{704}{9} + \frac{512}{3}\zeta_3 \right) n_f^2 \frac{(N^4 - 6N^2 + 18)}{96N^2} + \left( -\frac{80}{9} + \frac{704}{3}\zeta_3 \right) \frac{N^2(N^2 + 36)}{24}. \end{aligned} \quad (1.16)$$

In QCD, we have,  $C_A = 3$ ,  $C_F = 4/3$  and  $T_F = 1/2$ . From the expression of  $\beta_0$ , note that for  $n_f \leq 16$ ,  $\beta_0$  is positive. As a result, the beta function at leading order is negative, and the theory is asymptotically free. Thus one is allowed to perform perturbative calculations at high energies in QCD. The  $\beta$  function for QCD has been calculated upto five loops and the asymptotic freedom has been proved to hold even at higher perturbative orders.

### 1.3 IR divergence

The Infrared divergence appear in a theory when a massless gauge particle becomes either soft or collinear to the emitting particle. To determine their source, we consider a simple example of Figure (1.1), where the *blob* does not contain any IR divergences and we denote it by  $\mathcal{M}_0$ . From  $\mathcal{M}_0$ , a fermion is being emitted, further from this fermion a photon is being emitted. The matrix element for this diagram is then given by,

$$\mathcal{M} = e\bar{u}(p)\gamma^\mu \frac{\not{p} + \not{k}}{(p+k)^2 + i\epsilon} \mathcal{M}_0, \quad (1.17)$$

In the limit  $k \ll p$ , neglecting all other factors we can write down denominator of the above equation

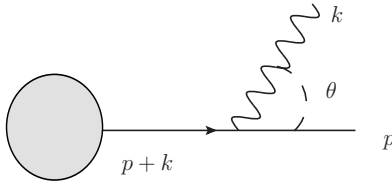


Figure 1.1: Emission of one soft photon from a hard matrix element.

as,

$$\frac{1}{(p+k)^2} = \frac{1}{2 p \cdot k} \simeq \frac{1}{p_0 k_0 (1 - \cos \theta)} \quad (1.18)$$

where we have considered that both the photon and the fermion are massless. The singularities in the amplitude of Eq. (1.17) when the denominator of the above equation vanishes. Note that we have three possible sources of singularities:

- (i) when photon becomes soft, that is,  $k_0 \rightarrow 0$
- (ii) when fermion becomes soft, that is,  $p_0 \rightarrow 0$
- (iii) when photon becomes collinear to fermion, that is,  $\cos \theta \rightarrow 1$ .

We encounter divergences only from the configurations of (i) and (iii), however (ii) always leads to integrable singularities because of an additional power of momentum originating from the wave functions of spinors in the numerator of Eq. (1.17). Note that in a case where fermions are massive, the only singularities that can appear in this configuration is when the photon becomes soft.

Due to the infrared safety of a physical observable, the IR singularities cancel among the real and virtual contribution at a given perturbative order. The cancellation of singularities at all perturbative orders is guaranteed by the Bloch and Nordsieck theorem [59]. Here, we show briefly this one loop cancellation for  $e^+e^- \rightarrow \mu^+\mu^-$  process.

In the soft limit squared four momentum of the photon vanishes and thus one cannot identify between a soft virtual and a real photon. Thus in this limit at one-loop, the physical process does not contain only  $\mu^+\mu^-$  final states, but also contains the state  $\mu^+\mu^-\gamma$ . The IR singularities that appear in the cross-section for one-loop correction of  $e^+e^- \rightarrow \mu^+\mu^-$  cancels out with the singularities associated with the cross-section of  $e^+e^- \rightarrow \mu^+\mu^-\gamma$ .

The diagrams for  $e^+e^- \rightarrow \mu^+\mu^-\gamma$  are shown in Fig. (1.2). The cross-section for these diagrams are obtained by writing down the scattering amplitude using the Feynman rules of appendix A and then performing the three-body phase space integration. The final expression for cross-section is given by [57],

$$\sigma_R^d = \sigma_0 \frac{e_R^2}{\pi^2} \left( \frac{4\pi e^{-\gamma_E} \mu_R^2}{Q^2} \right)^{4-d} \left( \frac{1}{\epsilon^2} + \frac{13}{12\epsilon} - \frac{5\pi^2}{24} + \frac{259}{144} + \mathcal{O}(\epsilon) \right). \quad (1.19)$$

Here,  $Q^2 = (p_1+p_2)^2$  is the center-of-mass energy,  $\sigma_0$  is the tree level cross-section which is computed in 4 dimension instead of  $d$  dimensions,  $e_R$  is the renormalized coupling and  $\mu_R$  is the renormalization

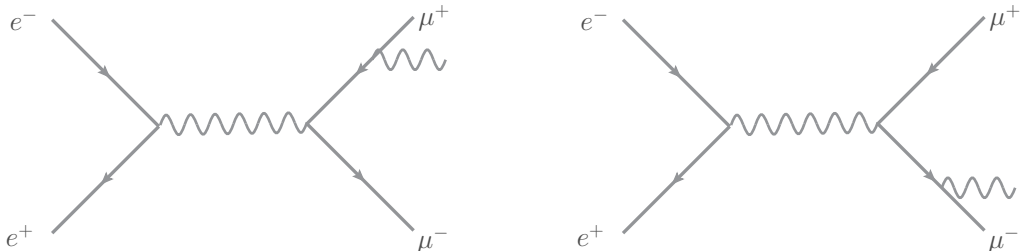


Figure 1.2: Real emission diagram

scale. Note that the cross-section is divergent in  $\epsilon \rightarrow 0$  limit. The singularities associated with the double pole ( $1/\epsilon^2$ ) is due to the configuration where the emitted photon is both soft and collinear simultaneously, however the single poles ( $1/\epsilon$ ) are related to the configuration when the emitted photon is either soft wide angle or hard collinear.

The Feynman diagram for virtual exchange of one gluon is shown in Fig. 1.3. The cross-section for this diagram is calculated by writing down the scattering amplitude and then performing the two-body phase space integration. The final result of the cross-section for one-loop correction is given by [57],

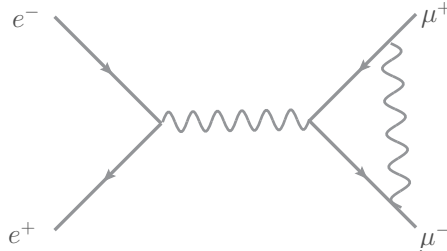


Figure 1.3: Virtual correction diagram

$$\sigma_v^d = -\sigma_0 \frac{e_R^2}{\pi^2} \left( \frac{4\pi e^{-\gamma_E} \mu_R^2}{Q^2} \right)^{4-d} \left( \frac{1}{\epsilon^2} + \frac{13}{12\epsilon} - \frac{5\pi^2}{24} + \frac{29}{18} + \mathcal{O}(\epsilon) \right). \quad (1.20)$$

Clearly, the cross-section due to virtual exchange of photon is divergent in the  $\epsilon \rightarrow 0$  limit.

The total cross-section at  $\mathcal{O}(\alpha_s)$  is the obtained by adding the contributions coming from real emission diagrams and the virtual exchange diagram, and is given by,

$$\sigma_{\text{tot}} = \sigma_v^d + \sigma_R^d = \sigma_0 \frac{3e_R^2}{16\pi^2}, \quad (1.21)$$

which is finite, that is, free from any IR divergences.

In QCD, the cancellation of singularities is guaranteed by the KLN theorem [60, 61], which states that, in a theory with massless fields, transition rates are free of the infrared divergence (soft and collinear) if summation over the initial and final degenerate states is performed. However in QCD, the initial state singularities do not get cancelled after adding the real and virtual contributions. It seems a violation of KLN theorem, however note that in QCD forming degenerate states is not possible as the hadrons cannot be described as perturbative objects. Note that in QCD the double poles associated with the configuration when a gluon is becoming both soft and collinear get cancelled, however the single poles do not get cancelled. A common way of removing this collinear poles from the final result is to perform mass factorization. The cancellation of final state real and virtual singularities give rise the large logarithms. These logarithms are large in certain kinematic limits and may disturb the convergence of the perturbation series, and as a consequence they need to resummed to obtain a precise and sensible prediction.

More precisely, the incomplete cancellation of real and virtual diagrams leave behind logarithms of the form  $\log(Q^2/\mu_R^2)$ , which can be potentially large, and we need to resum these logs to get a physically justified result.

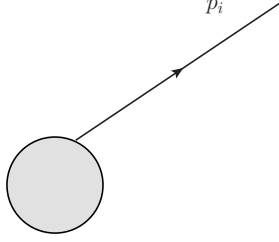


Figure 1.4: Born diagram

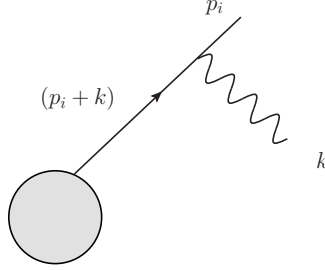


Figure 1.5: Soft photon emission from an outgoing electron line with momentum  $k$

## 1.4 Exponentiation

In this section, we discuss the exponentiation of the effects of soft photons emission from the fermions. To discuss the exponentiation we consider a process shown in Fig. (1.4). The diagram shown in Fig. (1.5) shows an emission of an extra photon from the external fermion line.. The amplitude for this process is given by,

$$\mathcal{M}(p_i) = \bar{u}(p_i) \mathcal{M}_0(p_i) , \quad (1.22)$$

where  $\mathcal{M}_0$  denotes the contribution arising from the *blob*, and is free from any kind of IR divergences; and  $\bar{u}(p_i)$  denotes the spinor associated with the fermion with momentum  $p_i$ . The amplitude then for emission of one photon from the fermion line is then given by,

$$\mathcal{M}(p_i) = -ie\bar{u}(p_i)\gamma^\mu \frac{i \left[ (\not{p}_i + \not{k}) + m \right]}{(p_i + k)^2 - m^2} \epsilon_\mu(k) \mathcal{M}_0(p_i + k) , \quad (1.23)$$

where  $e$  is the electron charge and  $\epsilon_\mu(k)$  is the photon polarization vector, carrying Lorentz index  $\mu$ . Now, in a configuration where photon is soft, we can perform the following approximations:

- we neglect the powers of  $k$  in the numerator, then using the relation between the Dirac gamma matrices and Dirac equation, we write the numerator as,

$$N^\mu = 2\bar{u}(p_i) p_i^\mu . \quad (1.24)$$

- Further, we neglect the  $k^2$  terms in the denominator, which gives

$$D = 2p_i \cdot k . \quad (1.25)$$

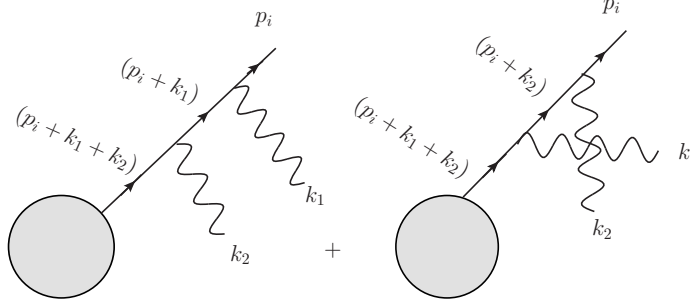


Figure 1.6: Two soft photon emissions in QED

- when the photon radiated is soft  $|\mathbf{k}| \ll |p_i|$ , then,

$$\mathcal{M}_0(p_i + k) \simeq \mathcal{M}_0(p_i) . \quad (1.26)$$

Finally, using Eq. (1.4), (1.25), (1.24), the matrix element of Eq. (1.23) is given by,

$$\mathcal{M}(p_i) = e \left[ \frac{p_i \cdot \epsilon(k)}{p_i \cdot k} \right] \mathcal{M}_0(p_i) . \quad (1.27)$$

From this equation, we can make two important observation:

1. The effect of emission of soft photon factorize from the hard part.
2. The factor for the emission of soft photons from a fermion line is described by Eikonal Feynman rule, given by,

$$\frac{p_i \cdot \epsilon(k)}{p_i \cdot k} . \quad (1.28)$$

Note that the Eikonal Feynman rules do not depend on the spin of the particle from which it is being emitted. The reason behind this fact is that the soft photons have very large Compton wavelength and thus cannot resolve the magnetic moment of the emitting particle.

## Real soft emissions

In a configuration when two soft photons are emitted from the same fermion, shown in Figure (1.6), the matrix element is given by,

$$\begin{aligned} \mathcal{M}(p_i) &= e^2 \left[ \frac{p_i^{\mu_1}}{p_i \cdot k_1} \frac{p_i^{\mu_2}}{p_i \cdot (k_1 + k_2)} + \frac{p_i^{\mu_2}}{p_i \cdot k_2} \frac{p_i^{\mu_1}}{p_i \cdot (k_1 + k_2)} \right] \epsilon_{\mu_1}(k_1) \epsilon_{\mu_2}(k_2) \mathcal{M}_0(p_i) \\ &= e^2 \left[ \left( \frac{p_i^{\mu_1}}{p_i \cdot k_1} \right) \left( \frac{p_i^{\mu_2}}{p_i \cdot k_2} \right) \right] \epsilon_{\mu_1}(k_1) \epsilon_{\mu_2}(k_2) \mathcal{M}_0(p_i) \\ &= e^2 \left[ \left( \frac{p_i \cdot \epsilon(k_1)}{p_i \cdot k_1} \right) \left( \frac{p_i \cdot \epsilon(k_2)}{p_i \cdot k_2} \right) \right] \mathcal{M}_0(p_i) , \end{aligned} \quad (1.29)$$

where  $k_1$  and  $k_2$  are momentum of the soft photons and  $\mathcal{M}_0$  is the hard matrix element. Note that the first factor inside the square bracket is due to the emission of photon with momentum  $k_1$ , while the second factor is due to the emission of photon with momentum  $k_2$ . Thus, the factor associated with the emission of one photon does not have the information about the second photon.

Now, doing the similar calculation for a process where  $n$  photons are being emitted from a fermion line with momentum  $p_i$ , shown in Fig. (1.7), the matrix element is given by,

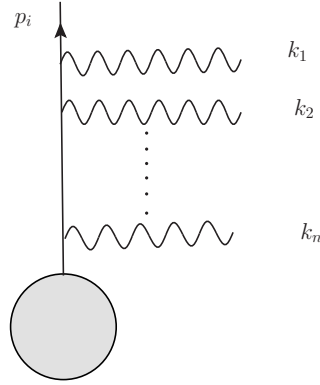


Figure 1.7:  $n$  soft photons attached to an external electron line

$$\equiv \bar{u}(p_i) \left( e \frac{p_i \cdot \epsilon(k_1)}{p_i \cdot k_1} \right) \left( e \frac{p_i \cdot \epsilon(k_2)}{p_i \cdot k_2} \right) \cdots \left( e \frac{p_i \cdot \epsilon(k_n)}{p_i \cdot k_n} \right) \mathcal{M}_0. \quad (1.30)$$

For a detailed derivation of the above equation, see Appendix (B). Similar to the case of emission of two soft photons, in this case a soft photon does not have the information about the other emitted photons from the same fermion lines.

Let us now consider QED form factor that contains two fermion lines attached to a hard interaction vertex and soft photons are being emitted from the fermion lines. A general diagram of this configuration is shown in Fig. (1.8) in which the *blob* contains all the information about hard interaction vertex, while the ellipse contains informations about the soft radiations. A formal proof of this type of factorization can be found in [62–65], for a recent review, see ref. [66].

The effect of the factorization discussed above is exponentiation, which we discuss very briefly here. The matrix element for the Feynman diagram shown in Fig. (1.8) is given by [67],

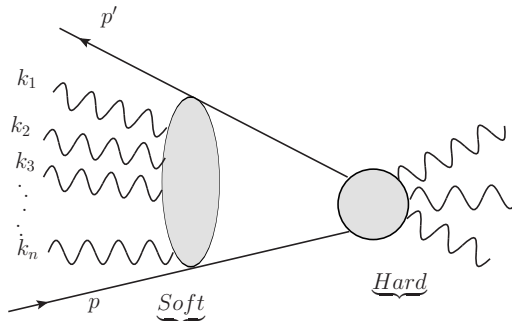


Figure 1.8: Factorization of soft and hard process

$$\begin{aligned} \mathcal{M} &= \bar{u}(p') i\mathcal{M}_0 u(p) \\ &\times e \left( \frac{p' \cdot \epsilon(k_1)}{p' \cdot k_1} - \frac{p \cdot \epsilon(k_1)}{p \cdot k_1} \right) \times e \left( \frac{p' \cdot \epsilon(k_2)}{p' \cdot k_2} - \frac{p \cdot \epsilon(k_2)}{p \cdot k_2} \right) \dots e \left( \frac{p' \cdot \epsilon(k_n)}{p' \cdot k_n} - \frac{p \cdot \epsilon(k_n)}{p \cdot k_n} \right) . \end{aligned} \quad (1.31)$$

Now, summing over polarizations using  $\sum_{pol} \epsilon_\mu \epsilon_\nu^* = -g_{\mu\nu}$ , the contribution in the cross-section due to the emission of soft photons is given by,

$$\int \frac{d^3k}{(2\pi)^3} \frac{1}{2k^0} e^{2(-g_{\mu\nu})} \left( \frac{p'^\mu}{p' \cdot k} - \frac{p^\mu}{p \cdot k} \right) \left( \frac{p'^\nu}{p' \cdot k} - \frac{p^\nu}{p \cdot k} \right) \equiv A . \quad (1.32)$$

Considering the energy of photon in the range  $\mu < E < E_l$ , the explicit calculation of  $A$  gives [67],

$$A = \frac{\alpha}{\pi} f_{IR}^{(real)}(q^2) \log \left( \frac{E_l^2}{\mu^2} \right) , \quad (1.33)$$

where

$$f_{IR}^{(real)}(q^2) = \int_0^1 \left( \frac{m^2 - q^2/2}{m^2 - q^2\zeta(1-\zeta)} \right) d\zeta - 1 , \quad (1.34)$$

and  $q^2 = (p' - p)^2$ ,  $E_l$  is the energy below which detector cannot detect,  $\mu$  is the infrared cut off. As  $q^2$  is negative and  $\zeta(1-\zeta)$  can only have a maximum value of  $1/4$ , the first term is bigger than 1, thus,  $f_{IR}^{(real)}(q^2)$  is positive. For the case in hand, there will be  $n$  factors of  $A$  and a overall symmetry factor of  $1/n!$  as the photons are identical particles.

In a collider one cannot perform a measurement where the collider can distinguish between (i) a final state with a certain number of fermions, (ii) and a final state with same number of fermions and soft photons. Thus by Bloch-Nordsieck we sum the contribution of these two processes in physical observables to obtain a finite result. Thus, using Block-Nordsieck theorem, we can write the cross-section for emission of  $n$ -photons as,

$$\begin{aligned} \sum_{n=0}^{\infty} \frac{d\sigma}{d\Omega} (p \rightarrow p' + n\gamma) &= \frac{d\sigma}{d\Omega} (p \rightarrow p') \sum_{n=0}^{\infty} \frac{1}{n!} A^n \\ &= \frac{d\sigma}{d\Omega} (p \rightarrow p') \cdot \exp(A) . \end{aligned} \quad (1.35)$$

This equation is important as it tells that the effects of emission of soft photons are factorized for both the scattering amplitudes and cross-section.

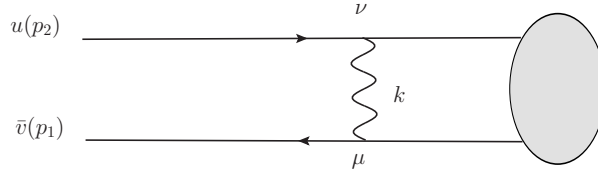


Figure 1.9: 1<sup>st</sup> order correction with only one photon



## Virtual soft emissions

Till now, we have discussed about the factorization of soft singularities for real emission diagrams. This kind of factorization is not only a feature of diagrams involving the real emission diagrams but also happens for diagrams involving virtual corrections.

Now, using the eikonal Feynman rules for virtual gluon exchange of Fig. (1.9), the matrix element is given by,

$$\mathcal{M}_v = \frac{-ie^2}{(2\pi)^4} \int d^4k \frac{1}{k^2 + i\epsilon} \frac{1}{(2p_1 \cdot k + k^2 + i\epsilon)} \frac{1}{(2p_2 \cdot k + k^2 + i\epsilon)} \times (-4p_1 \cdot p_2) \bar{v}(p_1) \dots u(p_2) . \quad (1.36)$$

$$\mathcal{M}_v = \mathcal{M}_0 \times B , \quad (1.37)$$

where,

$$B = -i \frac{e^2}{(2\pi)^4} \int d^4k \frac{1}{k^2 + i\epsilon} \frac{1}{(2p_1 \cdot k + k^2 + i\epsilon)} \frac{1}{(2p_2 \cdot k + k^2 + i\epsilon)} \times (-4p_1 \cdot p_2) , \quad (1.38)$$

and  $\mathcal{M}_0$  is the Born matrix element. The explicit form of  $B$  is given by [67]

$$B = -\frac{\alpha}{2\pi} f_{IR}^{(virtual)}(q^2) \log\left(\frac{-q^2}{\mu^2}\right) , \quad (1.39)$$

where,  $f_{IR}^{(virtual)}(q^2)$  has the same expression as of Eq. (1.34), with  $q^2 = (p_2 - p_1)^2$ . For exchange

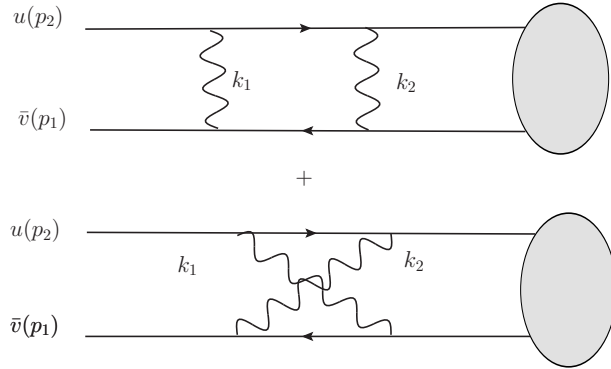


Figure 1.10:  $2^{nd}$  order correction with two photons

of two virtual photons between the fermion and the anti-fermion, we have contributions from two diagrams shown in Figure (1.10), the matrix element for these diagrams are given by,

$$\mathcal{M}_v = \mathcal{M}_0 \times \frac{1}{2!} B^2 . \quad (1.40)$$

The above result for two photons generalizes trivially to all orders in the perturbation theory. The matrix element for exchange of  $m$  virtual photons is given by,

$$\mathcal{M}_v = \mathcal{M}_0 \times \left( \frac{1}{m!} B^m \right) . \quad (1.41)$$

The term inside the bracket is  $m$ -th order term of an exponential. Thus, the generalized form for exchange of any number of soft photon can be written as,

$$\mathcal{M} = \sum \mathcal{M}_v = \mathcal{M}_0 \times \sum_{m=0}^{\infty} \frac{1}{m!} B^m = \mathcal{M}_0 \times \exp(B) . \quad (1.42)$$

Thus, the cross-section for emissions of virtual soft photons has the form

$$\frac{d\sigma}{d\Omega} = \left( \frac{d\sigma}{d\Omega} \right)_0 \times \exp(2B) . \quad (1.43)$$

Note that the factor  $B$  is one-loop correction and thus, the knowledge of one-loop result is sufficient to calculate the effects of soft photons at all orders in the perturbation theory.

## 1.5 Factorization and resummation

Factorization of Infrared singular parts from finite parts is the backbone of modern perturbative QCD. This type of factorization is based on the analytic structure of the loop integrals that generates IR singularities [60, 68–74] and power counting [75–77].

A general scattering amplitude factorizes into process independent soft and collinear functions and a process dependent hard function as,

$$\mathcal{M} = S \otimes J \otimes H , \quad (1.44)$$

where  $S$  contains the singularities associated with the emission of soft gluons,  $J$  contains the singularities related to the emission of collinear gluons and  $H$  is free from IR singularities and is in general process dependent.

The consequence of the factorization results in evolution equation and solving them results in exponentiation [78]. The generalization of exponentiation discussed in the previous section for QED generalizes non-trivially in non-abelian gauge theories as the gluons contain colour charges. However, the generalization of exponentiation for soft function has been achieved through a set of diagrams known as webs. The soft function can be written as,

$$S = \exp(W) . \quad (1.45)$$

where  $W$  are known as webs [79–84]. Webs are defined as the closed sets of diagrams that differ by the order of attachment to each fermion line (Wilson line). A generalization of webs and their application at four loops and beyond are discussed in [85, 86].

The jet functions follow an evolution equation controlled by jet anomalous dimension and solving the RG equation, one can also obtain exponentiation of the contributions coming from emission of collinear emissions.

The exponentiation of the effects of soft and collinear gluons are the facts that will be exploited throughout the thesis for resummation of these contributions. Thus, it is possible to capture the singularities appearing at higher orders by exponentiating the contributions from the lower order diagrams in both QED and QCD. We will now move on to discuss the factorization that happens

for cross-section in QCD and the method to resum large logarithms.

### 1.5.1 A demonstration of how large logarithms arise: The case of thrust distribution

In this section we will show a simple example of how to resum the large logarithms that appear in thrust distribution for  $e^+e^- \rightarrow q\bar{q}g$  process, which is relevant at colliders like LEP. Thrust is defined as

$$T = \text{Max}_{\mathbf{n}} \frac{\sum_i |\mathbf{p}_i \cdot \mathbf{n}|}{\sum_i E_i}, \quad (1.46)$$

where  $p_i$  are the momenta of the final state particles and  $\mathbf{n}$  is direction which maximises the numerator. It is straightforward to find  $T = 1$  for pencil like (back-to-back) events and  $T = 1/2$  for spherically symmetric events.

The differential cross-section with respect to thrust for  $e^+e^- \rightarrow q\bar{q}$  is given by,

$$\frac{1}{\sigma_0} \frac{d\sigma_0}{dT} = \delta(1 - T), \quad (1.47)$$

that is thrust is equal to 1 for this process. At next perturbative order in  $\alpha_s$ , we have the thrust distribution as,

$$\frac{1}{\sigma_0} \frac{d\sigma_0}{dT} = \frac{C_F \alpha_s}{2\pi} \left[ \frac{4}{1-T} \log \frac{1}{1-T} - \frac{3}{1-T} \right] + C_F \frac{\alpha_s}{4\pi} \delta(1 - T) \quad (1.48)$$

This distribution is divergent in the limit  $T \rightarrow 1$ . The experimental and fixed order theoretical distributions do not match at low values of  $T$ . The logarithms of the above equation are required to be resummed to obtain a sensible prediction. In the following two chapters of the thesis, we discuss two kinds of resummation:  $p_T$  resummation and Dressed gluon exponentiation.

In the following we give the derivation of the thrust distribution at NLO arising from the emission of a gluon in the final state. We consider that all final state particles are massless while computing thrust distribution at next-to-leading-order; however when we examine dressed gluon exponentiation, the gluon is not massless rather possesses virtuality  $k^2$ . In order to differentiate between massless and massive case scenario we have different attributes. When we study the massless case, we have the following characteristics:  $\gamma^* \rightarrow q(p_2)\bar{q}(p_1)g(p_3)$  yet in the massive case we have the following traits  $\gamma^* \rightarrow q(p_1)\bar{q}(p_2)g(k)$ . For matrix element square in the massless case, we use  $|\overline{\mathcal{M}}|^2$ , but in the massive case, we have  $\mathcal{M}$ . We are interested in the event shape variables in  $e^+e^-$  collider.

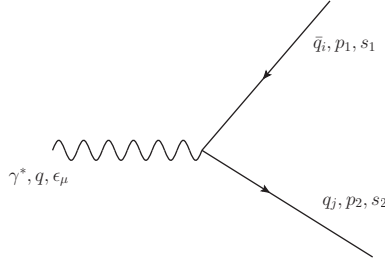


Figure 1.11: Born process

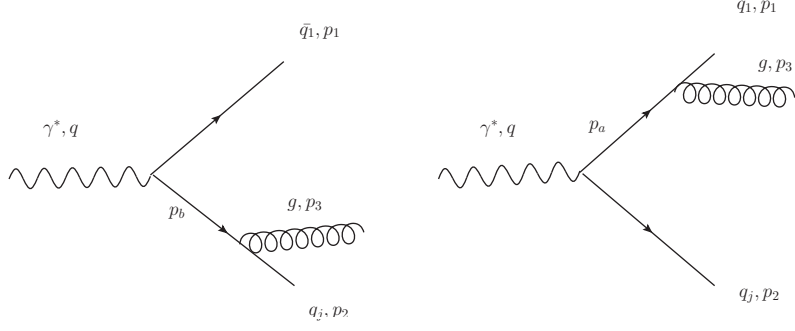


Figure 1.12: Feynman diagrams for real emission of one gluon

In order to study thrust we are interested in the process  $\gamma^* \rightarrow q\bar{q}g$ ;  $\sigma_0 = 3\alpha e_q^2 Q$  represents Born cross-section for the event  $\gamma^* \rightarrow q\bar{q}$ . Now, we will look into next-to leading order process which is  $\gamma^* \rightarrow q(p_2)\bar{q}(p_1)g(p_3)$ . The amplitude for these two diagrams given as

$$A = \bar{u}(p_2, s_2)(-ig_s\gamma_\nu T_{ij}^a) \left( \frac{i\cancel{p}_a}{p_a^2} \right) (-iee_q\gamma_\mu)v(p_1, s_1)\epsilon_\mu\epsilon'_\nu, \quad (1.49)$$

$$A' = \bar{u}(p_2, s_2)(-iee_q\gamma_\mu)v(p_1, s_1) \left( \frac{i\cancel{p}_b}{p_b^2} \right) (-ig_s\gamma_\nu T_{ij}^a)\epsilon_\mu\epsilon'_\nu, \quad (1.50)$$

Spin averaged matrix squared element

$$|\overline{\mathcal{M}}(\gamma^* \rightarrow q\bar{q}g)|^2 = |A|^2 + |A'|^2 + A(A')^* + A'A^*. \quad (1.51)$$

Conservation of momentum  $q = p_1 + p_2 + p_3$ . In center-of-mass frame,  $E_{cm} = Q = \sqrt{q^2}$ . We introduce dimensionless variables,  $x_i = 2E_i/Q$ . Here all particles involving decay are massless. In this scenario,  $p_i \cdot p_j = \frac{1}{2}Q^2(1 - x_k)$ . We will use the following relation corresponding to photon polarization  $\sum_\lambda \epsilon_\mu(\lambda)\epsilon_\nu^*(\lambda) = -g_{\mu\nu}$ . We will have the following constraint equation in terms of  $x_i$ 's.  $x_1 + x_2 + x_3 = 2$  We introduce the Mandelstam variables :

$$s = (p_1 + p_3)^2 = 2p_1 \cdot p_3 = Q^2(1 - x_2), \quad (1.52)$$

$$t = (p_2 + p_3)^2 = 2p_2 \cdot p_3 = Q^2(1 - x_1), \quad (1.53)$$

$$u = (p_1 + p_2)^2 = 2p_1 \cdot p_2 = Q^2(1 - x_3). \quad (1.54)$$

If  $|\overline{\mathcal{M}}|^2$  is a Lorentz scalar, it can be a function of  $p_1^2, p_2^2, p_3^2, p_1 \cdot p_2, p_1 \cdot p_3, p_2 \cdot p_3$ . As all the final state particles are massless we have  $p_1^2 = p_2^2 = p_3^2 = 0$ . Thus there are three variables of which  $|\overline{\mathcal{M}}|^2$  can be a function of. Now there is one scalar condition  $Q^2 = (p_1 + p_2 + p_3)^2$  thus there are really  $3 - 1 = 2$  variables, which we take to be  $(2 p_1 \cdot Q)/Q^2$ ,  $(2 p_2 \cdot Q)/Q^2$ .

First term of Eq. (1.51) becomes,

$$|A|^2 = \frac{g_s^2 e^2 e_q^2}{p_a^4} Tr[T_a T_a] Tr[\cancel{p}_2 \gamma_\nu \cancel{p}_a \gamma_\mu \cancel{p}_1 \gamma_\mu \cancel{p}_a \gamma_\nu] \quad (1.55)$$

$$\begin{aligned}
|A|^2 &= \frac{g_s^2 e^2 e_q^2}{t^2} 64 \left( \frac{1}{2}(u+s)t - \frac{1}{2}ut \right) \\
&= 32g_s^2 e^2 e_q^2 \frac{s}{t} = 32g_s^2 e^2 e_q^2 \frac{(1-x_2)}{(1-x_1)}
\end{aligned} \tag{1.56}$$

Similarly,

$$|A'|^2 = 32g_s^2 e^2 e_q^2 \frac{(1-x_1)}{(1-x_2)} \tag{1.57}$$

While,

$$A(A')^* = A^* A' = 32g_s^2 e^2 e_q^2 \frac{(1-x_3)}{(1-x_1)(1-x_2)} \tag{1.58}$$

$$|\overline{\mathcal{M}}(\gamma^* \rightarrow q\bar{q}g)|^2 = 32g_s^2 e^2 e_q^2 \frac{x_1^2 + x_2^2}{(1-x_1)(1-x_2)} \tag{1.59}$$

Differential decay rate given by the equation

$$dW = \frac{1}{2E_{cm}} |\overline{\mathcal{M}}|^2 \left( \prod_{i=1}^3 \frac{d^3 p_i}{(2\pi)^3 (2E_i)} \right) (2\pi)^4 \delta^4(q - p_1 - p_2 - p_3) \tag{1.60}$$

now, integration over 3-momenta of particle 3 (which is gluon) we will have,

$$\int dp_3 \delta^4(q - p_1 - p_2 - p_3) = \delta(Q - E_1 - E_2 - E_3) \tag{1.61}$$

$$s + t + u = Q^2 \tag{1.62}$$

For, massless particles,

$$|\mathbf{p}_i| = E_i$$

So,

$$\int \frac{d^3 p}{2E_i} = \frac{1}{2} \int E_i \sin \theta_i d\theta_i d\phi_i dE_i = \frac{4\pi}{2} \int E_i dE_i, \tag{1.63}$$

and

$$\begin{aligned}
&\frac{1}{(2\pi)^5} \int \int \frac{d^3 p_1}{2E_1} \frac{d^3 p_2}{2E_2} \frac{\delta(Q - E_1 - E_2 - E_3)}{2E_3} \\
&= \frac{1}{(2\pi)^5} \frac{4\pi \cdot 2\pi}{4} \int_0^\pi \sin \theta_1 d\theta_1 \frac{\delta(Q - E_1 - E_2 - E_3)}{2E_3} E_1 dE_1 E_2 dE_2 \\
&= \frac{1}{2} \frac{1}{(2\pi)^3} \int_{-1}^1 dz \frac{\delta(Q - E_1 - E_2 - E_3)}{2E_3} E_1 dE_1 E_2 dE_2,
\end{aligned} \tag{1.64}$$

where  $z = \cos \theta_{12}$  is the relative angle between particle 1 and 2. Now, we will use the following property of delta function

$$\delta(f(x)) = \sum_i \frac{\delta(x - x_i)}{|f'(x_i)|}, \tag{1.65}$$

if  $f(x_i) = 0$

$$(1 - x_i) = \frac{1}{2} x_j x_k (1 - \cos \theta_{jk}), \tag{1.66}$$

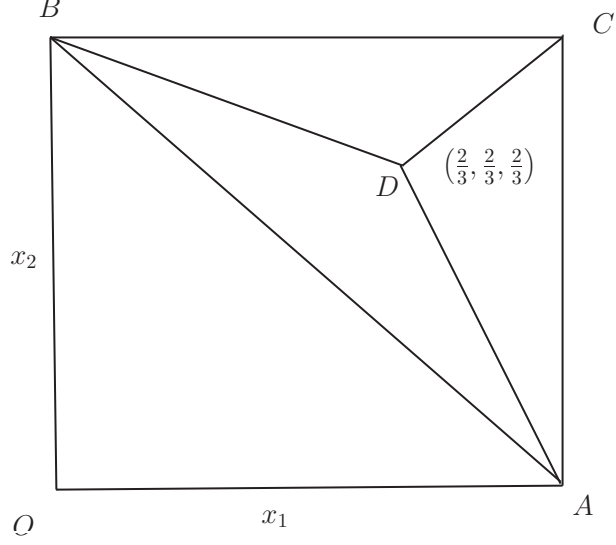


Figure 1.13: The phase space for  $q\bar{q}g$ , where all particles are massless. The lines AC, BC, AB correspond to  $x_1 = 1$ ,  $x_2 = 1$  and  $x_3 = 1$  respectively. At point D  $x_1, x_2, x_3$  all equal to value  $2/3$ . It is easy to check that any point in the plane identically satisfies the constraint  $x_1 + x_2 + x_3 = 2$ .

$$\begin{aligned} \frac{\delta(Q - E_1 - E_2 - E_3)}{2E_3} &= \delta((q - p_1 - p_2 - p_3)^2) \\ &= \delta\left(Q^2\left(1 - x_1 - x_2 + \frac{1}{2}(1 - z)\right)\right). \end{aligned} \quad (1.67)$$

Integrating this expression over  $z$  gives  $2/(Q^2 x_1 x_2)$ , such that Eq. (1.64) becomes

$$\frac{Q^2}{16(2\pi)^3} dx_1 dx_2. \quad (1.68)$$

Now, from Eq. (1.60) we have,

$$dW = \frac{Q}{(2\pi)^3} |\overline{\mathcal{M}}|^2 dx_1 dx_2, \quad (1.69)$$

finally we will have the following differential distribution,

$$\frac{1}{\sigma_0} \frac{d^2\sigma}{dx_1 dx_2} = \frac{2\alpha_s}{3\pi} \frac{x_1^2 + x_2^2}{(1 - x_1)(1 - x_2)}. \quad (1.70)$$

Eq. (1.70) will diverge if either  $x_1$  or  $x_2$  approaches 1. They both can simultaneously approaches 1 and in that case also the above equation diverge. This scenario happen when gluon becomes either soft or it become collinear to the quark or anti-quark. At next-to-leading-order  $d\sigma/dT$  can be calculated from Eq. (1.70); if we integrate over  $x_1$  and  $x_2$  with the constraint  $\delta(T - \text{Max}\{x_1, x_2, x_3\})$ . Working in centre of mass frame of  $\gamma^*$  where  $\vec{q} = 0$ , the energy fractions are  $x_i = 2E_i/Q$ . Where,  $q^\mu = (Q, 0, 0, 0)$  and  $p_i^\mu = (E_i, \mathbf{p}_i)$ . Calculation of thrust for this 3 body process will give us, considering  $\mathbf{p}_1 > \mathbf{p}_2$  and  $\mathbf{p}_3$

$$\sum_i |\mathbf{p}_i \cdot \mathbf{n}| = |\mathbf{p}_1 \cdot \mathbf{n}| + |\mathbf{p}_2 \cdot \mathbf{n}| + |\mathbf{p}_3 \cdot \mathbf{n}|. \quad (1.71)$$

As  $\mathbf{n} = \frac{\mathbf{p}_1}{|\mathbf{p}_1|}$ , that will give us

$$\sum_i |\mathbf{p}_i \cdot \mathbf{n}| = 2|\mathbf{p}_1| . \quad (1.72)$$

As we are considering massless case of final state particles, the value of thrust will come out to be

$$T = \frac{2E_1}{Q} = x_1 , \quad (1.73)$$

finally for any three body final states the expression for thrust in massless case become

$$T = \text{Max}\{x_1, x_2, x_3\} . \quad (1.74)$$

Figure (1.13) shows the Dalitz plot for the process at hand. The boundaries of phase space in Figure (1.13) are given by collinear configurations and the three vertices A, B, C corresponds to soft configurations. We can divide the region of integration into three such that in each region one of the  $x_i$  is the largest. Consider first the case  $T = x_1$ .

$$\begin{aligned} \frac{1}{\sigma_0} \frac{d\sigma}{dT} \Big|_{T=x_1} &= \frac{2\alpha_s}{3\pi} \int dx_1 dx_2 dx_3 \delta(x_1 + x_2 + x_3 - 2) \\ &\quad \times \delta(T - x_1) \theta(T - x_2) \theta(T - x_3) \frac{x_1^2 + x_2^2}{(1 - x_1)(1 - x_2)} \\ &= \frac{2\alpha_s}{3\pi} \int_{2(1-T)}^T dx_2 \frac{T^2 + x_2^2}{(1 - T)(1 - x_2)} \\ &= \frac{2\alpha_s}{3\pi} \left[ \frac{1 + T^2}{1 - T} \log \left( \frac{2T - 1}{1 - T} \right) + \frac{3T^2 - 14T + 8}{2(1 - T)} \right] . \end{aligned} \quad (1.75)$$

From the matrix squared element in Eq. (1.59) we see that the expression is symmetric under the exchange of  $x_1$  and  $x_2$ . So, for  $T = x_2$  we will have

$$\frac{1}{\sigma_0} \frac{d\sigma}{dT} \Big|_{T=x_2} = \frac{2\alpha_s}{3\pi} \left[ \frac{1 + T^2}{1 - T} \log \left( \frac{2T - 1}{1 - T} \right) + \frac{3T^2 - 14T + 8}{2(1 - T)} \right] . \quad (1.76)$$

For case  $T = x_3$  we will have the following expression

$$\begin{aligned} \frac{1}{\sigma_0} \frac{d\sigma}{dT} \Big|_{T=x_3} &= \frac{2\alpha_s}{3\pi} \int dx_1 dx_2 dx_3 \delta(x_1 + x_2 + x_3 - 2) \\ &\quad \times \delta(T - x_3) \theta(T - x_1) \theta(T - x_2) \frac{x_1^2 + x_2^2}{(1 - x_1)(1 - x_2)} \\ &= \frac{2\alpha_s}{3\pi} \int dx_1 dx_2 \delta(T - 2 + x_1 + x_2) \frac{x_1^2 + x_2^2}{(1 - x_1)(1 - x_2)} \\ &= \frac{2\alpha_s}{3\pi} \int_{2(1-T)}^T dx_2 \frac{(2 - T - x_2)^2 + x_2^2}{(T + x_2 - 1)(1 - x_2)} \\ &= \frac{4\alpha_s}{3\pi} \left[ \frac{1 + (1 - T)^2}{T} \log \left( \frac{2T - 1}{1 - T} \right) + 2 - 3T \right] . \end{aligned} \quad (1.77)$$

Adding the contributions from the three regions using Eqs. (1.75) - (1.77) we obtain the total thrust

distribution as

$$\frac{1}{\sigma_0} \frac{d\sigma}{dT} = \frac{2\alpha_s}{3\pi} \left[ \frac{2(3T^2 - 3T + 2)}{T(1-T)} \log\left(\frac{2T-1}{1-T}\right) - \frac{3(3T-2)(2-T)}{1-T} \right]. \quad (1.78)$$

The above equation diverges as  $T \rightarrow 1$  which is in agreement with the appearance of infrared singularities. Eq. (1.78) becomes unreliable when  $T$  is very close to 1 value. The logarithms appearing in the expression becomes large in that limiting case and correction terms become larger than the lowest order result and thus, the large logarithms need to be resummed.



## Chapter 2

# Resummed $p_T$ distribution of Pseudo-scalar Higgs

### 2.1 Introduction

The Standard Model is the most successful theory of particle physics – it explains the properties of the fundamental particles and their mutual interactions. The discovery of the Higgs boson in 2012 by the ATLAS [1] and the CMS [88] detectors at the Large Hadron Collider, has further cemented the status of the SM as the theory of particle physics. Even though the properties of the Higgs boson are in agreement with the SM predictions so far, SM is certainly not the complete theory of nature as it can not provide a description for the baryogenesis, the origin of neutrino masses. There is no resolution to the hierarchy problem within the framework of the SM, etc. Several of these issues can be addressed by introducing new fields in the theory thereby extending the model beyond the Standard Model. One of the goals of the LHC has been to discover the existence of any physics beyond the SM. A large class of such models predicts existence of multiple scalar or pseudo-scalar Higgs particles. The models like the Minimal Supersymmetric SM (MSSM) or Next-to-MSSM etc., predict existence of several Higgs bosons which differ among each other by their mass, charge, CP-parity and couplings. A simple example contains an additional Higgs doublet along with the usual Higgs doublet of the SM. After the symmetry breaking this gives rise to two CP-even (scalar) Higgs bosons ( $h, H$ ), one of which is identified with the SM Higgs boson ( $h$ ), a CP-odd (pseudo-scalar) Higgs boson ( $A$ ) as well as a pair of charged scalars ( $H^\pm$ ). This allows phenomenologically interesting scenarios particularly with pseudo-scalar resonances. One of the important goal at the LHC Run-II is to search for such resonances which requires a precise theoretical predictions for both inclusive as well as for exclusive observables.

In order to come up with a theoretical prediction one needs to first figure out what are the most dominant channels through which pseudo-scalar Higgs bosons are produced. It makes sense to concern ourselves with the calculation of cross-sections in production channels that are subdominant only after a precise prediction is available for the dominant channels. That is, we need to obtain results for which we might need to go to higher orders in perturbation theory to ensure that the theoretical uncertainties are under control.

The dominant production mode for pseudo-scalar Higgs boson is through the gluon fusion  $gg \rightarrow$

A. Therefore a large gluon flux can uplift its production cross-section to a great extent, and this is precisely the case at the LHC. Similar to the case of the Higgs boson production, the leading order (LO) prediction for  $gg \rightarrow A$  suffers from large theoretical uncertainties arising from its dependence on the renormalization scale  $\mu_R$  through the strong coupling constant. The next-to-leading order (NLO) correction [89–92] is known to increase the cross section by a large amount – 67% compared to the Born contribution. Furthermore the scale uncertainty also remains quite large, around 35%. These uncertainties arise from

1. the freedom that we have in choosing the renormalization scale  $\mu_R$ , as well as
2. the freedom that we have in choosing the factorization scale  $\mu_F$  that enter the parton densities and partonic cross-sections.

As is well known, these theoretical uncertainties are an artefact of the perturbation theory and reduce upon the inclusion of higher order corrections. A completely non-perturbative result would be completely free of these arbitrary renormalization and factorization scales.

The foregoing essentially means that we require a result that includes terms beyond NLO. For this reason the total (inclusive) cross section at the next-to-next-to-leading order (NNLO) was calculated in the early 2000s by several groups [93–97]. While NNLO correction reduces the scale uncertainties to 15% the cross-section jumps further by 15%. A 15% uncertainty is still high and to further reduce the scale dependences it is required that we go even higher in the perturbation order and obtain the full next-to-next-to-next-to-leading order (N<sup>3</sup>LO) corrections. The complexity in full N<sup>3</sup>LO correction is even higher and only recently [98] has been obtained for the SM Higgs boson production with infinite top mass limit which reduces the scale uncertainty to 3%. The large top mass approximations turned out to be a good approximation for the Higgs case and the predictions are found to be within 1% [99–101] and one could expect similar behaviour in pseudo-scalar production as well.

As we have discussed in the previous chapter of this thesis, large enhancements arise in perturbative results due to soft (and collinear) emissions as the matrix elements take large values for these emissions and actually blow up in the strict soft (or collinear) limit. Even though these enhancements do not appear in inclusive total cross-sections they become important if the emissions are restricted to the soft or the collinear configurations. Such a situation arises when one considers cross-section at the threshold of the production of the final state. This forces the emission to become soft and the parameter that controls the closeness to the threshold appears in the calculations as the argument of logarithms. Of course, the blunt poles in  $\epsilon$  are canceled against the virtual corrections the large logarithms enhance the cross-sections. As moving one order higher is technically very difficult, the first attempt towards the N<sup>3</sup>LO corrections is made through the calculation of the threshold enhanced soft-virtual (SV) corrections. For the Higgs production these are known for a long time up to N<sup>3</sup>LO<sub>SV</sub> [102–107]. Associated production [108] and bottom quark annihilation [109] are also known at the same accuracy.

As in the case of Higgs production, the effect of soft gluon emission at threshold of pseudo-scalar production has been computed at N<sup>3</sup>LO<sub>SV</sub> level [110]. Fixed order cross section may however give unreliable results in certain phase space regions due to large logarithms arising from gluon emission that are forced to be soft and, as we have seen in the previous chapter of this thesis, these needs to be resummed to all orders in the perturbation theory. The soft gluon resummation for inclusive

Higgs production accurate up to next-to-next-to-leading logarithmic (NNLO+NNLL) were obtained in [111]. The full N<sup>3</sup>LO result [98] enables to perform soft gluon resummation at next-to-next-to-next-to-leading logarithmic (N<sup>3</sup>LO+N<sup>3</sup>LL) [112–114] accuracy (see also [115] for renormalization group improved prediction.). For pseudo-scalar production, an approximate N<sup>3</sup>LO<sub>A</sub> result has been matched with N<sup>3</sup>LL threshold resummation in [9] (see [116, 117] for earlier works in this direction).

Resummation is especially important for exclusive observables. Rapidity distributions at NNLO+NNLL accuracy for the Higgs [118] and Drell-Yan [119] are predicted by resumming large threshold logarithms (see [62, 63, 120] for earlier works). Also see [121–125] for a different QCD approach and [126–128] for SCET approach..

Transverse momentum ( $p_T$ ) distribution is a very important and widely studied observable. Even though perturbation theory is the right tool to study transverse momentum distribution at values of  $p_T$  that are close to and above the typical hard scale  $M$  in the theory, it breaks down for small values of the transverse momentum. This breakdown occurs due to soft and collinear emissions when the  $p_T$  value of the observed final state is small, ie  $p_T \ll M$ . The reason behind this breakdown is the appearance of large logarithms of the type  $\ln^n(M^2/p_T^2)$  at each order in the perturbation theory, where the exponent of the logarithm increases with the perturbation order. By resumming these large logarithms [129–141], the predictivity of the QCD can be recovered in the full phase space region for  $p_T$  distribution.

Resummation of large logarithms is possible because the universal properties of the QCD in the infrared region [130–136, 139, 142, 143]. Soft-collinear effective theory (SCET) also provides tools for resummation using an effective field theory set up (see [144–148]). Resummation techniques have been used for Higgs boson  $p_T$  spectrum in gluon fusion up to NNLO+NNLL [149–157] and to the bottom quark annihilation up to NNLO+NNLL [158, 159]. The  $p_T$  distribution for the Higgs boson has been pushed to one order in logarithmic accuracy to NNLO+N<sup>3</sup>LL accuracy in [160–162]. Another approach to resum these large logarithms is through the parton shower (PS) simulations which has been also successful in recent times through the implementation in Monte Carlo generators like MADGRAPH5\_AMC@NLO [163], POWHEG [164] etc. mostly up to NLO+PS accuracy. However the accuracy of PS prediction is often not clear and has remained an active topic of research these days\*. Even though the resummation formulae provide us with results to be used in the low transverse momentum region we can not use them directly. A matching between the high  $p_T$  spectrum and low  $p_T$  spectrum has to be done before we can claim that we have a prediction of the distribution over the entire  $p_T$  range. This effectively brings in a matching scale (resummation scale or shower scale) which defines the infrared region and the hard region. Although its dependence is of higher logarithmic order, a suitable choice is needed to properly describe the full  $p_T$  spectrum in a meaningful way. We will discuss about the matching condition and matching scale in section 2.2.1.

A clear understanding of the pseudo-scalar properties is also based on the precise knowledge of differential observables like transverse momentum, rapidity etc. For the pseudo-scalar production in association with a jet, the two-loop virtual amplitudes can be found in [166], which is important to predict the differential distribution. The small  $p_T$  region of the pseudo-scalar  $p_T$  spectrum renders the fixed order prediction unreliable due to the large logarithms in this phase space region as is the case for the Higgs production. These logarithms have to be resummed in order to get a valid

---

\*For a recent study see [165] and references therein.

prediction and this has been carried out at next-to-leading logarithmic (NLO+NLL) in [8] using universal infrared behaviour of QCD. Before we proceed further, let us clarify our counting of orders for the distribution. In this thesis we count the  $gg \rightarrow A$ , which is proportional to  $\delta(p_T)$  as there is no emission of QCD particles in the final state as the Leading Order contribution.. Emission of a single QCD particle in the final state will contribute at the NLO and so on. The scale uncertainty in the peak region of the resummed result at the NLO+NLL is fairly large and was found to be 25% when the scale is varied simply by a typical factor of two. Along with the PDF uncertainty, the total theoretical uncertainties reach as large as 35% near the peak. These findings show that a calculation at the next order in perturbation theory is required to bring down these theoretical uncertainties. In this thesis we extend this accuracy to Next-to-Next-Leading-Logarithmic accuracy. We obtained different pieces necessary for  $p_T$  resummation of a pseudo-scalar Higgs boson up to NNLL accuracy. As we discussed above, we will be required to match with the fixed order predictions that are valid for higher values of  $p_T$  with the resummed results that are valid for low values of  $p_T$  in order to obtain a distribution that is valid for the  $p_T$  range. We use the ansatz prescribed in [9] to obtain the NNLO piece to a very good approximation and call it as  $\text{NNLO}_A$ . Finally the matched prediction is presented up to  $\text{NNLO}_A + \text{NNLL}$  accuracy for the pseudo-scalar  $p_T$  spectrum in light of phenomenological study both at 14 TeV and 13 TeV LHC.

The chapter is organised as follows: in Sec. 2.2 we set up the theoretical framework for the resummation of large logarithms for small  $p_T$  region relevant for pseudo-scalar Higgs boson production. In Sec. 2.3, we will provide a detailed phenomenological study of the  $p_T$  spectrum for different masses, scales and parton distribution functions (PDFs) relevant at the LHC. Finally we draw our conclusion in Sec. 2.4.

## 2.2 Theoretical Framework

In this section we give the resummation formula and discuss various coefficients that enter in it. We also describe the matching prescription that we follow to obtain the distribution valid over the entire  $p_T$  range.

### Resummation formula

Let  $M$  be the mass of the colourless final state (pseudo-scalar Higgs boson in our case). If we calculate the  $p_T$  distribution of  $M$  for transverse momentum values that are significantly smaller than  $M$ , large logarithms of the form  $\ln(p_T/M)$  arise in the distribution  $d\sigma/dp_T$  due to an incomplete cancellation of soft and collinear contributions. At each successive order in the strong coupling constant,  $\alpha_s (= g_s^2/4\pi)$ , the highest power of the logarithm that appears increases which renders the naïve perturbative expansion in  $\alpha_s$  invalid as  $p_T \rightarrow 0$ . However, thanks to the factorization of soft and collinear radiation from the hard processes we can resum these large logarithms to all orders in perturbation theory. The transverse momentum of all the final state particles –  $M$  and the QCD radiations, are tied together so that the total  $p_T$  of the final state vanishes. This is so because the incoming gluons that vanishing transverse momentum. Thus a Dirac delta function ensures that the sum of the transverse momenta of all the final state particles adds up to zero. Thus in order to factorise the phase space (the Dirac delta function) we need to work in the Fourier space conjugate to  $\mathbf{p}_T$  called impact parameter space in which the Delta function can be converted to an exponential

function. Suppose  $g(\mathbf{p}_T)$  is a function of the two dimensional vector transverse momentum vector  $\mathbf{p}_T$ . This is basically the projection of momentum vector  $\mathbf{p}$  in the plane transverse to the beam axis. Let us denote the variable conjugate to  $\mathbf{p}_T$  by the two dimensional vector  $\mathbf{b}$ . The Fourier transform of a function of the function  $g(\mathbf{p}_T)$  is then defined by:

$$g(\mathbf{p}_T) = \frac{1}{(2\pi)^2} \int d^2\mathbf{b} e^{-i\mathbf{b}\cdot\mathbf{p}_T} g(\mathbf{b}), \quad (2.1)$$

Note that the limit of vanishing transverse momentum,  $p_T \rightarrow 0$  corresponds to  $b \rightarrow \infty$ . As we discussed in the beginning of this section conservation of momentum puts a constraint that the transverse momentum  $\mathbf{p}_T$  of the final state massive particle (Higgs Boson or pseudo-scalar Higgs boson) should be equal to the sum of the transverse momenta  $\mathbf{l}_T = \sum_i \mathbf{l}_{i,T}$  of the outgoing partons. This constraint which appears as a Dirac delta function can be put in a factored form by going to the Fourier space –  $\mathbf{b}$  space, using

$$\delta(\mathbf{p}_T + \mathbf{l}_T) = \frac{1}{(2\pi)^2} \int d^2\mathbf{b} e^{-i\mathbf{b}\cdot(\mathbf{p}_T + \mathbf{l}_T)}. \quad (2.2)$$

It is easy to perform the integration over the angular variable utilising the rotational invariance and this gives Bessel function  $J_0$ . The distribution for low  $p_T$  values compared to  $M$  has the following behaviour which is obtained by resumming the large logarithms to all orders in perturbation theory:

$$\frac{d\sigma^{F,(\text{res})}}{dp_T^2} = \tau \int_0^\infty db \frac{b}{2} J_0(bp_T) W^F(b, M, \tau), \quad (2.3)$$

here  $S$  is the hadronic centre-of-mass energy and

$$\tau = M^2/S. \quad (2.4)$$

Note that this equation only defines  $W^F(b, M, \tau)$  and does not contain any physical information. The proper inclusion of terms  $p_T \gtrsim M$  will be described in Sec. 2.2.1. Here and in what follows, the superscript  $F$  is attached to final state specific quantities. In what follows, we will not work in the  $\tau$ -space but make a transition to the corresponding Mellin-space. This will be convenient because the convolutions that appear in the distribution would get turned into ordinary products. The Mellin transform of  $W^F(b, M, \tau)$  with respect to the variable  $\tau$  is defined by

$$W_N^F(b, M) = \int_0^1 d\tau \tau^{N-1} W^F(b, M, \tau), \quad (2.5)$$

which has the following form for Higgs and pseudo-scalar Higgs production [136, 139, 151]<sup>†</sup>

---

<sup>†</sup>Throughout this work the parameters that are not crucial for the discussion will be suppressed in function arguments.

$$\begin{aligned}
W_N^F(b, M) &= \hat{\sigma}_{gg}^{F,(0)} \exp \left[ - \int_{b_0^2/b^2}^{M^2} \frac{dl^2}{l^2} \left[ A_g(\alpha_s(l^2)) \ln \frac{M^2}{l^2} + B_g(\alpha_s(l^2)) \right] \right] \\
&\times \sum_{i,j} H_{g;\mu_1\nu_1,\mu_2\nu_2}^F C_{gi}^{\mu_1\nu_1} C_{gj}^{\mu_2\nu_2} f_{i,N}(b_0/b) f_{j,N}(b_0/b),
\end{aligned} \tag{2.6}$$

where

$$\hat{\sigma}_{gg}^{F,(0)} = \text{parton level cross-section at LO} \tag{2.7}$$

This is a result obtained after resumming the soft and collinear gluon emissions to all orders in the perturbation theory. Note that the argument  $k^2$  of the running coupling constant  $\alpha_s$  is the variable of integration and is one of the sources of the powers of  $\log(b)$ . The function  $f_{i,N}(q)$  in Eq. (2.6) is the Mellin transform of the density function  $f_i(x, q)$  of parton  $i$  in the proton, where  $x$  is the momentum fraction and  $q$  the momentum transfer. The numerical constant

$$b_0 = 2 \exp(-\gamma_E), \quad \text{Euler constant } \gamma_E = 0.5772\dots, \tag{2.8}$$

is introduced for convenience. Unless stated otherwise, we have put the renormalization and the factorization to be equal:  $\mu_F = \mu_R = M$ . We will use the short hand notation  $[H_g^F C_1 C_2]$  to denote the factors that appear in the second line in Eq. (2.6):

$$[H_g^F C_1 C_2]_{gg,ij} = H_{g;\mu_1\nu_1,\mu_2\nu_2}^F C_{gi}^{\mu_1\nu_1} C_{gj}^{\mu_2\nu_2}, \tag{2.9}$$

and the structure of partonic tensor,  $C_{gk}^{\mu\nu}$ , is given by

$$C_{gk}^{\mu\nu}(z; q_1, q_2, \mathbf{b}; \alpha_s) = d^{\mu\nu}(q_1, q_2) C_{gk}(z; \alpha_s) + D^{\mu\nu}(q_1, q_2; \mathbf{b}) G_{gk}(z; \alpha_s), \tag{2.10}$$

where

$$\begin{aligned}
d^{\mu\nu}(q_1, q_2) &= -g^{\mu\nu} + \frac{q_1^\mu q_2^\nu + q_2^\mu q_1^\nu}{q_1 \cdot q_2}, \\
D^{\mu\nu}(q_1, q_2; \mathbf{b}) &= d^{\mu\nu}(q_1, q_2) - 2 \frac{b^\mu b^\nu}{\mathbf{b}^2}.
\end{aligned} \tag{2.11}$$

The vector  $b^\mu = (0, \mathbf{b}, 0)$  is the two-dimensional impact parameter vector in the four-dimensional notation and  $q_1, q_2$  are the momenta of colliding partons. All the coefficients that appear in the resummation formula in Eq. (2.6) and Eq. (2.10) have series expansions in  $a_s = \alpha_s/4\pi$ :

$$\begin{aligned}
C_{gi}(z; \alpha_s) &= \delta_{gi} \delta(1-z) + \sum_{n=1}^{\infty} a_s^n C_{gi}^{(n)}(z), \\
G_{gi}(z; \alpha_s) &= \sum_{n=1}^{\infty} a_s^n G_{gi}^{(n)}(z), \quad H_g^F(\alpha_s) = 1 + \sum_{n=1}^{\infty} a_s^n H_g^{F,(n)}, \\
A_g(\alpha_s) &= \sum_{n=1}^{\infty} a_s^n A_g^{(n)}, \quad B_g(\alpha_s) = \sum_{n=1}^{\infty} a_s^n B_g^{(n)}.
\end{aligned} \tag{2.12}$$

The order upto which these coefficients are included in Eq. (2.6) determines the *logarithmic accuracy* of the resummed cross section;

- Leading Logarithmic (LL) accuracy: Only the coefficient  $A_g^{(1)}$  is included and all higher order coefficients are dropped.
- Next-to-Leading (NLL) Logarithmic accuracy: Only the coefficients  $A_g^{(2)}$ ,  $B_g^{(1)}$ ,  $C_{gi}^{(1)}$ , and  $H_g^{F,(1)}$  are included.
- All the coefficients that are required for the resummation of the transverse momentum distribution of the pseudo-scalar Higgs boson at Next-to-next-to-leading (NNLL) accuracy will be given in Sec. 2.2.2.

**Resummation Scheme:** The coefficients  $A_g$ ,  $B_g$ , and  $C_{gi}$  that enter in the resummation formula contain information about the soft and collinear radiation and is independent of the hard scattering process. Ofcourse, there is a freedom of absorbing the function  $H$  into these coefficients. Since these resummation coefficients are process independent (i.e. they do not depend on specific final state), the coefficients  $A_g$ ,  $B_g$ , and  $C_{gi}$  that enter in the resummation formula for the Higgs production with  $H_g^h = 1$  can be used for the pseudo-scalar production as well. This choice for the resummation coefficients will be termed as Higgs resummation scheme in this thesis (see [11] for details on resummation schemes).

As far as the resummation formula, that is valid for low transverse momentum values is concerned the information of pseudo-scalar Higgs enters through the the *hard coefficient*  $H_g^F$  and the Born factor  $\hat{\sigma}_{gg}^{F,(0)}$ . All the other coefficients are resummation coefficients are known in the Higgs scheme mentioned above up to the perturbative order required in this work (see Sec. 2.2.2), except for the two coefficients  $H_g^{A,(1)}$  and  $H_g^{A,(2)}$  that we need to evaluate upto NNLO. This will also be presented in Sec. 2.2.2.

In the infinite top quark mass limit the effective Lagrangian [167] describing pseudo-scalar production is given by

$$\mathcal{L}_{\text{eff}}^A = \Phi^A(x) \left[ -\frac{1}{8} C_G O_G - \frac{1}{2} C_J O_J \right], \quad (2.13)$$

where the operators are defined as,

$$O_G = G_a^{\mu\nu} \tilde{G}_{a,\mu\nu} \equiv \epsilon_{\mu\nu\rho\sigma} G_a^{\mu\nu} G_a^{\rho\sigma}, \quad O_J = \partial_\mu (\bar{\psi} \gamma^\mu \gamma_5 \psi). \quad (2.14)$$

The Wilson coefficients  $C_G$  and  $C_J$  are obtained by integrating out the loops resulting from top quark.  $G_a^{\mu\nu}$  and  $\psi$  represent gluonic field strength tensor and light quark fields, respectively. In this study we will only consider contributions arising from the operator  $O_G$  in the effective Lagrangian and will not include the contributions arising from  $O_J$  operator. The Born cross section for the pseudo-scalar production at the parton level including the finite top mass dependence is given by

$$\hat{\sigma}_{gg}^{A,(0)}(\mu_R^2) = \frac{\pi\sqrt{2}G_F}{16} a_s^2 \cot^2\beta |\tau_A f(\tau_A)|^2. \quad (2.15)$$

Here  $\tau_A = 4m_t^2/m_A^2$ ,  $m_t$  is the  $\overline{MS}$  top quark mass at scale  $\mu_R$ ,  $m_A$  is the mass of pseudoscalar

particle and the function  $f(\tau_A)$  is given by

$$f(\tau_A) = \begin{cases} \arcsin^2 \frac{1}{\sqrt{\tau_A}} & \tau_A \geq 1, \\ -\frac{1}{4} \left( \ln \frac{1-\sqrt{1-\tau_A}}{1+\sqrt{1-\tau_A}} + i\pi \right)^2 & \tau_A < 1. \end{cases} \quad (2.16)$$

In the above equation,  $G_F$  is the Fermi constant and  $\cot \beta$  is the ratio between vacuum expectation values of the Higgs doublets.

## Perturbative expansion of resummation formula:

Note that the parton densities that appear in Eq. (2.6) are evaluated not at the factorization scale  $\mu_F$  but at  $b_0/b$ . Evolving the parton densities from  $b_0/b$  to  $\mu_F$  in Eq. (2.6) (see Ref. [11]), one can define the partonic resummed cross section  $\mathcal{W}_{ij,N}^F$  through

$$W_N^F(b, M) = \sum_{i,j} \mathcal{W}_{ij,N}^F(b, M, \mu_F) f_{i,N}(\mu_F) f_{j,N}(\mu_F). \quad (2.17)$$

Now we can separate the large logarithms that appear in  $\mathcal{W}_{ij,N}^F$  from the remaining terms. However, we have a freedom in what we choose as the argument of the logarithm. Instead of working (resumming) with  $L = \ln(M^2 b^2/b_0^2)$  we can equally well choose to work with  $L = \ln(Q^2 b^2/b_0^2)$ , where  $Q$  is some arbitrary scale of the order of  $M$ . The difference between these two choices is not a divergent quantity but a finite one. Thus we write  $\mathcal{W}^F$  as

$$\mathcal{W}_{ij,N}^F(b, M, \mu_F) = \hat{\sigma}_{gg}^{F,(0)} \left\{ \mathcal{H}_{gg \leftarrow ij,N}^F(M, Q, \mu_F) + \Sigma_{gg \leftarrow ij,N}^F(L, M, Q, \mu_F) \right\}, \quad (2.18)$$

where  $L = \ln(Q^2 b^2/b_0^2)$  denotes the logarithms that are being resummed in  $\mathcal{W}^F$  and  $Q$  is an arbitrary *resummation scale*. Note that the left hand side of the above equation is independent of the resummation scale  $Q$  and so is the right hand side. However a truncation of the perturbative expansion in the right hand side will introduce a dependence on  $Q$ . This dependence on  $Q$  will be however, of higher order in the strong coupling constant. Note that the dependence on  $b$  — the variable conjugate to  $p_T$  — is contained entirely in the functions  $\Sigma_{c\bar{c} \leftarrow ij}^F$ . Furthermore  $\Sigma_{c\bar{c} \leftarrow ij}^F$  are so defined that they vanish at  $L = 0$ ; for the perturbative expansions up to NNLO refer to Ref. [11]. The hard-collinear function  $\mathcal{H}_{gg \leftarrow ij,N}^F$  depends on the coefficients  $H_g^F$  and  $C_{g_i}$  of Eq. (2.12).

### 2.2.1 Matching the cross section across the large and small $p_T$ regions

The resummed result given in the previous section is valid at small values of transverse momentum where the logarithms of  $p_T$  are summed to all orders, and to emphasize that these results are accurate to a certain logarithmic accuracy such as NLL or NNLL we attach a subscript to the resummed cross section:  $(d\sigma^{F,(\text{res})}/dp_T^2)_{\text{l.a.}}$ . As the IR and collinear radiation does not give any enhancements at the high values of transverse momentum, the fixed order results accurately describe the distribution which we will denote by  $(d\sigma^F/dp_T^2)_{\text{f.o.}}$ . To obtain a prediction valid over the entire  $p_T$  region, which we denote by  $(\frac{d\sigma^F}{dp_T^2})_{\text{f.o.}+1.\text{a.}}$ , we following the additive matching procedure defined below:



$$\left(\frac{d\sigma^F}{dp_T^2}\right)_{\text{f.o.}+\text{l.a.}} = \left(\frac{d\sigma^F}{dp_T^2}\right)_{\text{f.o.}} + \left(\frac{d\sigma^{F,(\text{res})}}{dp_T^2}\right)_{\text{l.a.}} - \left(\frac{d\sigma^{F,(\text{res})}}{dp_T^2}\right)_{\text{l.a.}} \Big|_{\text{f.o.}}. \quad (2.19)$$

Here the first term on the right hand side is the fixed order result which is what is relevant at large values of transverse momentum; the second term provide the resummed result that is valid at low values of the transverse momentum. Clearly, the enhanced effects of soft and collinear radiation is included twice: first in the fixed order result and then in the second term which is the resummed result. The purpose of the third term is to remove this double counting. At low  $p_T$  the divergences in  $p_T$  spectrum arising due to the fixed order result in the first term are subtracted by the last term, which is nothing but the expansion of the resummation formula in  $a_s$  truncated to appropriate order. Even, though this takes care of the double counting at low values of the transverse momentum, the third term has still an undesired effect: it contributes at large values of transverse momentum! At large values of  $p_T$  we can reduce the effect of the last term by making the replacement [11]

$$L \rightarrow \tilde{L} \equiv \ln \left( \frac{Q^2 b^2}{b_0^2} + 1 \right). \quad (2.20)$$

Now as  $p_T \rightarrow \infty$  or equivalently  $b \rightarrow 0$  the argument of the logarithm approaches unity and thus the logarithm vanishes.

## 2.2.2 Resummation coefficients and determination of $H_g^{A,(2)}$

Here we list down the  $A_g^{(1)}$ ,  $B_g^{(1)}$ ,  $A_g^{(2)}$  [135, 137],  $B_g^{(2)}$  [138, 168, 169],  $A_g^{(3)}$  [170] coefficients along with  $C_{gi}$  [138, 168, 169, 171] and  $G_{gi}$  [151] coefficients that enter into the computation. Whenever, a coefficient is scheme dependent we have given it in the Higgs scheme.

$$\begin{aligned} A_g^{(1)} &= 4C_A, \\ A_g^{(2)} &= 8C_A \left[ \left( \frac{67}{18} - \frac{\pi^2}{6} \right) C_A - \frac{5}{9} n_f \right], \\ A_g^{(3)} &= 64C_A \left[ C_A^2 \left( \frac{11\pi^4}{720} - \frac{67\pi^2}{216} + \frac{245}{96} + \frac{11}{24} \zeta_3 \right) + C_A n_f \left( \frac{5\pi^2}{108} - \frac{209}{432} - \frac{7}{12} \zeta_3 \right) \right. \\ &\quad \left. + C_F n_f \left( -\frac{55}{96} + \frac{1}{2} \zeta_3 \right) - \frac{1}{108} n_f^2 + 8\beta_0 \left( C_A \left( \frac{101}{216} - \frac{7}{16} \zeta_3 \right) - \frac{7}{108} n_f \right) \right], \\ B_g^{(1)} &= -\frac{2}{3} (11C_A - 2n_f), \\ B_g^{(2)} &= 16C_A^2 \left( \frac{23}{24} + \frac{11}{18} \pi^2 - \frac{3}{2} \zeta_3 \right) + \frac{1}{2} C_F n_f - C_A n_f \left( \frac{1}{12} + \frac{\pi^2}{9} \right) - \frac{11}{8} C_F C_A, \\ C_{gg}^{(1)} &= [(5 + \pi^2)C_A - 3C_F] \delta(1-z), \\ C_{gq}^{(1)} &= 2C_F z, \\ G_{gg}^{(1)} &= 4C_A \frac{1-z}{z}, \\ G_{gq}^{(1)} &= 4C_F \frac{1-z}{z}, \end{aligned} \quad (2.21)$$

where  $\beta_0 = (11 C_A - 2 n_f)/3$ , with the SU(N) QCD color factors  $C_F = (N^2 - 1)/2N$ ,  $C_A = N$  and  $n_f = 5$  is the number of active quark flavors. The coefficients  $A_g^{(i)}$ ,  $B_g^{(1)}$ ,  $C_{gq}^{(1)}$ ,  $G_{gg}^{(1)}$  and  $G_{gq}^{(1)}$  are scheme independent. The scheme dependent coefficients  $B_g^{(2)}$  and  $C_{gg}^{(1)}$  have been given above in Higgs scheme.

## 2.3 The results: Hard coefficients and matched distributions

In this section we will first calculate the hard coefficients  $H_g^{A,(1)}$  and  $H_g^{A,(2)}$ , then we will describe how we obtain the fixed order  $p_T$  distribution that we need for the matching, and finally obtain the distributions.

### 2.3.1 Evaluation of hard coefficient

The only coefficients that remain to be determined are the first and second order hard coefficients. These can be extracted from the knowledge of form factors up to 2-loop for the pseudo-scalar. The unrenormalised form factors  $\hat{\mathcal{F}}_g^{A,(n)}$  up to 2-loop are given here

$$\mathcal{F}_g^A \equiv \sum_{n=0}^2 \left[ \hat{a}_s^n \left( \frac{-q^2}{\mu^2} \right)^{n \frac{\epsilon}{2}} S_\epsilon^n \hat{\mathcal{F}}_g^{A,(n)} \right]. \quad (2.22)$$

We present the unrenormalised results after factoring out Born term for the choice of the scale  $\mu_R^2 = \mu_F^2 = -q^2$  as follows:

$$\begin{aligned} \hat{\mathcal{F}}_g^{A,(1)} &= C_A \left\{ -\frac{8}{\epsilon^2} + 4 + \zeta_2 + \epsilon \left( -6 - \frac{7}{3} \zeta_3 \right) + \epsilon^2 \left( 7 - \frac{\zeta_2}{2} + \frac{47}{80} \zeta_2^2 \right) \right\}, \\ \hat{\mathcal{F}}_g^{A,(2)} &= C_F n_f \left\{ -\frac{80}{3} + 6 \ln \left( \frac{q^2}{m_t^2} \right) + 8 \zeta_3 \right\} + C_A n_f \left\{ -\frac{8}{3\epsilon^3} + \frac{20}{9\epsilon^2} + \frac{1}{\epsilon} \left( \frac{106}{27} + 2\zeta_2 \right) \right. \\ &\quad \left. - \frac{1591}{81} - \frac{5}{3} \zeta_2 - \frac{74}{9} \zeta_3 \right\} + C_A^2 \left\{ \frac{32}{\epsilon^4} + \frac{44}{3\epsilon^3} + \frac{1}{\epsilon^2} \left( -\frac{422}{9} - 4\zeta_2 \right) + \frac{1}{\epsilon} \left( \frac{890}{27} - 11\zeta_2 \right) \right. \\ &\quad \left. + \frac{50}{3} \zeta_3 \right\} + \frac{3835}{81} + \frac{115}{6} \zeta_2 - \frac{21}{5} \zeta_2^2 + \frac{11}{9} \zeta_3 \left\}. \quad (2.23) \end{aligned}$$

The strong coupling constant  $a_s \equiv a_s(\mu_R^2)$  is renormalised at the mass scale  $\mu_R$  and is related to the unrenormalised one,  $\hat{a}_s \equiv \hat{g}_s^2/16\pi^2$ , through

$$\hat{a}_s S_\epsilon = \left( \frac{\mu^2}{\mu_R^2} \right)^{\epsilon/2} Z_{a_s} a_s, \quad (2.24)$$

with  $S_\epsilon = \exp[(\gamma_E - \ln 4\pi)\epsilon/2]$  and the scale  $\mu$  is introduced to keep the unrenormalised strong coupling constant dimensionless in  $d = 4 + \epsilon$  space-time dimensions. The renormalization constant  $Z_{a_s}$  up to  $\mathcal{O}(a_s^3)$  is given by

$$Z_{a_s} = 1 + a_s \left[ \frac{2}{\epsilon} \beta_0 \right] + a_s^2 \left[ \frac{4}{\epsilon^2} \beta_0^2 + \frac{1}{\epsilon} \beta_1 \right] + a_s^3 \left[ \frac{8}{\epsilon^3} \beta_0^3 + \frac{14}{3\epsilon^2} \beta_0 \beta_1 + \frac{2}{3\epsilon} \beta_2 \right]. \quad (2.25)$$

The coefficients of the QCD  $\beta$  function  $\beta_i$  are given by [172]

$$\begin{aligned}\beta_0 &= \frac{11}{3}C_A - \frac{2}{3}n_f, \\ \beta_1 &= \frac{34}{3}C_A^2 - 2n_f C_F - \frac{10}{3}n_f C_A, \\ \beta_2 &= \frac{2857}{54}C_A^3 - \frac{1415}{54}C_A^2 n_f + \frac{79}{54}C_A n_f^2 + \frac{11}{9}C_F n_f^2 - \frac{205}{18}C_F C_A n_f + C_F^2 n_f,\end{aligned}\quad (2.26)$$

where  $n_f$  is the number of active light quark flavors. The operator renormalization is needed to remove the additional UV divergences and UV finite form factor is given by

$$[\mathcal{F}_g^A]_R = Z_g^A \mathcal{F}_g^A, \quad (2.27)$$

where the operator renormalization constant up to  $\mathcal{O}(a_s^3)$  is given by

$$\begin{aligned}Z_g^A &= 1 + a_s \left[ \frac{22}{3\epsilon} C_A - \frac{4}{3\epsilon} n_f \right] + a_s^2 \left[ \frac{1}{\epsilon^2} \left\{ \frac{484}{9} C_A^2 - \frac{176}{9} C_A n_f + \frac{16}{9} n_f^2 \right\} + \frac{1}{\epsilon} \left\{ \frac{34}{3} C_A^2 \right. \right. \\ &\quad \left. \left. - \frac{10}{3} C_A n_f - 2 C_F n_f \right\} \right] + a_s^3 \left[ \frac{1}{\epsilon^3} \left\{ \frac{10648}{27} C_A^3 - \frac{1936}{9} C_A^2 n_f + \frac{352}{9} C_A n_f^2 - \frac{64}{27} n_f^3 \right\} \right. \\ &\quad \left. + \frac{1}{\epsilon^2} \left\{ \frac{5236}{27} C_A^3 - \frac{2492}{27} C_A^2 n_f - \frac{308}{9} C_A C_F n_f + \frac{280}{27} C_A n_f^2 + \frac{56}{9} C_F n_f^2 \right\} \right. \\ &\quad \left. + \frac{1}{\epsilon} \left\{ \frac{2857}{81} C_A^3 - \frac{1415}{81} C_A^2 n_f - \frac{205}{27} C_A C_F n_f + \frac{2}{3} C_F^2 n_f + \frac{79}{81} C_A n_f^2 + \frac{22}{27} C_F n_f^2 \right\} \right].\end{aligned}\quad (2.28)$$

We can obtain the hard coefficient function by removing infrared singularities from renormalised form factor given in Eq. (2.27) by multiplying the IR subtraction operators [173]. This gives the hard function in what is called hard scheme. We would however use the  $B$  and  $C$  functions in the Higgs scheme. Finally, hard coefficient functions can be calculated in the Higgs scheme by using following relations [159]:

$$\begin{aligned}H_g^{A,(1)} &= H_{g,\text{hard}}^{A,(1)} - H_{g,\text{hard}}^{h,(1)}, \\ H_g^{A,(2)} &= H_{g,\text{hard}}^{A,(2)} - H_{g,\text{hard}}^{h,(2)} + \left( H_{g,\text{hard}}^{h,(1)} \right)^2 - H_{g,\text{hard}}^{A,(1)} H_{g,\text{hard}}^{h,(1)},\end{aligned}\quad (2.29)$$

where the subscript ‘hard’ denotes hard scheme. The first and second order coefficients that appear in the expansion of the hard function when calculated in the Higgs scheme are

$$\begin{aligned}H_g^{A,(1)} &= \frac{3}{2}C_F - \frac{1}{2}C_A, \\ H_g^{A,(2)} &= \frac{1}{12}C_F + \frac{5}{96}C_A + \frac{41}{144}C_A n_f + \left( -\frac{13}{8} + \frac{1}{4} \log \frac{m_A^2}{m_t^2} \right) C_F n_f \\ &\quad + \left( \frac{37}{24} + \frac{11}{8} \log \frac{m_A^2}{m_t^2} \right) C_A C_F + \left( \frac{137}{288} - \frac{7}{8} \log \frac{m_A^2}{m_t^2} \right) C_A^2.\end{aligned}\quad (2.30)$$

### 2.3.2 Fixed order distribution at NNLO

It has been long observed that the inclusive pseudo-scalar Higgs coefficient function can be obtained from the scalar Higgs coefficient at each order of perturbation theory by a simple rescaling (see Eq. 13-16 of [9]) after factoring out the born cross-section. The rescaling is exact at NLO; and at NNLO the correction terms do not contain scales explicitly and are suppressed by partonic  $(1-z)^2$ . The fact that at NLO the rescaling is exact, is already highly non-trivial and is a direct consequence of similarity of the two processes. At NNLO level the difference is only sub-dominant. We use the same scaling factor to obtain the approximate fixed order  $p_T$  spectrum (denoted as NNLO<sub>A</sub>) for pseudo-scalar since both the processes share similar kinematics. The only difference comes from the vertex corrections through virtual loop calculation which only affects the low  $p_T$  spectrum and does not affect the very high  $p_T$  tail. Thus we have obtained the approximate fixed order  $p_T$  distribution for pseudo-scalar Higgs from scalar-Higgs spectrum by multiplying same rescaling factor as in Eq. 13 in Ref. [9]. We find that at NNLO level in the high  $p_T$  tail, only the rescaling coefficient from one lower order contributes to the  $p_T$  spectrum. In particular the contribution comes from  $H_g^{A,(1)}$ . The fixed order distribution obtained this way has been matched to the NNLL resummed spectrum at low  $p_T$  completely within HqT framework. In the next section we describe the detailed phenomenology for the matched  $p_T$  spectrum.

### 2.3.3 Matched distributions

In this subsection we present the phenomenological aspects of the differential distribution that we have obtained using our FORTRAN code, which we created by modifying the publicly available code HqT [10–12]. We studied the distributions for the LHC centre-of-mass energy both at 13 TeV and 14 TeV. Our default choices for different quantities in this study are:

**For 14 TeV centre-of-mass energy,**

1. Pseudo-scalar mass  $m_A = 200$  GeV,
2. Resummation scale  $Q = m_A$ ,
3. MMHT 2014 [174] parton density sets with the corresponding  $\alpha_s$ .

**For 13 TeV centre-of-mass energy,**

1. Pseudo-scalar mass  $m_A = 200$  GeV,
2. Resummation scale  $Q = m_A/2$ ,
3. MMHT 2014 [174] parton density sets with the corresponding  $\alpha_s$ .

In Fig. 2.1 (14 TeV) and Fig. 2.2 (13 TeV) we study the effect of resummation over the fixed order result, where in each figure, the left panel shows the result for NLO and NLO+NLL; the right for NNLO<sub>A</sub> and NNLO<sub>A</sub>+NNLL. For LHC 14TeV we set  $\mu_R = \mu_F = m_A$ ; for LHC 13 TeV we keep  $\mu_R = \mu_F = m_A/2$  and use MMHT2014 PDF sets for both the cases. We observe that the divergent behaviour of the distribution at fixed order is cured upon resummation. Precisely, at NLO the distribution diverges to positive infinity and at NNLO<sub>A</sub> to negative infinity. Upon resummation a regular behaviour is displayed in both the cases.

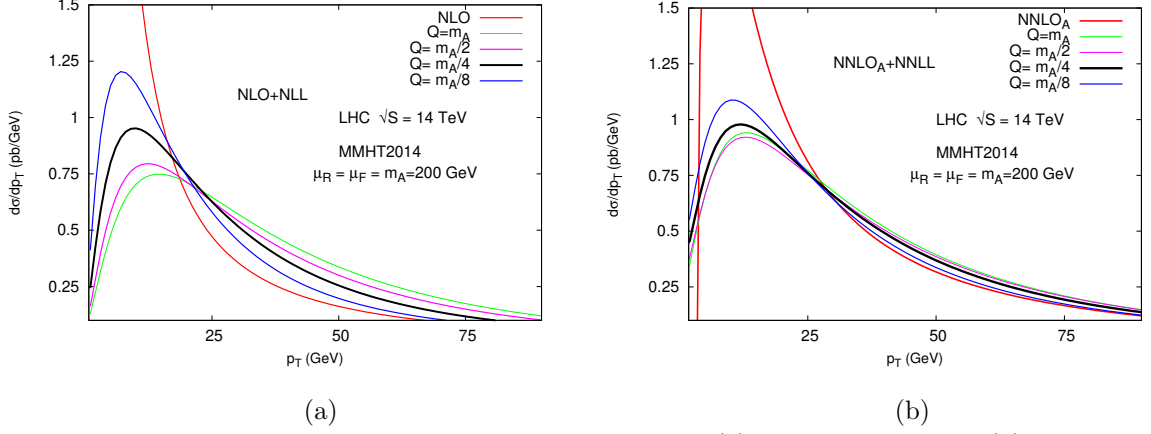


Figure 2.1: Resummation scale variation for (a) NLO+NLL and (b) NNLO<sub>A</sub>+NNLL at 14 TeV

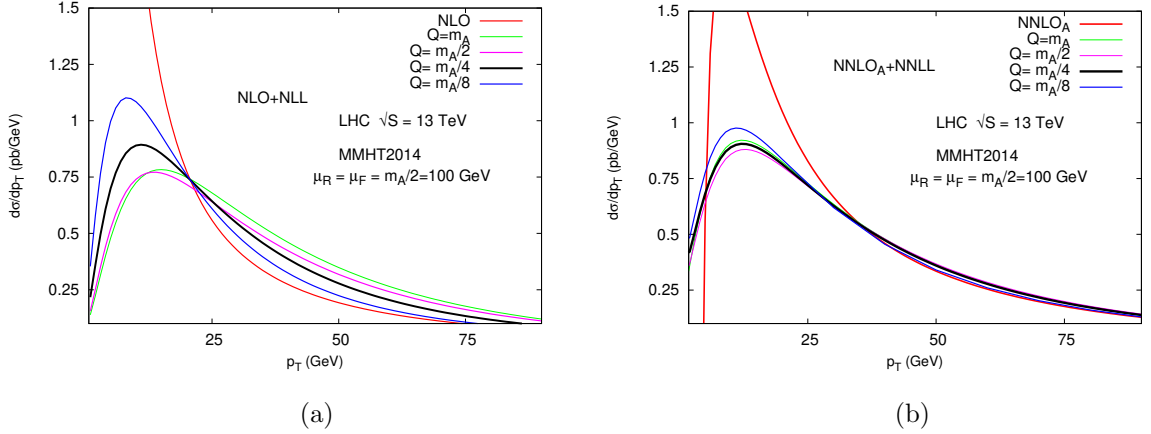


Figure 2.2: Resummation scale variation for (a) NLO+NLL and (b) NNLO<sub>A</sub>+NNLL at 13 TeV

**Uncertainty due to  $Q$ :** in Fig. 2.1 and Fig. 2.2 we also show the sensitivity of the resummed results to the choice of resummation scale  $Q$ , where we have varied  $Q$  from  $m_A$  to  $m_A/8$ . For each diagram, in the left panel we see the results are quite sensitive to the choice, where by sensitivity we mean the range of variation of the maxima of distribution for different choices of  $Q$ . Not surprisingly, upon going to the next logarithmic accuracy (right panel) the sensitivity is significantly reduced around the peak region and the results at moderate values of  $p_T$  are almost insensitive to the choice. It is reassuring that in the right panel at moderate and large values of  $p_T$  the resummed curve is coincident with the fixed order curve, as desired. We note that the position of the peak is unchanged in going to the next order. For  $Q = m_A$  and centre-of-mass energy 14 TeV we see that the peak value changes by 25% in going from NLO+NLL to NNLO<sub>A</sub>+NNLL. Similarly for  $Q = m_A/2$  and centre-of-mass energy 13 TeV, the peak value changes by 11% upon going from NLO+NLL to the next level of accuracy.

**Uncertainty due to  $\mu_R$  and  $\mu_F$ :** in Fig. 2.3(a) and Fig. 2.3(b) we show the sensitivity of our

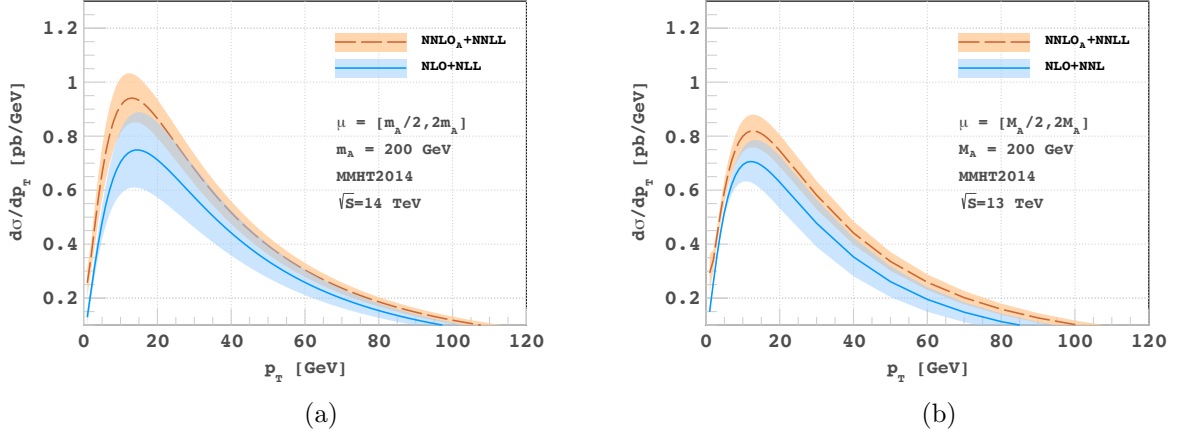


Figure 2.3:  $\mu_R$  and  $\mu_F$  variation at NLO+NLL and NNLO<sub>A</sub>+NNLL for (a) 14 TeV and (b) 13 TeV

results to the variation of  $\mu_R$  and  $\mu_F$ . The bands in this figure have been obtained by varying of  $\mu_R$  and  $\mu_F$  independently in the range  $[m_A/2, 2m_A]$ , while excluding the regions where  $\mu_R/\mu_F > 2$  or  $\mu_R/\mu_F < 1/2$ . More specifically, for 14 TeV centre-of-mass energy we see that at the peak, the variation is about 38% for NLO+NLL which gets reduced to about 19% upon going to the next level of accuracy. Similarly for 13 TeV centre-of-mass energy we see that at the peak the variation is about 22% for NLO+NLL and about 15% for NNLO<sub>A</sub>+NNLL. We have also studied the individual variation of  $\mu_R$  and  $\mu_F$  for both the energies at the LHC in Fig. 2.4 and Fig. 2.5 respectively. In Fig. 2.4 we keep  $\mu_F = m_A$  and vary  $\mu_R$  in the range  $[m_A/2, 2m_A]$ . For 14 TeV centre-of-mass energy we find that at the peak, the variation for NLO+NLL is about 32%, which gets reduced to about 17% at NNLO<sub>A</sub>+NNLL. Similarly for 13 TeV centre-of-mass energy we see that at the peak the variation is about 21% for NLO+NLL and about 13% for NNLO<sub>A</sub>+NNLL. In Fig. 2.5 we set  $\mu_R = m_A$  and vary  $\mu_F$  in the same range as above. For 14 TeV centre-of-mass energy we find that at the peak, the variation for NLO+NLL is about 4%, which gets reduced to about 2% at NNLO<sub>A</sub>+NNLL. Similarly for 13 TeV centre-of-mass energy we see that at the peak the variation is about 4% for NLO+NLL and about 0.5% for NNLO<sub>A</sub>+NNLL.

**Combined uncertainty due to  $Q$ ,  $\mu_R$  and  $\mu_F$ :** in Fig. 2.6(a) and Fig. 2.6(b) we show the sensitivity of our results to the variation of  $Q$ ,  $\mu_R$  and  $\mu_F$ . The bands in this figure show independent variation of  $Q$ ,  $\mu_R$  and  $\mu_F$  in the range  $[m_A/2, 2m_A]$  with constraints  $\mu_R/\mu_F \in [1/2, 2]$ ,  $Q/\mu_R \in [1/2, 2]$  and  $Q/\mu_F \in [1/2, 2]$ . When we take into account all scale variations together we notice that both at 13 TeV and 14 TeV the variation at the peak is 38% for NLO+NLL which gets reduced to 20% upon going to the next level of accuracy. It is to be noted that this amount of decrement is almost same as the case discussed in Fig. 2.3(a).

**Uncertainty due to parton density sets:** as there are several PDF groups in the literature, it is necessary to estimate the uncertainty resulting from the choice of PDFs within each set of a

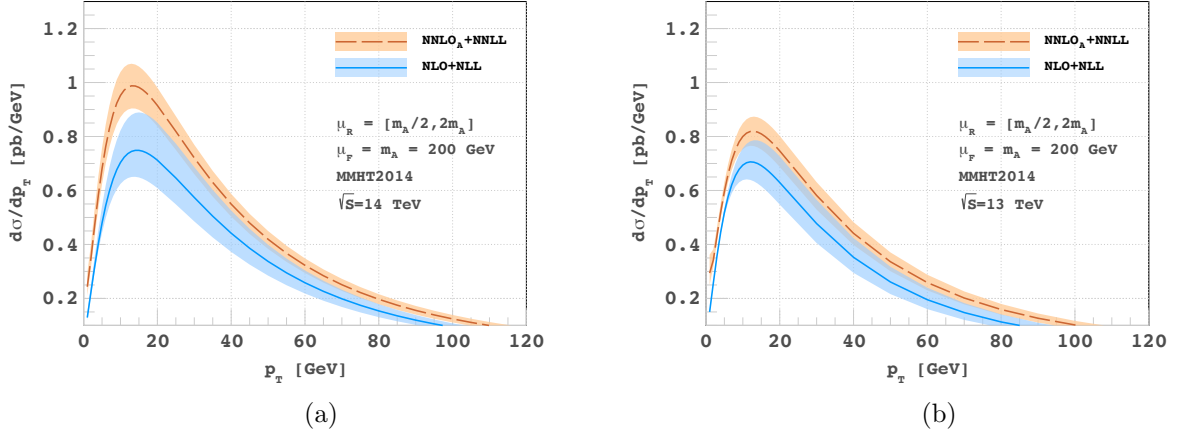


Figure 2.4: Variation of  $\mu_R$  at NLO+NLL and NNLO<sub>A</sub>+NNLL keeping  $\mu_F$  fixed at  $m_A$  for (a) 14 TeV and (b) 13 TeV

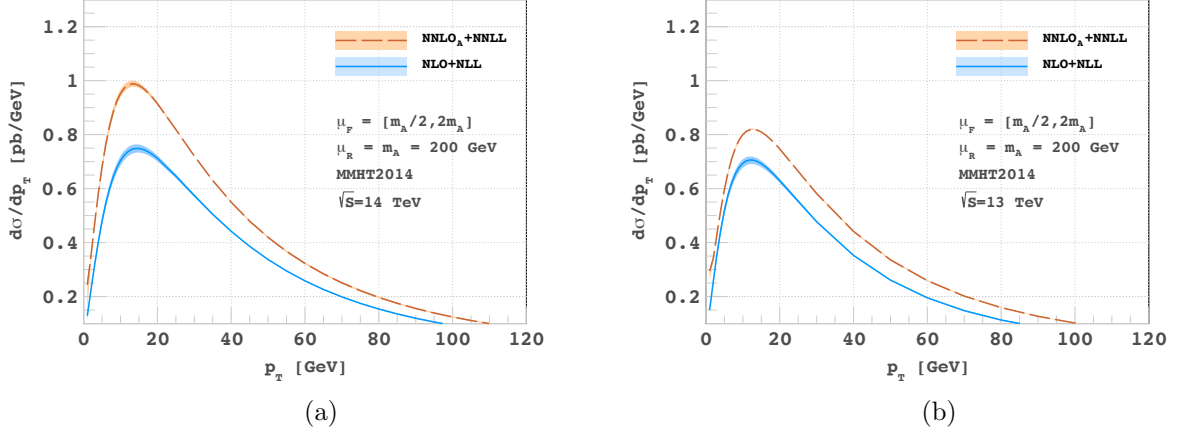


Figure 2.5: Variation of  $\mu_F$  at NLO+NLL and NNLO<sub>A</sub>+NNLL keeping  $\mu_R$  fixed at  $m_A$  for (a) 14 TeV and (b) 13 TeV

given PDF group. Using PDFs from different PDF groups namely MMHT2014 [174], ABMP [175], NNPDF3.1 [176] and PDF4LHC [177] we have obtained the differential  $p_T$  distributions along with the corresponding PDF uncertainty. In Fig. 2.7(a), we have demonstrated the uncertainty bands for various PDF sets as a function of  $p_T$  at energies of 14 TeV. In order to demonstrate the correlation of PDF uncertainty with the  $p_T$  values we have tabulated in Table 2.1, the corresponding results for few benchmark values of  $p_T$  along with percentage uncertainties. We have also performed the same exercise for 13 TeV centre of mass energy, as shown in Fig. 2.7(b). We have tabulated the results for few benchmark values of  $p_T$  along with percentage uncertainties in Table 2.2.

**Pseudo-scalar Higgs mass variation:** in Fig. 2.8(a) and Fig. 2.8(b) we show how the distribution behaves as the mass of the final state is changed. We have kept the renormalization and

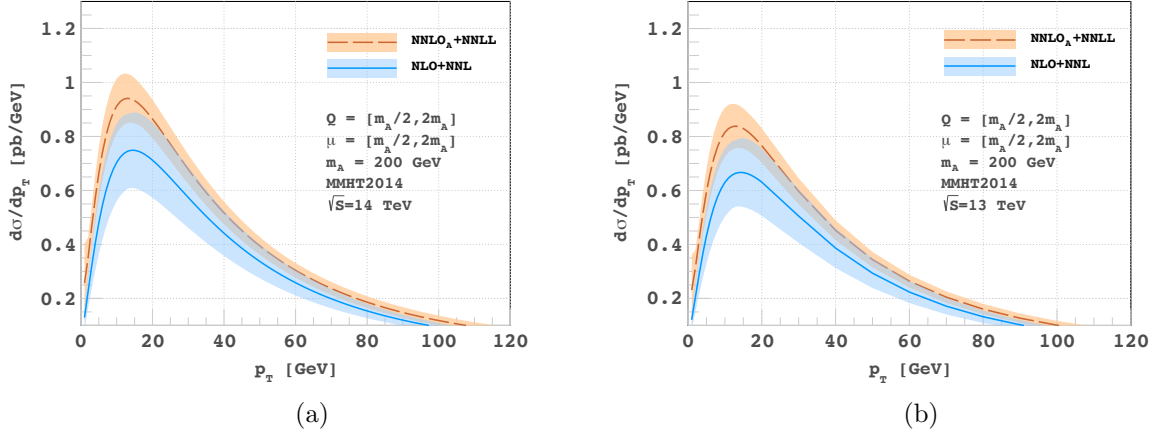


Figure 2.6:  $Q$ ,  $\mu_R$  and  $\mu_F$  variation at NLO+NNL and NNLO<sub>A</sub>+NNLL for (a) 14 TeV and (b) 13 TeV

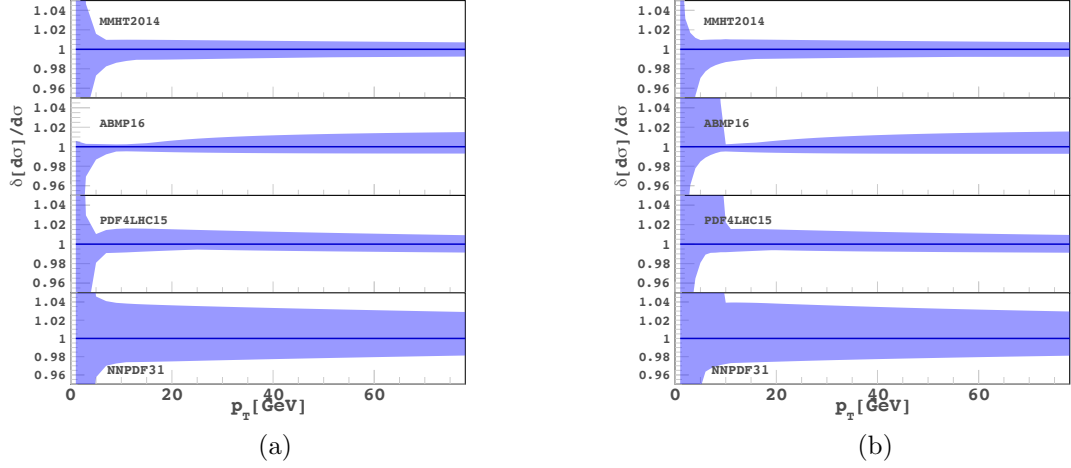


Figure 2.7: PDF variation at NNLO<sub>A</sub>+NNLL for (a) 14 TeV and (b) 13 TeV using various sets. The y-axis represents the ratio of extremum variation over the central PDF set.

factorization scales fixed at 200 GeV for 14 TeV, at 100 GeV for 13 TeV LHC energies and varied  $m_A$  from 100 to 300 GeV. We see that the cross-section decreases with the increase in the mass of the final state.



$q_T$	MMHT	ABMP	NNPDF	PDF4LHC
7.0	$0.802^{+0.97\%}_{-1.75\%}$	$0.828^{+0.26\%}_{-0.78\%}$	$0.821^{+4.09\%}_{-3.00\%}$	$0.804^{+1.45\%}_{-0.91\%}$
13.0	$0.941^{+0.98\%}_{-1.07\%}$	$0.928^{+0.31\%}_{-0.49\%}$	$0.960^{+3.77\%}_{-2.60\%}$	$0.943^{+1.60\%}_{-0.80\%}$
19.0	$0.882^{+0.96\%}_{-1.05\%}$	$0.847^{+0.58\%}_{-0.55\%}$	$0.897^{+3.65\%}_{-2.53\%}$	$0.884^{+1.54\%}_{-0.67\%}$
25.0	$0.772^{+0.94\%}_{-1.01\%}$	$0.729^{+0.83\%}_{-0.60\%}$	$0.783^{+3.55\%}_{-2.45\%}$	$0.774^{+1.46\%}_{-0.56\%}$
31.0	$0.660^{+0.91\%}_{-0.96\%}$	$0.616^{+0.99\%}_{-0.63\%}$	$0.669^{+3.46\%}_{-2.38\%}$	$0.662^{+1.38\%}_{-0.61\%}$

Table 2.1:  $q_T$  distributions at NNLO<sub>A</sub>+NNLL using different PDF sets along with percentage uncertainties for  $q_T = 7.0, 13.0, 19.0, 25.0, 31.0$  for  $\sqrt{s} = 14$  TeV.

$q_T$	MMHT	ABMP	NNPDF	PDF4LHC
7.0	$0.762^{+0.99\%}_{-1.87\%}$	$0.783^{+18.52\%}_{-0.85\%}$	$0.780^{+22.04\%}_{-3.30\%}$	$0.761^{+23.32\%}_{-0.89\%}$
13.0	$0.880^{+1.01\%}_{-1.11\%}$	$0.864^{+0.34\%}_{-0.54\%}$	$0.898^{+3.93\%}_{-2.67\%}$	$0.882^{+1.56\%}_{-0.75\%}$
19.0	$0.820^{+0.98\%}_{-0.97\%}$	$0.783^{+0.57\%}_{-0.61\%}$	$0.834^{+3.84\%}_{-2.56\%}$	$0.822^{+1.51\%}_{-0.62\%}$
26.0	$0.698^{+0.94\%}_{-0.92\%}$	$0.654^{+0.85\%}_{-0.66\%}$	$0.707^{+3.70\%}_{-2.45\%}$	$0.700^{+1.43\%}_{-0.68\%}$
32.0	$0.596^{+0.91\%}_{-0.89\%}$	$0.552^{+0.99\%}_{-0.63\%}$	$0.602^{+3.60\%}_{-2.37\%}$	$0.597^{+1.35\%}_{-0.72\%}$

Table 2.2:  $q_T$  distributions at NNLO<sub>A</sub>+NNLL using different PDF sets along with percentage uncertainties for  $q_T = 7.0, 13.0, 19.0, 26.0, 32.0$  for  $\sqrt{s} = 13$  TeV.

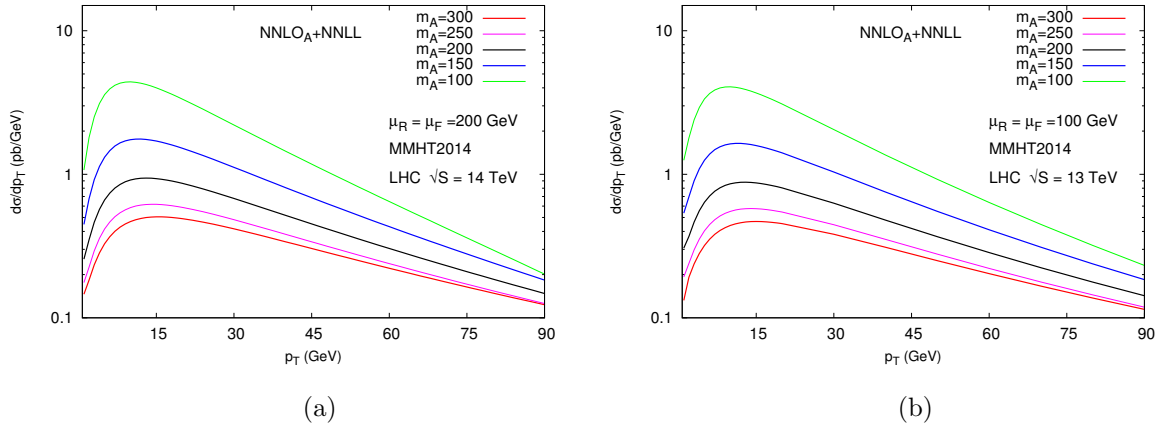


Figure 2.8: Pseudo-scalar Higgs mass variation at NNLO<sub>A</sub>+NNLL for (a) 14 TeV and (b) 13 TeV

## 2.4 Conclusions

In this study we obtained the resummed  $p_T$  distribution for pseudo-scalar Higgs bosons at the LHC for both the centre-of-mass energy 14 TeV and 13 TeV at next-to-next-to-leading logarithmic accuracy by matching the resummed curve with approximated fixed order next-to-next-to-leading

order result. We showed that we achieve a very significant reduction in sensitivity to the choices of resummation, renormalization and factorization scales that are artefact of perturbation theory. We also studied the uncertainty due to different choices of parton density sets. These results provide us with precise estimate for the distribution especially in the region around 15 GeV where the cross-section is large and the fixed order results are completely unreliable due to the breakdown of fixed order perturbation series.

# Chapter 3

## Power corrections to event shapes

### 3.1 Introduction

Infrared-safe event shape variables play a very significant role in understanding the collider data both at the lepton and hadron colliders. Several shape variables have been studied in the literature and among them the most studied variables are the Thrust, C-parameter and Angularity. These shape variables, (one of which, the Thrust was introduced in (1.5.1))

- are essential tools for the precise determination of the strong coupling constant, and
- they are classic testing grounds for both analytical and numerical models of hadronization.

As we saw in (1.5.1) large logarithmic corrections to the distributions of event shape variables arise at fixed orders in perturbation theory, when the shape variable  $e$  takes values corresponding to pencil like configurations. In Eq. (1.78) we see that these large logarithms appear as  $\log(1 - T)/(1 - T)$ , which is divergent in the soft-collinear limit where  $T \rightarrow 1$ . The term  $\log(1 - T)/(1 - T)$  is a leading logarithmic term at the leading power; leading power in  $1 - T$ . In the same Eq. (1.78) we also see that subleading logarithms at leading power ( $\log^0(1 - T)/(1 - T)$ ) are also present.

Not only that owing to their infrared and collinear safety, they can be computed in perturbation theory in QCD, the large logarithmic corrections to the distributions can be resummed to all orders by a variety of methods. At fixed orders, the state of the art is next-to-next-to-leading order (NNLO) accuracy [29–33], while the next to leading log (NLL) resummation has been known for a while [34–37]. In recent years, the NNLL resummation framework has also been developed [13, 38–48].

In this work we will be concerned with analytic estimates of non-perturbative corrections, which are suppressed by powers of  $\Lambda/Q$  (where  $\Lambda$  is the QCD scale and  $Q$  is the center-of-mass energy) with respect to the perturbative result. The basic idea of such analytic estimates goes back to the Operator Product Expansion (OPE), and was first applied to observable that do not admit an OPE in the early papers [178–180]. Very roughly speaking, one notes that a generic (dimensionless) observable in perturbative QCD is a sum of a ‘leading power’ perturbative series plus power corrections, of the general form

$$\sigma\left(\frac{Q}{\mu}, \alpha_s\right) = \sigma_{\text{pert}}\left(\frac{Q}{\mu_f}, \frac{\mu_f}{\mu}, \alpha_s\right) + \sum_n \sigma_n\left(\frac{\mu_f}{\mu}, \alpha_s\right) \left(\frac{\mu_f}{Q}\right)^n, \quad (3.1)$$

where  $\mu_f$  is a perturbative factorization scale, ultimately to be traded for the strong interaction scale  $\Lambda$ . Generically, with a dimensional regulator, different terms in the sum in Eq. (3.1) mix with each other under renormalization. In dimensional regularization, the same effect arises in a subtler fashion: each term in Eq. (3.1) is ambiguous due to the divergence of the corresponding perturbative expansion, which manifests itself via singularities in the Borel plane. These ambiguities are power-suppressed and are compensated by corresponding ambiguities in subsequent terms in the sum in Eq. (3.1). This opens the way for a perturbative estimate of hadronization corrections based on the study of singularities in the Borel plane. Phenomenological studies of event shapes and other basic QCD observables with these tools were first systematically pursued in [181], and subsequently developed in a vast literature, reviewed in [182]. The phenomenological importance of these power-suppressed corrections cannot be understated: for example, they are crucial for a precise determination of the strong coupling [13–17].

In the case of event shape distributions, denoted by  $d\sigma/de$  below, the situation is more subtle. Such distributions peak in the two-jet region, which can be taken to correspond to  $e \rightarrow 0$ , and which is dominated by soft and collinear emissions; in this region, the distributions are typically affected by enhanced power corrections of the form  $(\Lambda/(eQ))^n$ , associated with the emission of soft gluons, as well as corrections scaling as  $(\Lambda^2/(eQ^2))^n$ , associated with hard collinear gluon emission. We will refer to the first of these as ‘soft’ power corrections, and to the second ones as ‘collinear’ power corrections for the sake of brevity. When  $e \sim \Lambda/Q$ , which is typically close to the peak of the distribution at least at LEP energies, all soft power corrections become equally important and need to be resummed in order to get a stable prediction. At even smaller values of  $e$ ,  $e \sim \Lambda^2/Q^2$ , collinear power corrections become relevant as well.

An elegant and efficient method to handle simultaneously large perturbative logarithms (up to NLL accuracy) and power corrections in the two-jet region is Dressed Gluon Exponentiation (DGE) [49], which has already been applied to a variety of event shapes [50–52], as well as to other important QCD observables [53–55]. DGE, aside from consistently including the NLL resummation of Sudakov logarithms, provides a renormalon-based estimate of both soft and collinear power corrections. Collinear power corrections have been shown to enjoy a degree of universality [50, 51, 54] across several inclusive observables. When, however, this universality breaks down, as for example in [52, 183], collinear power corrections can be very cumbersome to compute; furthermore, they only become relevant at extremely small values of the event shape, usually out of experimental range, or in a region where very few data points are available.

These facts suggest that it would be useful to construct a systematic approximation to DGE which would suffice to capture all soft power corrections, while remaining simple to implement in practice. In this chapter, we will introduce such an approximation, which essentially consists in combining DGE with the eikonal approximation for the relevant matrix elements. We call the resulting construction Eikonal Dressed gluon exponentiation or EDGE. The universality and simplicity of soft emission can then be used to express soft power corrections to a large class of event shapes in terms of a very simple integral, which reproduces known results for all event shapes for which soft power corrections are known. This chapter is structured as follows: 3.2 briefly summarizes the essential aspects of DGE, section 3.3 shows how to implement EDGE using energy fractions by taking examples from three very well known event shapes: thrust,  $C$ -parameter and angularities, section 3.4 describes the implementation of EDGE using the transverse momentum and the rapidity, in section

3.5 we present Sudakov exponent and discuss power corrections.

## 3.2 Dressed Gluon Exponentiation

The starting point for DGE is the event shape distribution in the single dressed gluon approximation, which is constructed from the one-loop real emission contribution to the event shape for a gluon with virtuality  $k^2 \neq 0$ . From this, one easily obtains [179] the (renormalon) resummation of quark vacuum polarization corrections which dominates in the large  $N_f$  limit. One can write the result as

$$\frac{1}{\sigma} \frac{d\sigma}{de}(e, Q^2) \Big|_{SDG} = -\frac{C_F}{2\beta_0} \int_0^1 d\xi \frac{d\mathcal{F}(e, \xi)}{d\xi} A(\xi Q^2), \quad (3.2)$$

where  $\beta_0 = \frac{11}{12}C_A - \frac{1}{6}N_f$ ,  $\xi = k^2/Q^2$ , and  $A(\xi Q^2)$  is the large- $\beta_0$  running coupling ( $A = \beta_0\alpha_s/\pi$ ) on the time-like axis. In the  $\overline{\text{MS}}$  scheme, it admits the Borel representation

$$A(\xi Q^2) = \int_0^\infty du (Q^2/\Lambda^2)^{-u} \frac{\sin \pi u}{\pi u} e^{\frac{5}{3}u} \xi^{-u}. \quad (3.3)$$

The cornerstone of Eq. (3.2) is the characteristic function  $\mathcal{F}(e, \xi)$ , which is the one-loop event shape distribution with a non-vanishing gluon virtuality  $k^2$  [181, 184],

$$\mathcal{F}(e, \xi) = \int dx_1 dx_2 \mathcal{M}(x_1, x_2, \xi) \delta(e - \bar{e}(x_1, x_2, \xi)), \quad (3.4)$$

where  $x_i$  are the customary energy fraction variables,  $\mathcal{M}$  is the matrix element for the emission of a gluon with  $k^2 \neq 0$ , and  $\bar{e}$  is the explicit expression of the event shape in terms of the kinematic variables. Interchanging the order of integrations in Eq. (3.2) we can construct a Borel representation as

$$\frac{1}{\sigma} \frac{d\sigma}{de}(e, Q^2) \Big|_{SDG} = \frac{C_F}{2\beta_0} \int_0^\infty du (Q^2/\Lambda^2)^{-u} B(e, u), \quad (3.5)$$

where the Borel function  $B(e, u)$  is defined by

$$B(e, u) = -\frac{\sin \pi u}{\pi u} e^{\frac{5}{3}u} \int_0^\infty d\xi \xi^{-u} \frac{d\mathcal{F}(e, \xi)}{d\xi}. \quad (3.6)$$

The Borel function  $B(e, u)$  has a simple structure in the  $u$  plane, without renormalon singularities. Renormalon poles are however generated when the single dressed gluon distribution is exponentiated via a Laplace transform [49].

The additive property of the event shapes with respect to the multiple gluon emissions together with the factorization of soft and collinear emissions from the *hard* part of the matrix element leads to the exponentiation of the logarithmically enhanced terms in the Laplace space and the resummed cross section is given by [50, 51],

$$\frac{1}{\sigma} \frac{d\sigma(e, Q^2)}{de} = \int_{C-i\infty}^{C+i\infty} \frac{d\nu}{2\pi i} e^{\nu e} \exp[S(\nu, Q^2)], \quad (3.7)$$

where  $C$  lies to the right of the singularities of the integrand. The Sudakov exponent has the form

[185],

$$S(\nu, Q^2) = \int_0^1 de \frac{1}{\sigma} \frac{d\sigma(e, Q^2)}{de} \Big|_{SDG} (e^{-\nu e} - 1). \quad (3.8)$$

The Sudakov region  $e \rightarrow 0$  corresponds to  $\nu \rightarrow \infty$ . Using Eq. (3.5), the Sudakov exponent takes the form

$$S(\nu, Q^2) = \frac{C_F}{2\beta_0} \int_0^\infty du \left( \frac{Q^2}{\Lambda^2} \right)^{-u} B_\nu^e(u), \quad (3.9)$$

where the Borel function in the Laplace space,  $B_\nu^e(u)$ , is defined as

$$B_\nu^e(u) = \int_0^1 de B(e, u) (e^{-\nu e} - 1). \quad (3.10)$$

This exponentiation effectively resums both large Sudakov logarithms and power corrections in the two-jet region.

### 3.3 Borel function using Eikonal Dressed Gluon Exponentiation

In this article we undertake the calculation of the Borel function that was defined in Eq. (3.6) for three very well known event shape variables: (a) the thrust [18–21], (b) the  $C$ -parameter [22–25] and, (c) the angularities [26–28], and we propose a simplified version of the well-established method of Dressed Gluon Exponentiation (DGE), which we call Eikonal DGE (EDGE), which determines all dominant power corrections to event shapes by means of strikingly elementary calculations. We believe our method can be generalized to hadronic event shapes and jet shapes of relevance for LHC physics. There are two aspects to this simplification. First, as we will see in the later parts of this article, we only need to work with the squared matrix element in the eikonal limit. Second, and more importantly, the event shape definitions can be simplified (*eikonalized*) to significantly simplify the computations, however, still capturing the dominant power corrections. The definition of thrust is simple enough and does not require any *eikonalization*, however we will introduce the *eikonalized* versions of  $C$ -parameter and angularities for the computation of their respective Borel functions.

As discussed above we need to construct the characteristic function  $\mathcal{F}(e, \xi)$  for these three event shape variables for the order  $\alpha_s$  process  $\gamma^* \rightarrow q\bar{q}g$ . The color stripped squared matrix element after removing the coupling is

$$\mathcal{M}(x_1, x_2, \xi) = \frac{(x_1 + \xi)^2 + (x_2 + \xi)^2}{(1 - x_1)(1 - x_2)} - \frac{\xi}{(1 - x_1)^2} - \frac{\xi}{(1 - x_2)^2}, \quad (3.11)$$

where the energy fractions are defined by

$$x_1 = \frac{2p_1 \cdot Q}{Q^2}, \quad x_2 = \frac{2p_2 \cdot Q}{Q^2}, \quad x_3 = \frac{2k \cdot Q}{Q^2}. \quad (3.12)$$

Here  $k$  denotes the momentum of the off-shell gluon and,  $p_1$  and  $p_2$  are the momenta of the quark and

anti-quark respectively. Momentum conservation  $Q = p_1 + p_2 + k$  gives the constraint  $x_1 + x_2 + x_3 = 2$ . Figure (3.1) gives the Dalitz plot for this processes. In the soft gluon limit we approximate the squared matrix element to,

$$\mathcal{M}_{\text{soft}}(x_1, x_2, \xi) = \frac{2}{(1-x_1)(1-x_2)}. \quad (3.13)$$

Note that this is the same as what we would write in the soft gluon limit for the case of massless gluon.

Next we will take the mentioned three shape variables in turn and construct eikonalized versions of them and then compute the corresponding characteristic functions, and their Borel functions.

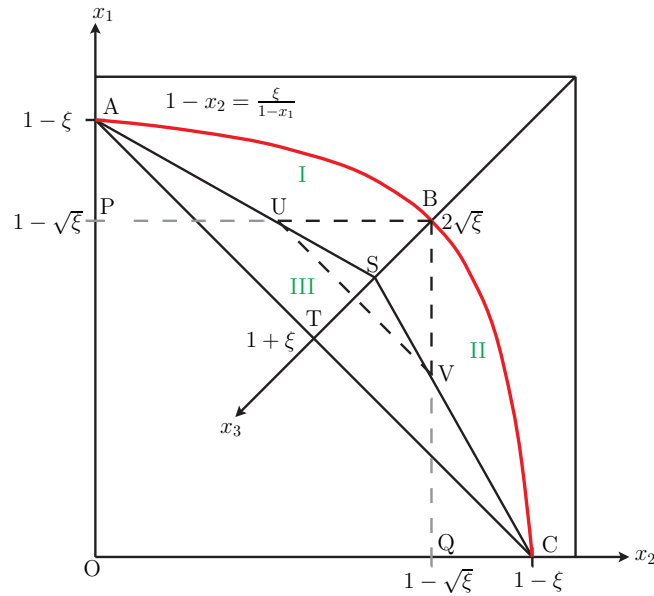


Figure 3.1: Dalitz plot showing phase space for  $\gamma \rightarrow q\bar{q}g$  with off-shell gluon. The energy momentum conservation condition  $x_1 + x_2 + x_3 = 2$  is satisfied throughout this  $x_1 - x_2$  plane and the actual length along  $x_3$  axis is  $\sqrt{2}$  times the measured length. The collinear limit (when the gluon is collinear to the quark) corresponds to  $x_1 = 1 - \xi$ ,  $x_2 = 0$ , while the soft limit (when the gluon is soft to the quark) corresponds to  $x_1 = x_2 = 1 - \sqrt{\xi}$ . The soft boundary of the phase space  $1 - x_2 = \xi/(1 - x_1)$  is denoted by the red curve.

### 3.3.1 Thrust

Thrust is one of the most studied event shapes and it has a historical connection with the determination of strong coupling constant  $\alpha_s$ . It is defined as [20]

$$T = \text{Max}_{\mathbf{n}} \frac{\sum_i |\mathbf{p}_i \cdot \mathbf{n}|}{\sum_i E_i}, \quad (3.14)$$

where  $\mathbf{p}_i$  denotes the 3-momentum of the  $i$ -th particle in the final state and  $\mathbf{n}$  is a unit vector. In order to determine the range of  $T$ , we need to consider two extreme cases: a most spherical configuration and a pencil like configuration. For a spherical configuration,  $T$  attains a minimum

value  $1/2$  and for a pencil like configuration,  $T$  attains a maximum value 1. Thus, thrust varies in the range  $1/2 \leq T \leq 1$ . For a three particles final state, the numerator in Eq. (3.14) is maximum when  $\mathbf{n}$  is along the direction of the largest  $\mathbf{p}_i$ . Thus, the thrust for all massless particles final state is given by

$$T = \text{Max}\{x_1, x_2, x_3\}. \quad (3.15)$$

In presence of a massive off-shell gluon in the final state, the definition of thrust needs some simple modifications which was first given in [186] and has the form,

$$T = \text{Max}\left\{x_1, x_2, \sqrt{x_3^2 - 4\xi}\right\}. \quad (3.16)$$

Substituting in the definition Eq. (3.4) of the characteristic function, the squared matrix element Eq. (3.13) and the definition of thrust Eq. (3.16), we obtain

$$\mathcal{F}(T, \xi) = \int \int dx_1 dx_2 \frac{2}{(1-x_1)(1-x_2)} \delta\left(T - \text{Max}\left\{x_1, x_2, \sqrt{x_3^2 - 4\xi}\right\}\right). \quad (3.17)$$

When the radiated (dressed) gluon is soft, this integral receives contributions from the regions I and II as shown in Figure (3.1). Region I contributes when  $x_1$  is the largest, and region II contributes when  $x_2$  is the largest of  $x_1, x_2, \sqrt{x_3^2 - 4\xi}$ . Naming these contributions as  $\mathcal{F}_1(T, \xi)$  and  $\mathcal{F}_2(T, \xi)$  respectively, we have

$$\mathcal{F}(T, \xi) \simeq \mathcal{F}_1(T, \xi) + \mathcal{F}_2(T, \xi), \quad (3.18)$$

where

$$\begin{aligned} \mathcal{F}_1(T, \xi) &= \int_{2-T-\sqrt{T^2+4\xi}}^{\frac{1-\xi-T}{1-T}} dx_2 \mathcal{M}(T, x_2, \xi) \\ \mathcal{F}_2(T, \xi) &= \int_{2-T-\sqrt{T^2+4\xi}}^{\frac{1-\xi-T}{1-T}} dx_1 \mathcal{M}(x_1, T, \xi), \end{aligned} \quad (3.19)$$

Note that the integrals  $\mathcal{F}_1$  and  $\mathcal{F}_2$  are same due to the symmetry of  $\mathcal{M}(x_1, x_2, \xi)$  under interchange of  $x_1$  and  $x_2$ . The limits of the integration are determined by the boundary of the phase space shown in red in the Figure (3.1). The characteristic function immediately evaluates to

$$\mathcal{F}(t, \xi) = -\frac{4}{t} \log\left(\frac{\xi}{t(q-t)}\right), \quad (3.20)$$

where  $t \equiv 1 - T$  and  $q = \sqrt{T^2 + 4\xi}$ . Now, using Eqs. (3.6) and (3.20) the Borel function for the thrust takes the form,

$$B(t, u) = \frac{4 \sin \pi u}{\pi u} \frac{1}{t} e^{\frac{5u}{3}} \int_{t^2}^t \xi^{-u-1} d\xi, \quad (3.21)$$



where the lower limit is determined using the collinear gluon boundary conditions,  $x_1 = 1 - \xi$ ,  $x_2 = 0$  and the upper limit is determined from the soft gluon boundary condition  $x_1 = x_2 = 1 - \sqrt{\xi}$ . Evaluating the integral we immediately obtain

$$B(t, u) = \frac{\sin \pi u}{\pi u} e^{\frac{5u}{3}} \frac{4}{u} \frac{1}{t} \left( \frac{1}{t^{2u}} - \frac{1}{t^u} \right), \quad (3.22)$$

this agrees with the leading singular terms of the same function presented in [185]. Thus, it is possible to calculate the leading singular terms in  $\mathcal{F}(t, \xi)$  and  $B(t, u)$  using the eikonal matrix element.

### 3.3.2 $C$ -parameter

The  $C$ -parameter was originally defined in [22, 25] using the eigenvalues of the matrix

$$\theta_{\alpha\beta} = \frac{1}{\sum_j |\mathbf{p}^{(j)}|} \sum_i \frac{\mathbf{p}_\alpha^{(i)} \mathbf{p}_\beta^{(i)}}{|\mathbf{p}^{(i)}|}, \quad (3.23)$$

where  $\mathbf{p}_\alpha^{(i)}$  are the spatial component of the momentum of  $i$ -th particle. If the eigenvalues of the above matrix are denoted by  $\lambda_1$ ,  $\lambda_2$  and  $\lambda_3$ , then the  $C$ -parameter is given by

$$C = 3(\lambda_1 \lambda_2 + \lambda_2 \lambda_3 + \lambda_1 \lambda_3). \quad (3.24)$$

This can be cast into a Lorentz invariant form

$$C = 3 - \frac{3}{2} \sum_{i,j} \frac{(p^{(i)} \cdot p^{(j)})^2}{(p^{(i)} \cdot q)(p^{(j)} \cdot q)}, \quad (3.25)$$

where  $p^{(i)}$  denotes the four momentum of the  $i$ -th particle and  $q$  denotes the total four-momentum.  $C$  takes a minimum value 0 for a two-jet event and  $C$  attains a maximum value 1 for a spherical event. If, however, the final state has a planar configuration the largest value that the parameter can attain is  $3/4$ . This upper limit also applies for the case of 3-body final state that concerns us. The above expression of the  $C$ -parameter and its rescaled version can be written down using the energy fractions and the virtuality of the off-shell gluon.

$$c = \frac{C}{6} = \frac{(1-x_1)(1-x_2)(x_1+x_2-1+2\xi) - \xi^2}{x_1 x_2 (2-x_1-x_2)}. \quad (3.26)$$

Now, we define the eikonalized version of the  $c$ -parameter

$$c_{eik}(x_1, x_2) = \frac{(1-x_1)(1-x_2)}{(1-x_1) + (1-x_2)}, \quad (3.27)$$

which coincides with the above definition in the soft gluon limit. Note that  $c_{eik}$  is not a function of the virtuality  $\xi$ . We will use  $c_{eik}$  to calculate the characteristic function for  $C$ -parameter; it is convenient to change variables from  $x_1$  and  $x_2$  into  $y = 2 - x_1 - x_2$  and  $z = (1 - x_2)/y$ . In these new variables  $c_{eik}(y, z) = yz(1 - z)$ . The characteristic function (Eq. (3.4)) in this limit takes the

form,

$$\mathcal{F} = \int dy dz y \mathcal{M}_{\text{soft}}(y, z, \xi) \delta(c_{\text{eik}}(y, z) - c), \quad (3.28)$$

where,

$$\mathcal{M}_{\text{soft}}(y, z, \xi) = \frac{2}{y^2 z(1-z)} \quad (3.29)$$

The symmetry of  $\mathcal{M}$  under  $x_1 \leftrightarrow x_2$  appears as symmetry under  $z \rightarrow 1-z$ . In order to perform the integral in Eq. (3.28), it is required to determine the limits of the  $z$ -integration using the boundary of the soft region that is given by  $x_2 = (1 - \xi - x_1)/(1 - x_1)$ . The integral in Eq. (3.28) has an explicit form,

$$\mathcal{F} = \int_{2\sqrt{\xi}}^{1+\xi} dy \int_{\frac{1}{2}-\frac{1}{2}\sqrt{1-4\xi/y^2}}^{\frac{1}{2}+\frac{1}{2}\sqrt{1-4\xi/y^2}} dz \frac{2}{yz(1-z)} \frac{1}{y\sqrt{1-4c/y}} \left( \delta(z-z_1) + \delta(z-z_2) \right), \quad (3.30)$$

where

$$z_1 = \frac{1}{2} + \frac{1}{2}\sqrt{1-4c/y} \quad \text{and} \quad z_2 = \frac{1}{2} - \frac{1}{2}\sqrt{1-4c/y}. \quad (3.31)$$

This integral has a symmetry under  $z \leftrightarrow (1-z)$  interchange, therefore the integral over  $z$  equals twice the integral between  $z = 1/2$  and the upper limit in Eq. (3.30), where only the  $\delta(z-z_1)$  is relevant. The condition  $z \leq \frac{1}{2} + \frac{1}{2}\sqrt{1-4\xi/y^2}$  implies that  $y \geq \xi/c$ . With this the integral in Eq. (3.30) takes the form

$$\mathcal{F} = \frac{4}{c} \int_{\xi/c}^{1+\xi} dy \frac{1}{y\sqrt{1-4c/y}}. \quad (3.32)$$

Evidently, it is only the lower limit of the integration that gives rise to singular contribution in the  $\xi \rightarrow 0$  limit. As we are only interested in the derivative of  $\mathcal{F}$ , we get, without even evaluating the integral

$$\frac{d\mathcal{F}}{d\xi} = -\frac{4}{c\xi} \frac{\sqrt{\xi}}{\sqrt{\xi-4c^2}}. \quad (3.33)$$

Contrast this to the computation of  $d\mathcal{F}/d\xi$  presented in [51] where the computation proceeds with the full definition of the  $c$ -parameter. In that paper the authors had to deal with the complicated elliptic integrals and had to carefully consider small  $c$  and small  $\xi$  limits. These complications are completely absent in our method.

Now we are in the position to compute the Borel function  $B(c, u)$  for the  $c$ -parameter. We have to substitute  $d\mathcal{F}/d\xi$  into Eq. (3.5),

$$B(c, u) = \frac{4 \sin \pi u}{\pi u} \frac{1}{c} e^{\frac{5u}{3}} \int_{4c^2}^{1-\frac{c}{c}} d\xi \frac{\xi^{-u}}{\sqrt{\xi(\xi-4c^2)}} \quad (3.34)$$

where the lower limit in the above integral is determined using  $x_1 = x_2 = 1 - \sqrt{\xi}$  (soft limit), and the upper limit is determined using  $x_1 = 1 - \xi$ ,  $x_2 = 0$  (collinear limit). We are interested

in the logarithmically enhanced terms, thus we can replace the upper limit of the integration by  $c/(1-c) \approx c$ . Carrying out the integral yields the Borel function

$$B(c, u) = 4 \frac{\sin \pi u}{\pi u} e^{\frac{5u}{3}} \frac{1}{c} \left[ \frac{1}{(2c)^{2u}} \frac{\sqrt{\pi} \Gamma(u)}{\Gamma(u + \frac{1}{2})} - \frac{1}{uc^u} \right]. \quad (3.35)$$

Our result agrees with the soft contribution of the same function presented in [51]. We conclude thus, that the leading singular terms in  $\mathcal{F}(c, \xi)$  and  $B(c, \xi)$  can be captured with significant ease if we use the eikonal version  $c_{eik}$  that we have introduced for the  $c$ -parameter.

### 3.3.3 Angularities

As a demonstration of the wide applicability of our method we consider one more event shape variable – the angularities. Angularities are novel observables that allow us to transform between recoil-insensitive to recoil-sensitive observables in a continuous manner. Angularities were first introduced almost twenty years ago in [26–28] and they were defined as

$$\tau_a = \frac{1}{Q} \sum_i E_i (\sin \theta_i)^a (1 - |\cos \theta_i|)^{1-a}, \quad (3.36)$$

where  $\theta_i$  is the angle made by  $i$ -th particle with the thrust axis,  $E_i$  is the energy of the particle  $i$  and  $a$  is a continuous parameter. The thrust axis is defined as the axis with respect to which Eq. (3.36) is minimized at  $a = 0$ . One can easily realize that angularities with  $a = 0$  corresponds to  $1 - T$ , where  $T$  is the thrust, while  $a = 1$  refers to jet broadening [187]. The continuous parameter  $a$  has a range  $-\infty < a < 2$ , where the upper limit on  $a$  is fixed by infrared safety. In terms of  $x_i$  and  $\xi$  angularities were defined in [52] as,

$$\begin{aligned} \tau_a(x_1, x_2, \xi) = & \frac{1}{x_1} (1 - x_1)^{1-a/2} \left[ (1 - x_2 - \xi)^{1-a/2} (x_1 + x_2 - 1 + \xi)^{a/2} \right. \\ & \left. + (1 - x_2 - \xi)^{a/2} (x_1 + x_2 - 1 + \xi)^{1-a/2} \right], \end{aligned} \quad (3.37)$$

where, thrust axis is considered along  $\mathbf{p}_1$  (quark momentum). As we did for the  $c$ -parameter we introduce an eikonal version of the angularities:

$$\tau_a^{eik}(x_1, x_2, \xi) = (1 - x_1)^{1-a/2} (1 - x_2)^{a/2}. \quad (3.38)$$

Now, Using Eq. (3.4) and (3.13) the characteristics function takes the form,

$$\mathcal{F} = \int dx_1 dx_2 \frac{2}{(1 - x_1)(1 - x_2)} \delta(\tau_a^{eik}(x_1, x_2, \xi) - \tau_a). \quad (3.39)$$

It is straight-forward to perform the  $x_1$  integration to obtain

$$\mathcal{F} = \frac{4}{\tau_a(1 - \frac{a}{2})} \int dx_2 \frac{1}{1 - x_2}. \quad (3.40)$$

We determine the upper limit of this integration using the soft boundary  $1 - x_2 = \xi/(1 - x_1)$ . As shown in [52], the lower limit of this integration does not contribute to the logarithmically enhanced

terms. The upper limit of the integration is

$$1 - \left( \frac{\xi^{1-\frac{a}{2}}}{\tau_a} \right)^{\frac{1}{1-a}}.$$

We finally have the characteristics function

$$\mathcal{F}(\tau_a, \xi) = -\frac{4}{\tau_a} \frac{1}{1-a} \log \xi. \quad (3.41)$$

Taking the derivative with respect to  $\xi$  and substituting in Eq. (3.6) we get the Borel function

$$B(\tau_a, u) = \frac{4 \sin \pi u}{\pi u} \frac{1}{1-a} \frac{1}{\tau_a} e^{\frac{5u}{3}} \int_{\tau_a^2}^{\tau_a^{\frac{2}{2-a}}} d\xi \xi^{-u-1}, \quad (3.42)$$

where the limits are determined using the collinear and soft gluon boundary conditions mentioned in Figure (3.1). Upon performing the integration in Eq. (3.42) we obtain

$$B(\tau_a, u) = \frac{\sin \pi u}{\pi u} e^{\frac{5}{3}u} \frac{4}{1-a} \frac{1}{\tau_a} \left[ \frac{1}{\tau_a^{2u}} - \frac{1}{\tau_a^{\frac{2u}{2-a}}} \right], \quad (3.43)$$

which agrees with the soft contribution of the same function presented in [52]. We have, thus obtained, the leading singular terms in  $\mathcal{F}(\tau_a, \xi)$  and  $B(\tau_a, \xi)$ , which are responsible for power corrections by considering the eikonal matrix element and the eikonal version of the angularities  $\tau_a^{eik}(x_1, x_2, \xi)$  which again substantially simplifies the computation.

### 3.4 Borel function using Eikonal Dressed Gluon Exponentiation in the light-cone variables

In this section, we will follow the same steps of Sec. (3.3) and calculate Borel function for thrust,  $C$ -parameter and angularities using a different set of kinematic variables. Instead of the energy fractions that we used in the previous section we would employ the transverse momentum  $k_\perp$  and rapidity  $y$  of the massive eikonal gluon. In the soft gluon approximation, a number of event shapes for massless particles were defined in [188, 189]. We will consider a class of event shapes which, for massive soft gluon emission, can be written as

$$\bar{e}(k, Q) = \sqrt{\frac{k_\perp^2 + k^2}{Q^2}} h_e(y), \quad (3.44)$$

where  $k_\perp$  and  $y$  denote transverse momentum of the gluon and pseudo-rapidity measured with respect to the thrust axis respectively. The function  $h_e(y)$  characterizes the given event shape. Some of the approximations described below apply to more general event shapes as well, but the results are especially simple for those which can be cast in the form of Eq. (3.44).

The contribution from the emission of a soft off-shell gluon can easily be computed applying the eikonal approximation to the vertex for the emission from the hard parton. Since off-shell soft-gluon phase space factorizes [49] from the hard partons, and also the matrix element factorizes, the soft

cross section takes on a simple and universal form,

$$\frac{d\sigma}{\sigma} = \frac{1}{3} \frac{4}{k^2 + k_{\perp}^2} dk_{\perp}^2 dy. \quad (3.45)$$

The characteristic function is also then given, in the soft limit, by a simple and universal expression

$$\mathcal{F}(e, \xi) = \int dk_{\perp}^2 dy \frac{2}{k^2 + k_{\perp}^2} \delta(e - \bar{e}(k^2, k_{\perp}^2, y)), \quad (3.46)$$

which integrates to the remarkably simple form,

$$\mathcal{F}(e, \xi) = \frac{8}{e} \int_{y_{\min}} dy \quad (3.47)$$

where the only information on the chosen observable is the phase space boundary given by the minimum rapidity  $y_{\min}$ . The upper limit of integration is not relevant, since it does not give any singular contributions in the  $\xi \rightarrow 0$  limit, which is the only significant limit for power corrections.

Up to now, we have kept the discussion generic, for any shape belonging to the class given in Eq. (3.44). Let us now illustrate the results by looking at some specific examples.

### 3.4.1 Thrust

The thrust for a generic process is defined in Eq. (3.15). In the two jet events all event shape variables that we consider tends to 0, except thrust which tends to 1. Thus, it is convenient to define  $t = 1 - T$ . In the soft gluon approximation, thrust in terms of the  $k_{\perp}$  and rapidity  $y$  is given by [188]

$$t = \frac{1}{Q} \sqrt{k_{\perp}^2 + k^2} e^{-|y|}. \quad (3.48)$$

Note that, for our case the gluon is massive and  $k^2 \neq 0$ . In order to perform the integral in Eq. (3.47), we need to determine the lower limit of the rapidity. The lower limit of rapidity  $y$  is determined by putting  $k_{\perp} = 0$  in Eq. (3.48), thus minimum rapidity is given by,

$$y_{\min} = \ln\left(\frac{1}{t} \sqrt{\xi}\right). \quad (3.49)$$

Now, using Eq. (3.47) and (3.49) the characteristics function has the form,

$$\mathcal{F} = -\frac{8}{t} \log\left(\frac{\sqrt{\xi}}{t}\right). \quad (3.50)$$

The Borel function  $B(t, u)$  is then given by

$$B(t, u) = \frac{\sin \pi u}{\pi u} e^{\frac{5}{3}u} \frac{4}{u} \frac{1}{t} \left[ \frac{1}{t^{2u}} - \frac{1}{t^u} \right], \quad (3.51)$$

which is in well agreement with the soft approximated version of the characteristics function and Borel function presented in [185].

### 3.4.2 $C$ -parameter

The  $C$ -parameter for a generic process is defined in Eq. (3.3.2). The  $C$ -parameter in the soft approximation and expressed using  $k_\perp$  and  $y$  is given by [188]

$$c = \frac{C}{6} = \frac{1}{2Q} \sqrt{k^2 + k_\perp^2} \frac{1}{\cosh y}. \quad (3.52)$$

As for the case of thrust we determine the lower limit of rapidity by putting  $k_\perp = 0$  and obtain

$$y_{\min} = \cosh^{-1} \left( \sqrt{\xi}/(2c) \right). \quad (3.53)$$

Now, substituting  $y_{\min}$  in Eq. (3.47) we obtain the characteristic function in the soft gluon limit:

$$\mathcal{F} = -\frac{8}{c} \cosh^{-1} \left( \frac{\sqrt{\xi}}{2c} \right). \quad (3.54)$$

This yields the Borel function

$$B(c, u) = 4 \frac{\sin \pi u}{\pi u} e^{5u/3} \frac{1}{c} \left[ \frac{1}{(2c)^{2u}} \frac{\sqrt{\pi} \Gamma(u)}{\Gamma(u + \frac{1}{2})} - \frac{1}{uc^u} \right], \quad (3.55)$$

in full agreement with the soft contribution to the same function in [51]. Notice that, while collinear effects present in [51] are not properly reproduced, as expected, the cancellation of the pole at  $u = 0$ , which is a consequence of the IR safety of the event shape, is preserved.

### 3.4.3 Angularities

In the soft gluon limit, angularities takes the form [188, 189],

$$\tau_a = \frac{1}{Q} \sqrt{k^2 + k_\perp^2} e^{-|y|(1-a)}, \quad (3.56)$$

and the minimum rapidity is given by

$$y_{\min} = \frac{1}{1-a} \ln \left( \frac{1}{\tau_a} \sqrt{\xi} \right). \quad (3.57)$$

Now, using Eq. (3.47), one easily finds

$$\frac{d\mathcal{F}(\tau_a, \xi)}{d\xi} = -\frac{1}{1-a} \frac{4}{\tau_a \xi}. \quad (3.58)$$

The Borel function  $B(\tau_a, u)$  is then given by

$$B(\tau_a, u) = \frac{\sin \pi u}{\pi u} e^{\frac{5}{3}u} \frac{4}{1-a} \frac{1}{u} \frac{1}{\tau_a} \left[ \frac{1}{\tau_a^{2u}} - \frac{1}{\tau_a^{\frac{2u}{2-a}}} \right], \quad (3.59)$$

again in agreement with the soft contribution to the results of [52], and reproducing, in the limit  $a \rightarrow 0$ , the results for thrust of Ref. [50].

### 3.5 The Sudakov exponent

In this section, we will describe the computation of Sudakov exponent for thrust. Similar conclusions hold true for the other two shape variables as well that we have considered in this article. We can calculate the Borel function in the Laplace space  $B_\nu^t(u)$  in the eikonal limit using  $B(t, u)$  that we wrote above in Eq. (3.22), we obtain,

$$B_\nu^{t,\text{eik}}(u) = \frac{4 \sin \pi u}{\pi u} e^{\frac{5u}{3}} \frac{1}{u} \left[ \left( \nu^{2u} \gamma(-2u, \nu) + \frac{1}{2u} \right) - \left( \nu^u \gamma(-u, \nu) + \frac{1}{u} \right) \right], \quad (3.60)$$

where, we have used

$$\int_0^1 \frac{dt}{t} e^{u \log \frac{1}{t}} (e^{-\nu t} - 1) = \nu^u \gamma(-u, \nu) + \frac{1}{u}, \quad (3.61)$$

and  $\gamma(-u, \nu) = \Gamma(-u) - \Gamma(-u, \nu)$ . In the Sudakov region ( $\nu \rightarrow \infty$ ), we can replace  $\gamma(-u, \nu)$  by  $\Gamma(-u, \nu)$ . Retaining only the logarithmically enhanced terms (powers of  $\log \nu$ ), in the small  $u$  limit  $B_\nu^t(u)$  takes the form,

$$B_\nu^{t,\text{eik}}(u) = 2 e^{\frac{5}{3}u} \frac{\sin \pi u}{\pi u} \left[ \Gamma(-2u) \left( \nu^{2u} - 1 \right) \frac{2}{u} - \Gamma(-u) \left( \nu^u - 1 \right) \frac{2}{u} \right]. \quad (3.62)$$

The first term inside the square brackets corresponds to large-angle soft gluon emissions and the second term to collinear gluon emissions. Note that this expression is free from any  $u = 0$  singularities. There are two sources of the poles in this expression:  $\Gamma(-2u)$  has poles for all positive integers and half-integers, and  $\Gamma(-u)$  has poles for all positive integers. However, the pre-factor  $\sin \pi u$  regulates the poles at the integer values of  $u$ . Thus,  $B_\nu^{t,\text{eik}}$  has renormalon poles only at half-integer values of  $u$ .

We will now compare our result with the full result for  $B_\nu^t$  presented in [51, 185] which is given by,

$$B_\nu^t(u) = 2 e^{\frac{5}{3}u} \frac{\sin \pi u}{\pi u} \left[ \Gamma(-2u) (\nu^{2u} - 1) \frac{2}{u} - \Gamma(-u) (\nu^u - 1) \left( \frac{2}{u} + \frac{1}{1-u} + \frac{1}{2-u} \right) \right]. \quad (3.63)$$

Note the poles at  $u = 1$  and  $u = 2$  which are absent in the collinear term of our eikonalized  $B_\nu^{t,\text{eik}}(u)$ . We further notice that no spurious renormalon poles are present in the eikonalized version. Recall that, for thrust approximation was done only for the matrix element and not for the definition of the variable. To show that our eikonal versions of the shape variables do not spoil the above feature we present the results for the  $c$ -parameter. The eikonal version and full result [51] are as follows:

$$B_\nu^{c,\text{eik}}(u) = 2 \frac{\sin \pi u}{\pi u} e^{\frac{5u}{3}} \left[ \Gamma(-2u) (\nu^{2u} - 1) 2^{1-2u} \frac{\sqrt{\pi} \Gamma(u)}{\Gamma(u + \frac{1}{2})} - \frac{2}{u} \Gamma(-u) (\nu^u - 1) \right], \quad (3.64)$$

$$B_\nu^c(u) = 2 \frac{\sin \pi u}{\pi u} e^{\frac{5u}{3}} \left[ \Gamma(-2u) (\nu^{2u} - 1) 2^{1-2u} \frac{\sqrt{\pi} \Gamma(u)}{\Gamma(\frac{1}{2} + u)} - \Gamma(-u) (\nu^u - 1) \left( \frac{2}{u} + \frac{1}{1-u} + \frac{1}{2-u} \right) \right]. \quad (3.65)$$

Again, no spurious poles are introduced. As expected, the EDGE does not reproduce the collinear

renormalon singularities as it cannot capture the hard-collinear emissions correctly.

The perturbative coefficients of the Sudakov exponent in the large- $\beta_0$  limit can be determined by expanding  $B_\nu^t(u)$  in powers of  $u$  and replacing  $u^n$  by  $n!/(\beta_0\alpha_s/\pi)^{n+1}$ . We notice that the large-angle soft gluon emission terms – the coefficient of  $\Gamma(-2u)$ , are identical in the eikonalized and full versions of the Borel function in the Laplace space. This implies that the leading logs – the terms of the form  $L^{n+1}\alpha_s^n$  where  $L = \log \nu$ , will be the same between the two. The differences in the sub-leading logarithms appear due to the absence of the  $u = 1$  and  $u = 2$  poles in the collinear terms. We will now expand the two functions to the first few orders to demonstrate the matching of the LL terms and the discrepancy in the sub-leading logarithms. The expansion of the full result gives,

$$\begin{aligned}
B_\nu^t(u) = & -2L^2 + 0.691L \\
& + (-2L^3 - 5.297L^2 - 6.485L)u \\
& + (-1.167L^4 - 5.527L^3 - 14.491L^2 - 31.655L)u^2 \\
& + (-0.5L^5 - 3.262L^4 - 12.329L^3 - 39.003L^2 - 80.940L)u^3 \\
& + (-0.172L^6 - 1.405L^5 - 6.832L^4 - 28.452L^3 - 87.21L^2 - 175.80L)u^4 \\
& + \mathcal{O}(u^5) + \dots
\end{aligned} \tag{3.66}$$

whereas, the expansion of the eikonal result gives,

$$\begin{aligned}
B_\nu^{t,\text{eik}}(u) = & -2L^2 - 2.31L \\
& + (-2L^3 - 6.79L^2 - 15.71L)u \\
& + (-1.167L^4 - 6.02L^3 - 19.10L^2 - 44.59L)u^2 \\
& + (-0.5L^5 - 3.38L^4 - 13.86L^3 - 45.47L^2 - 93.66L)u^3 \\
& + (-0.172L^6 - 1.429L^5 - 7.216L^4 - 30.61L^3 - 93.57L^2 - 187.395L)u^4 \\
& + \mathcal{O}(u^5) + \dots
\end{aligned} \tag{3.67}$$

As expected, the leading logarithms are appearing correctly in the eikonal approximated version of the Borel function in the Laplace space. We observe that the differences in NLL and NNLL terms between  $B_\nu^t$  and  $B_\nu^{t,\text{eik}}$  are decreasing as we go higher order in  $u$ .

Let us now discuss the power corrections. The Sudakov exponent is an integral over  $u$  and the poles of  $B_\nu^t$  that occur on the real  $u$ -axis make it an ill defined integral. The integral can be defined by shifting the poles above or below the axis or equivalently indenting the contour below or above the poles. This however, introduces an ambiguity that is proportional to the residue of the poles. The poles of  $B_\nu^t$  that occur at  $u = m/2$ , where  $m$  is an odd integer give the ambiguity [51] originating from the large-angle soft gluon emissions. From Eq. (3.9) we see that the ambiguity would be of the form  $(\Lambda\nu/Q)^m$  which implies the existence of non-perturbative power corrections of the same form. In Table (3.1) we present the residues of poles at  $u = m/2$  arising from  $B_\nu^{t,\text{eik}}(u)$  which contribute to the soft power corrections. The full result  $B_\nu^t(u)$  also has poles at  $u = 1$  and  $u = 2$  which give indications to the size of the collinear power corrections whereas these are absent in  $B_\nu^{t,\text{eik}}(u)$ . Thus, the collinear power corrections exist only for  $\nu^1$  and  $\nu^2$ , and using the full expression for  $B_\nu^t(u)$  we find that they are given by  $-2(\frac{\Lambda}{Q})^2$  and  $-\frac{1}{2}(\frac{\Lambda}{Q})^4$  respectively. Note that, in the calculation of the residues for the collinear terms we have ignored the  $\mathcal{O}(1)$  factor  $C_F/2\beta_0$ . We see, thus, that the



residue of the collinear power correction is suppressed by  $\bar{\Lambda}/Q$  as compared to the soft correction for  $\nu^1$  term. For example at the LEP where  $Q = 209$  Gev and  $\bar{\Lambda} = 200 e^{\frac{5}{6}}$  Mev, the ratio of the size of the collinear correction to the soft correction for  $\nu^1$  is approximately  $-0.0017$ . Thus, at colliders like LEP, the soft power corrections are more important as compared to the collinear corrections. As pointed out in [185], the dominant power correction arising from the residue at  $u = 1/2$  is proportional to  $\nu$  and thus generates a shift in the resummed cross-section.

For the other event shapes considered in this article one can calculate the Borel function in Laplace space using EDGE. It remains true that soft power corrections are dominant over the collinear corrections for all the event shapes considered in this paper.

Correction	Residue
$\nu^1$	$8 \frac{\bar{\Lambda}}{Q}$
$\nu^3$	$-\frac{4}{27} \left(\frac{\bar{\Lambda}}{Q}\right)^3$
$\nu^5$	$\frac{1}{375} \left(\frac{\bar{\Lambda}}{Q}\right)^5$
$\nu^7$	$-\frac{1}{30870} \left(\frac{\bar{\Lambda}}{Q}\right)^7$

Table 3.1: The size of the residues of renormalon singularities for soft power corrections. The numbers quoted are  $\pi$  times the residue and  $\bar{\Lambda} = \Lambda e^{5/6}$ . We ignore here the  $\mathcal{O}(1)$  factor  $C_F/2\beta_0$  in Eq. (3.9).

### 3.6 Conclusions

In this work, we have introduced Eikonal Dressed Gluon Exponentiation which is a combination of Dressed Gluon Exponentiation and Eikonal approximation. Using our method, we have demonstrated for several event shapes at  $e^+e^-$  colliders that the leading singular contributions for the respective Borel functions in the single dressed gluon approximation are produced with remarkably simple calculations. It is straightforward to construct the Sudakov exponent in the large- $\beta_0$  limit for the power corrections using the procedure presented in [49, 186]. This exponentiation effectively resums both the large Sudakov logarithms and the power corrections. We observe that EDGE does not introduce any spurious renormalons and correctly produces the dominant power corrections originating from soft emissions.

We have shown that in order to accurately capture the leading singular terms of the characteristic function  $\mathcal{F}(e, \xi)$  and Borel function  $B(e, \xi)$  for an event shape variable  $e$ , it is sufficient to use the eikonal squared matrix element  $\mathcal{M}$ , together with the eikonal version of the event shape variable. Typically the shape variables such as  $C$ -parameter and angularities have complicated expressions especially so when the final state gluon is off the mass shell. We have demonstrated that the simplification of the computations is achieved, both when one uses the energy fractions as the variables, and also when we uses light-cone variables to parameterize the phase space of the eikonal dressed gluon. When using the latter variables, we observe that the minimum value of rapidity  $y_{\min}$  is the source of the leading singular terms in  $\mathcal{F}(e, \xi)$ . We believe that this method is sufficiently simple and flexible to be implemented also in the more intricate environment of hadron collisions, where hadronic event shapes and jet shapes provide important tools for QCD analyses.

## Chapter 4

# Conclusions and Future directions

Resummation is a well-known method to obtain precise theoretical predictions for several relevant physical quantities in the present and future colliders. The method of resummation is crucially based on the concept of factorization of Infrared singularities from hard (finite) part of a scattering amplitude and cross-section. In this thesis we have studied resummed  $p_T$  distribution for pseudo-scalar Higgs bosons and power corrections of event shape variables.

### Resummed $p_T$ distribution for pseudo-scalar Higgs bosons

We have studied the resummed  $p_T$  distribution for pseudo-scalar Higgs bosons at the LHC for both the centre-of-mass energy 13 TeV and 14 TeV at next-to-next-to-leading logarithmic accuracy by matching the resummed curve with approximated fixed order next-to-next-to-leading order result.

Our results show a significant reduction in sensitivity to the choices of resummation, renormalization and factorization scales that are artefact of the perturbation theory. In our work, we also studied the uncertainty due to different choices of parton density sets. These results provide us with precise estimate for the distribution especially in the region around 15 GeV where the cross-section is large and the fixed order results are completely unreliable due to the breakdown of fixed order perturbation series.

### Power corrections of event shape variables

We have introduced Eikonal Dressed Gluon Exponentiation by combining Dressed Gluon Exponentiation [49] and Eikonal approximation. As an application of our method, we have calculated the leading singular contributions of the characteristic function and their respective Borel functions for the event shapes in the single dressed gluon approximation for  $e^+e^-$  collider. Our method greatly simplifies the calculations of the leading singular contributions. We have shown that this simplification in the calculation happens while using both the energy fractions and the light-cone variables. We have also observed that while using light-cone variables, the minimum value of rapidity is the source of leading singular terms.

It is straightforward to construct the Sudakov exponent in the large- $\beta_0$  limit for the power corrections using the procedure presented in [49, 186]. This exponentiation effectively resums both the large Sudakov logarithms and the power corrections. We observe that EDGE does not introduce

any spurious renormalons and correctly produces the dominant power corrections originating from soft emissions.

We believe that this method is sufficiently simple and flexible to be implemented also in the more intricate environment of hadron collisions, where hadronic event shapes and jet shapes provide important tools for QCD analyses.

# Appendix A

## Useful Relations needed for this thesis

### A.1 Feynman Rules

Feynman rules are like cornerstone of theoretical QFT. We need results from the theory side, which can be derived using Feynman rules, in order to forecast and match experimental data. In the Figure (A.1) all momenta are incoming and at each vertex momentum is conserved.

fermion propagator :	$\frac{i\delta^{ij}}{\not{p} - m + i\epsilon}$
gluon propagator :	$-i \frac{g^{\mu\nu} + (1 - \xi) \frac{p^\mu p^\nu}{p^2}}{p^2 + i\epsilon} \delta^{ab}$
ghost propagator :	$\frac{i\delta^{ab}}{p^2 + i\epsilon}$
quark gluon vertex :	$i\hat{g}_s \gamma^\mu T_{ij}^a$
ghost gluon vertex :	$-\hat{g}_s f^{abc} p^\mu$
3 gluon vertex :	$\hat{g}_s f^{abc} [g^{\mu\nu} (k - p)^\rho + g^{\nu\rho} (p - q)^\mu + g^{\rho\mu} (q - k)^\nu]$
4 gluon vertex :	$-i\hat{g}_s^2 [f^{abe} f^{cde} (g^{\nu\rho} g^{\nu\sigma} - g^{\mu\sigma} g^{\nu\rho}) + f^{ace} f^{bde} (g^{\mu\nu} g^{\rho\sigma} - g^{\mu\sigma} g^{\nu\rho}) + f^{ade} f^{bce} (g^{\mu\nu} g^{\rho\sigma} - g^{\mu\rho} g^{\nu\sigma})]$

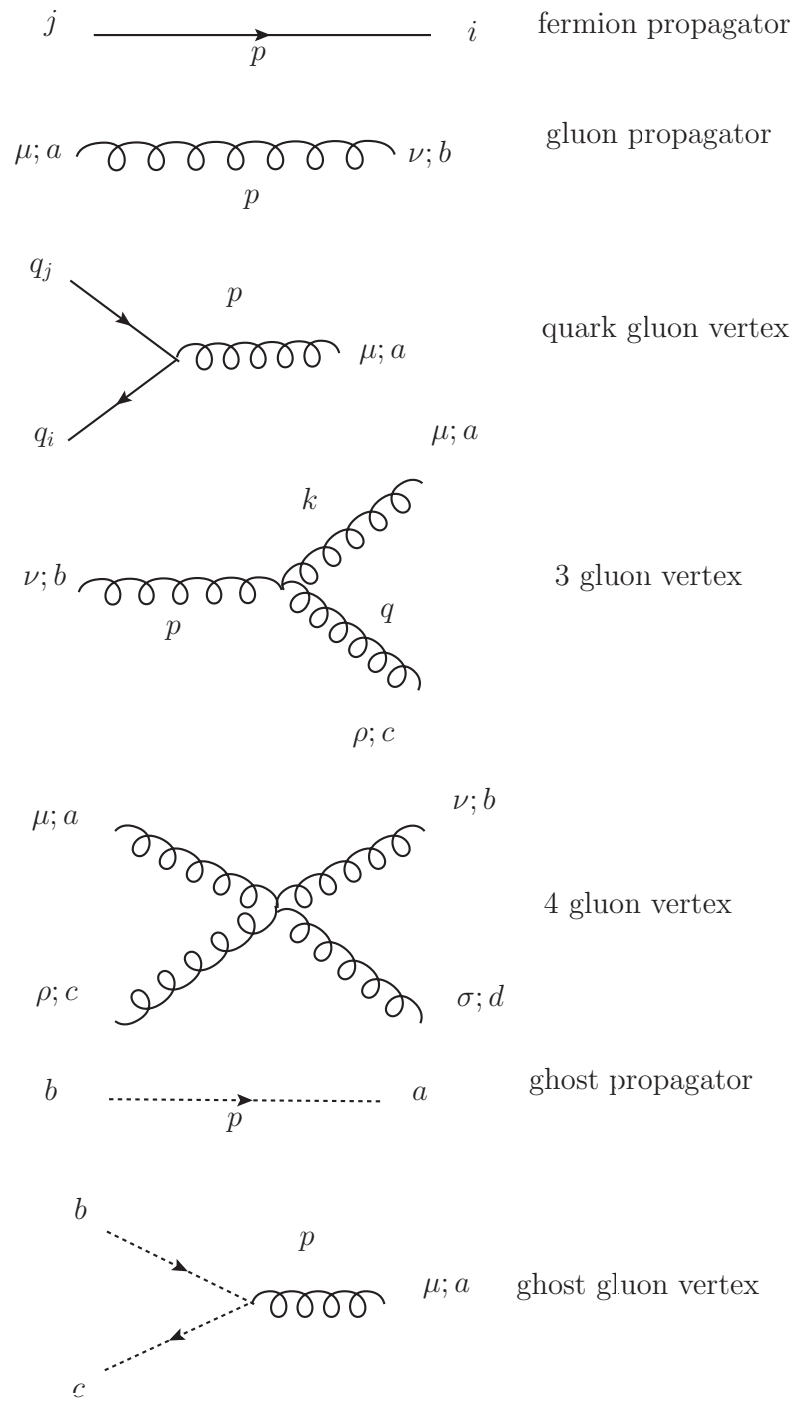


Figure A.1: QCD Feynman rules

## A.2 Relations between Gamma Matrices

In  $d$  dimensions,

$$\begin{aligned} g^{\mu\nu} g_{\mu\nu} &= d \\ \{\gamma^\mu, \gamma^\nu\} &= 2g^{\mu\nu} \\ \text{tr}[1] &= d \end{aligned} \tag{A.1}$$

In  $d = 4 - \varepsilon$  dimensions,

$$\begin{aligned} \gamma^\mu \gamma^\nu \gamma_\mu &= -(2 - \varepsilon) \gamma^\nu \\ \gamma^\mu \gamma^\nu \gamma^\rho \gamma_\mu &= 4g^{\nu\rho} - \varepsilon \gamma^\mu \gamma^\rho \\ \gamma^\mu \gamma^\nu \gamma^\rho \gamma^\sigma \gamma_\mu &= -2\gamma^\sigma \gamma^\rho \gamma^\nu + \varepsilon \gamma^\nu \gamma^\rho \gamma^\sigma \end{aligned} \tag{A.2}$$

For  $d = 4 - 2\varepsilon$  dimensions, just replace  $\varepsilon$  by  $2\varepsilon$

## A.3 Trace Technology

$$\begin{aligned} (\bar{v} \gamma^\mu u)^* &= u^\dagger (\gamma^\mu)^\dagger (\gamma^0)^\dagger v = u^\dagger (\gamma^\mu)^\dagger \gamma^0 v = u^\dagger \gamma^0 \gamma^\mu v = \bar{u} \gamma^\mu v \\ (\bar{v} \gamma^{\mu_1} \gamma^{\mu_2} u)^* &= \bar{u} \gamma^{\mu_2} \gamma^{\mu_1} v \\ (\bar{u} S^{\mu\alpha} v \epsilon_\alpha)^* &= \bar{v} S^{\mu\alpha} u \epsilon_\alpha^* \\ \sum_s \bar{u}^s(p) u^s(p) &= \not{p} + m \\ \sum_{s'} \bar{v}^{s'}(p) v^{s'}(p) &= \not{p} - m \\ \not{p} \gamma^\mu &= 2p^\mu - \gamma^\mu \not{p} \end{aligned} \tag{A.3}$$

## A.4 Casimir Invariants of SU(N)

In QCD, we generally talk about only the two most valuable representations, namely fundamental and adjoint representations. The lowest non-trivial representation is called fundamental representation. For SU(N) fundamental representation is presented by  $(N \times N)$  matrices but for adjoint representation matrices are  $((N^2 - 1) \times (N^2 - 1))$ . Both representations are basis-dependent, but we can also represent basis-independently through the introduction of Casimirs. Casimir operators are those which commute with other generators of the group. According to the Schur's lemma Casimir operators should be proportional to Identity. For, SU(N) group, we define,

$$J^2 = \sum_a T_R^a T_R^a = C_2(R) \mathbb{1} . \tag{A.4}$$

In any representation the generators can be chosen so that,

$$\text{tr}[T_R^a T_R^b] = T(R) \delta^{ab} , \tag{A.5}$$

where  $T(R)$  is the index of the representation. For fundamental representation,  $T_F = 1/2$  and for adjoint representation,  $T_A = N$ . Now set  $a = b$  and sum over  $a$  is implicit then,

$$d(R) C_2(R) = T(R) d(G) , \tag{A.6}$$

where,  $d(R)$  is the dimension of the representation, for example  $d(\text{fund}) = N$  and  $d(\text{adj}) = N^2 - 1$  and  $d(G)$  is the dimension of the group; number of group generators for  $SU(N)$  group is  $d(SU(N)) = N^2 - 1$ . So, casimir for the fundamental representation,  $C_F = (N^2 - 1)/2N$  and for the adjoint representation,  $C_A = N$ .

# Appendix B

## Proof of some relations used in the main section

### B.1 Proof of the eikonal identity regarding soft photon emissions

If  $n$  photons are coming out from an outgoing electron line with momenta  $k_1, \dots, k_n$  ( see Figure (1.7) ), there will be  $n!$  permutations possible. Let  $\Pi$  indicate one such permutation where  $\Pi(i)$  is the number between 1 and  $n$  to which  $i$  is assigned. Using this notation as a guide we will prove the following identity (see [67], for example).

$$\sum_{\substack{\text{all} \\ \text{permutations} \\ \Pi}} \frac{1}{p \cdot k_{\Pi(1)}} \frac{1}{p \cdot (k_{\Pi(1)} + k_{\Pi(2)})} \cdots \frac{1}{p \cdot (k_{\Pi(1)} + k_{\Pi(2)} + \cdots + k_{\Pi(n)})} \\ = \frac{1}{p \cdot k_1} \frac{1}{p \cdot k_2} \frac{1}{p \cdot k_3} \cdots \frac{1}{p \cdot k_n}$$

Let's check the above formula for  $n = 2$

$$\begin{aligned} & \sum_{\Pi} \frac{1}{p \cdot k_{\Pi(1)}} \frac{1}{p \cdot (k_{\Pi(1)} + k_{\Pi(2)})} \\ &= \frac{1}{p \cdot k_1} \frac{1}{p \cdot (k_1 + k_2)} + \frac{1}{p \cdot k_2} \frac{1}{p \cdot (k_2 + k_1)} \\ &= \frac{1}{p \cdot (k_1 + k_2)} \left[ \frac{1}{p \cdot k_1} + \frac{1}{p \cdot k_2} \right] \\ &= \frac{1}{p \cdot (k_1 + k_2)} \frac{p \cdot k_2 + p \cdot k_1}{(p \cdot k_1)(p \cdot k_2)} \\ &= \frac{1}{p \cdot k_1} \frac{1}{p \cdot k_2} \end{aligned}$$

we notice that the last factor for any  $n$  is always same for every permutation  $\Pi$ . For  $n = 2$  this factor

$$\frac{1}{p \cdot (k_1 + k_2)} \tag{B.1}$$



So, we can write the L.H.S of the formula as follows

$$\begin{aligned} L.H.S &= \sum_{\text{all permutations } \Pi} \frac{1}{p \cdot k_{\Pi(1)}} \frac{1}{p \cdot (k_{\Pi(1)} + k_{\Pi(2)})} \cdots \frac{1}{p \cdot (k_{\Pi(1)} + k_{\Pi(2)} + \cdots + k_{\Pi(n)})} \\ &= \frac{1}{p \cdot \sum k} \sum_{i=1}^n \sum_{\Pi'(i)} \frac{1}{p \cdot k_{\Pi(1)}} \frac{1}{p \cdot (k_{\Pi(1)} + k_{\Pi(2)})} \cdots \frac{1}{p \cdot (k_{\Pi(1)} + k_{\Pi(2)} + \cdots + k_{\Pi(n-1)})} \end{aligned}$$

where,

$$\sum_{\Pi} = \sum_{i=1}^n \sum_{\Pi'(i)} \quad (\text{B.2})$$

$\Pi'(i)$  is the set of all permutations except  $i$ .

$$L.H.S = \frac{1}{p \cdot \sum k} \sum_{i=1}^n \frac{1}{p \cdot k_1} \frac{1}{p \cdot k_2} \cdots \frac{1}{p \cdot k_{i-1}} \frac{1}{p \cdot k_{i+1}} \cdots \frac{1}{p \cdot k_n} \quad (\text{B.3})$$

write down explicitly,

$$\begin{aligned} L.H.S &= \frac{1}{p \cdot \sum k} \left[ \frac{1}{(p \cdot k_2)(p \cdot k_3) \cdots (p \cdot k_n)} + \frac{1}{(p \cdot k_1)(p \cdot k_3) \cdots (p \cdot k_n)} + \cdots \right. \\ &\quad \left. + \frac{1}{(p \cdot k_1)(p \cdot k_2)(p \cdot k_3) \cdots (p \cdot k_{i-1})(p \cdot k_{i+1}) \cdots (p \cdot k_n)} + \frac{1}{(p \cdot k_1)(p \cdot k_2) \cdots (p \cdot k_{n-1})} \right] \end{aligned}$$

If we now multiply and divide each term in this sum by  $(p \cdot k_i)$  we will have

$$\begin{aligned} L.H.S &= \frac{1}{p \cdot \sum k} \left[ \frac{p \cdot k_1}{(p \cdot k_2)(p \cdot k_3) \cdots (p \cdot k_n)} + \frac{p \cdot k_2}{(p \cdot k_1)(p \cdot k_3) \cdots (p \cdot k_n)} + \cdots \right. \\ &\quad \left. + \frac{p \cdot k_i}{(p \cdot k_1)(p \cdot k_2)(p \cdot k_3) \cdots (p \cdot k_{i-1})(p \cdot k_{i+1}) \cdots (p \cdot k_n)} + \frac{p \cdot k_n}{(p \cdot k_1)(p \cdot k_2) \cdots (p \cdot k_{n-1})} \right] \\ &= \frac{1}{p \cdot \sum k} \left[ \frac{(p \cdot k_1) + (p \cdot k_2) + \cdots + (p \cdot k_n)}{\prod_i (p \cdot k_i)} \right] \\ &= \frac{1}{p \cdot \sum k} \frac{p \cdot \sum k}{\prod_i (p \cdot k_i)} \\ &= \frac{1}{\prod_i (p \cdot k_i)} \\ &= \frac{1}{p \cdot k_1} \frac{1}{p \cdot k_2} \frac{1}{p \cdot k_3} \cdots \frac{1}{p \cdot k_n} \quad (\text{B.4}) \end{aligned}$$

## B.2 Borel Summation and Renormalons

In perturbative QCD observables are expanded in series with the strong coupling constant as expansion parameter. In general, perturbative series are divergent and, at best, asymptotic. We can try to give a value to the sum of a divergent series in various ways whenever we come across one. Here, we will concentrate on the Borel summation method. Let us pretend that  $R$  is a divergent series.

$$R \sim \sum_{n=0}^{\infty} r_n \alpha_s^{n+1} \quad (\text{B.5})$$

The series diverges as  $r_n \sim n!$  when  $n \rightarrow \infty$ . The Borel transform of  $R$  is defined as

$$B[R](u) = \sum_{n=0}^{\infty} r_n \frac{u^n}{n!} \quad (\text{B.6})$$

We can define the Borel integral as

$$\tilde{R} = \int_0^{\infty} du e^{-u/\alpha_s} B[R](u) \quad (\text{B.7})$$

Next we show that  $\tilde{R}$  has the same series expansion of  $R$

$$\begin{aligned} \tilde{R} &= \int_0^{\infty} du e^{-u/\alpha_s} B[R](u) \\ &= \int_0^{\infty} du e^{-u/\alpha_s} \sum_{n=0}^{\infty} r_n \frac{u^n}{n!} \\ &= \sum_{n=0}^{\infty} \alpha_s^{n+1} \int_0^{\infty} du e^{-u} u^n \\ &= \sum_{n=0}^{\infty} \frac{r_n}{n!} \alpha_s^{n+1} \Gamma(n+1) \\ &= \sum_n r_n \alpha_s^{n+1} \end{aligned} \quad (\text{B.8})$$

If  $\tilde{R}$  exists, we say that Borel sum of  $R$  exists.

Let us consider the gauge invariant observables  $R$  and subtract the tree level contribution from it. So, the higher order corrections look like  $\sum_{n=0}^{\infty} r_n \alpha_s^{n+1}$ , where  $r_0$  originates from diagrams with a single gluon line. The coefficients  $r_n$  are polynomials in  $n_f$  [190].

$$r_n = r_{n0} + r_{n1} n_f + \dots + r_{nn} n_f^n . \quad (\text{B.9})$$

The set of bubble diagrams give the coefficient  $r_{nn}$  with largest power of  $n_f$ . The renormalized fermion loop is defined as follows

$$\Pi(k^2) = -\beta_{0f} \alpha_s \left[ \ln \left( -\frac{k^2}{\mu^2} \right) + C \right] , \quad (\text{B.10})$$

with a scheme dependent constant  $C$ , in the  $\overline{MS}$  scheme  $C = -5/3$ .  $\beta_{0f}$  is the fermion contribution to the one-loop  $\beta$  function [191]. Let us define Borel transform by

$$B[R](u) = \sum_n \frac{r_n}{n!} (-\beta_{0f})^{-n} u^n . \quad (\text{B.11})$$

This Borel transform can be used as a generating function for perturbative coefficients:

$$r_n = (-\beta_{0f})^{-n} \left. \frac{d^n}{du^n} B[R](u) \right|_u = 0 . \quad (\text{B.12})$$

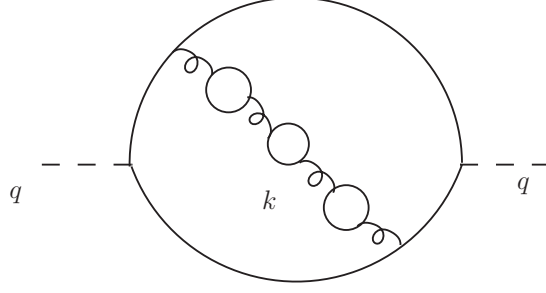


Figure B.1: Bubble chain diagram where we can see fermion loop insertion into a single gluon line which leads to renormalon

In order to evaluate  $B \left[ \frac{\alpha_s}{1+\Pi(k^2)} \right]$  we first expand the following

$$\begin{aligned} \frac{\alpha_s}{1+\Pi(k^2)} &= \frac{\alpha_s}{1 - \beta_{0f}\alpha_s \ln \left( -\frac{k^2}{\mu^2} e^C \right)} \\ &= \alpha_s \left[ 1 + \beta_{0f}\alpha_s \ln \left( -\frac{k^2}{\mu^2} e^C \right) + (\beta_{0f})^2 \alpha_s^2 \ln^2 \left( -\frac{k^2}{\mu^2} e^C \right) + \dots \right], \end{aligned} \quad (\text{B.13})$$

once we have the above expansion we can immediately identify

$$r_n = \beta_{0f} \ln \left( -\frac{k^2}{\mu^2} e^C \right). \quad (\text{B.14})$$

Using Eq. (B.11) we can now do the Borel summation

$$\begin{aligned} B[R](u) &= \sum_n \frac{\beta_{0f} \ln \left( -\frac{k^2}{\mu^2} e^C \right)}{n!} (-\beta_{0f})^{-n} u^n \\ &= \exp \left[ \ln \left( -\frac{k^2}{\mu^2} e^C \right)^{-u} \right] \\ &= \left( -\frac{k^2}{\mu^2} e^C \right)^{-u}. \end{aligned} \quad (\text{B.15})$$

The following relations are used to calculate the Borel transform of bubble graphs [191]

$$B \left[ \frac{\alpha_s}{1+\Pi(k^2)} \right] = \left( -\frac{k^2}{\mu^2} e^C \right)^{-u}. \quad (\text{B.16})$$

$$B \left[ \frac{\beta_{0f}\alpha_s^2}{|1+\Pi(k^2)|} \right] = -\frac{\sin(\pi u)}{\pi} \left( -\frac{k^2}{\mu^2} e^C \right)^{-u}. \quad (\text{B.17})$$

# Bibliography

- [1] G. Aad et al. Observation of a new particle in the search for the Standard Model Higgs boson with the ATLAS detector at the LHC. *Phys. Lett. B* 716, (2012) 1–29.
- [2] S. Chatrchyan et al. Observation of a New Boson at a Mass of 125 GeV with the CMS Experiment at the LHC. *Phys. Lett. B* 716, (2012) 30–61.
- [3] R. Barate et al. Search for the standard model Higgs boson at LEP. *Phys. Lett. B* 565, (2003) 61–75.
- [4] Precision Electroweak Measurements and Constraints on the Standard Model .
- [5] T. Aaltonen et al. Combination of Tevatron Searches for the Standard Model Higgs Boson in the  $W^+W^-$  Decay Mode. *Phys. Rev. Lett.* 104, (2010) 061,802.
- [6] R. Abdul Khalek et al. Science Requirements and Detector Concepts for the Electron-Ion Collider: EIC Yellow Report .
- [7] A. Accardi et al. Electron Ion Collider: The Next QCD Frontier: Understanding the glue that binds us all. *Eur. Phys. J. A* 52, (2016) 268.
- [8] B. Field. Next-to-leading log resummation of scalar and pseudoscalar Higgs boson differential cross-sections at the CERN LHC and Tevatron. *Phys. Rev. D* 70, (2004) 054,008.
- [9] T. Ahmed, M. Bonvini, M. C. Kumar, P. Mathews, N. Rana, V. Ravindran, and L. Rottoli. Pseudo-scalar Higgs boson production at  $N^3 LO_A + N^3 LL'$ . *Eur. Phys. J. C* 76, (2016) 663.
- [10] G. Bozzi, S. Catani, D. de Florian, and M. Grazzini. The  $q(T)$  spectrum of the Higgs boson at the LHC in QCD perturbation theory. *Phys. Lett. B* 564, (2003) 65–72.
- [11] G. Bozzi, S. Catani, D. de Florian, and M. Grazzini. Transverse-momentum resummation and the spectrum of the Higgs boson at the LHC. *Nucl. Phys. B* 737, (2006) 73–120.
- [12] D. de Florian, G. Ferrera, M. Grazzini, and D. Tommasini. Transverse-momentum resummation: Higgs boson production at the Tevatron and the LHC. *JHEP* 11, (2011) 064.
- [13] R. Abbate, M. Fickinger, A. H. Hoang, V. Mateu, and I. W. Stewart. Thrust at  $N^3LL$  with Power Corrections and a Precision Global Fit for  $\alpha_s(m_Z)$ . *Phys. Rev. D* 83, (2011) 074,021.
- [14] A. H. Hoang, D. W. Kolodrubetz, V. Mateu, and I. W. Stewart. Precise determination of  $\alpha_s$  from the  $C$ -parameter distribution. *Phys. Rev. D* 91, (2015) 094,018.

- [15] S.-Q. Wang, S. J. Brodsky, X.-G. Wu, J.-M. Shen, and L. Di Giustino. Novel method for the precise determination of the QCD running coupling from event shape distributions in electron-positron annihilation. *Phys. Rev. D* 100, (2019) 094,010.
- [16] S. Marzani, D. Reichelt, S. Schumann, G. Soyez, and V. Theeuwes. Fitting the Strong Coupling Constant with Soft-Drop Thrust. *JHEP* 11, (2019) 179.
- [17] T. Gehrmann, G. Luisoni, and P. F. Monni. Power corrections in the dispersive model for a determination of the strong coupling constant from the thrust distribution. *Eur.Phys.J. C* 73, (2013) 2265.
- [18] S. Brandt, C. Peyrou, R. Sosnowski, and A. Wroblewski. The Principal axis of jets. An Attempt to analyze high-energy collisions as two-body processes. *Phys. Lett.* 12, (1964) 57–61.
- [19] G. L. Kane, J. Pumplin, and W. Repko. Transverse Quark Polarization in Large p(T) Reactions,  $e^+e^-$  Jets, and Leptoproduction: A Test of QCD. *Phys. Rev. Lett.* 41, (1978) 1689.
- [20] E. Farhi. A QCD Test for Jets. *Phys. Rev. Lett.* 39, (1977) 1587–1588.
- [21] G. Altarelli. Partons in Quantum Chromodynamics. *Phys. Rept.* 81, (1982) 1.
- [22] J. F. Donoghue, F. Low, and S.-Y. Pi. Tensor Analysis of Hadronic Jets in Quantum Chromodynamics. *Phys. Rev. D* 20, (1979) 2759.
- [23] G. C. Fox and S. Wolfram. Observables for the Analysis of Event Shapes in  $e^+e^-$  Annihilation and Other Processes. *Phys. Rev. Lett.* 41, (1978) 1581.
- [24] J. Bjorken and S. J. Brodsky. Statistical Model for electron-Positron Annihilation Into Hadrons. *Phys. Rev. D* 1, (1970) 1416–1420.
- [25] G. Parisi. Super Inclusive Cross-Sections. *Phys. Lett. B* 74, (1978) 65–67.
- [26] C. F. Berger and G. F. Sterman. Scaling rule for nonperturbative radiation in a class of event shapes. *JHEP* 0309, (2003) 058.
- [27] C. F. Berger, T. Kucs, and G. F. Sterman. Event shape / energy flow correlations. *Phys.Rev. D* 68, (2003) 014,012.
- [28] C. F. Berger, T. Kucs, and G. F. Sterman. Interjet energy flow / event shape correlations. *Int. J. Mod. Phys. A* 18, (2003) 4159–4168.
- [29] A. Gehrmann-De Ridder, T. Gehrmann, E. Glover, and G. Heinrich. NNLO corrections to event shapes in  $e^+e^-$  annihilation. *JHEP* 0712, (2007) 094.
- [30] S. Weinzierl. Event shapes and jet rates in electron-positron annihilation at NNLO. *JHEP* 0906, (2009) 041.
- [31] T. Gehrmann, A. Huss, J. Mo, and J. Niehues. Second-order QCD corrections to event shape distributions in deep inelastic scattering. *Eur. Phys. J. C* 79, (2019) 1022.
- [32] A. Kardos, G. Somogyi, and A. Verbytskyi. Determination of  $\alpha_S$  beyond NNLO using event shape averages. *Eur. Phys. J. C* 81, (2021) 292.

- [33] A. Gehrmann-De Ridder, T. Gehrmann, E. Glover, and G. Heinrich. NNLO moments of event shapes in  $e^+e^-$  annihilation. *JHEP* 05, (2009) 106.
- [34] S. Catani, L. Trentadue, G. Turnock, and B. Webber. Resummation of large logarithms in  $e^+e^-$  event shape distributions. *Nucl.Phys.* B407, (1993) 3–42.
- [35] A. Banfi, G. P. Salam, and G. Zanderighi. Phenomenology of event shapes at hadron colliders. *JHEP* 06, (2010) 038.
- [36] A. Banfi, G. P. Salam, and G. Zanderighi. Principles of general final-state resummation and automated implementation. *JHEP* 03, (2005) 073.
- [37] A. Banfi, G. Salam, and G. Zanderighi. Semi-numerical resummation of event shapes. *JHEP* 01, (2002) 018.
- [38] A. Banfi, H. McAslan, P. F. Monni, and G. Zanderighi. The two-jet rate in  $e^+e^-$  at next-to-next-to-leading-logarithmic order. *Phys. Rev. Lett.* 117, (2016) 172,001.
- [39] T. Becher and G. Bell. NNLL Resummation for Jet Broadening. *JHEP* 1211, (2012) 126.
- [40] A. H. Hoang, D. W. Kolodrubetz, V. Mateu, and I. W. Stewart.  $C$ -parameter distribution at  $\text{N}^3\text{LL}'$  including power corrections. *Phys. Rev. D* 91, (2015) 094,017.
- [41] A. Budhraj, A. Jain, and M. Procura. One-loop angularity distributions with recoil using Soft-Collinear Effective Theory. *JHEP* 08, (2019) 144.
- [42] G. Bell, A. Hornig, C. Lee, and J. Talbert.  $e^+e^-$  angularity distributions at NNLL' accuracy. *JHEP* 01, (2019) 147.
- [43] A. H. Hoang, D. W. Kolodrubetz, V. Mateu, and I. W. Stewart. State-of-the-art predictions for  $C$ -parameter and a determination of  $\alpha_s$ . *Nucl. Part. Phys. Proc.* 273-275, (2016) 2015–2021.
- [44] D. W. Kolodrubetz. Accuracy and Precision in Collider Event Shapes. Ph.D. thesis, MIT, Cambridge, CTP 2016.
- [45] C. Lepenik and V. Mateu. NLO Massive Event-Shape Differential and Cumulative Distributions. *JHEP* 03, (2020) 024.
- [46] C. Lee, A. Hornig, and G. Ovanessian. Probing the Structure of Jets: Factorized and Resummed Angularity Distributions in SCET. *PoS EFT09*, (2009) 010.
- [47] A. Hornig, C. Lee, and G. Ovanessian. Effective Predictions of Event Shapes: Factorized, Resummed, and Gapped Angularity Distributions. *JHEP* 05, (2009) 122.
- [48] A. Banfi, H. McAslan, P. F. Monni, and G. Zanderighi. A general method for resummation of event-shape distributions in  $e^+e^-$  annihilation. *JHEP* 05, (2015) 102.
- [49] E. Gardi. Dressed gluon exponentiation. *Nucl.Phys.* B622, (2002) 365–392.
- [50] E. Gardi and J. Rathsman. The Thrust and heavy jet mass distributions in the two jet region. *Nucl.Phys.* B638, (2002) 243–287.

- [51] E. Gardi and L. Magnea. The C parameter distribution in  $e^+ e^-$  annihilation. *JHEP* 0308, (2003) 030.
- [52] C. F. Berger and L. Magnea. Scaling of power corrections for angularities from dressed gluon exponentiation. *Phys.Rev.* D70, (2004) 094,010.
- [53] M. Cacciari and E. Gardi. Heavy quark fragmentation. *Nucl.Phys.* B664, (2003) 299–340.
- [54] E. Gardi. Radiative and semileptonic B meson decay spectra: Sudakov resummation beyond logarithmic accuracy and the pole mass. *JHEP* 0404, (2004) 049.
- [55] J. R. Andersen and E. Gardi. Taming the anti-B  $\rightarrow X(s)\gamma$  spectrum by dressed gluon exponentiation. *JHEP* 0506, (2005) 030.
- [56] G. 't Hooft and M. J. G. Veltman. Regularization and Renormalization of Gauge Fields. *Nucl. Phys. B* 44, (1972) 189–213.
- [57] M. D. Schwartz. Quantum Field Theory and the Standard Model. Cambridge University Press, 2014.
- [58] F. Herzog, B. Ruijl, T. Ueda, J. A. M. Vermaseren, and A. Vogt. The five-loop beta function of Yang-Mills theory with fermions. *JHEP* 02, (2017) 090.
- [59] F. Bloch and A. Nordsieck. Note on the Radiation Field of the electron. *Phys. Rev.* 52, (1937) 54–59.
- [60] T. Kinoshita. Mass singularities of Feynman amplitudes. *J. Math. Phys.* 3, (1962) 650–677.
- [61] T. D. Lee and M. Nauenberg. Degenerate Systems and Mass Singularities. *Phys. Rev.* 133, (1964) B1549–B1562.
- [62] G. F. Sterman. Summation of Large Corrections to Short Distance Hadronic Cross-Sections. *Nucl. Phys.* B281, (1987) 310–364.
- [63] S. Catani and L. Trentadue. Resummation of the QCD Perturbative Series for Hard Processes. *Nucl. Phys.* B327, (1989) 323–352.
- [64] S. Forte and G. Ridolfi. Renormalization group approach to soft gluon resummation. *Nucl. Phys. B* 650, (2003) 229–270.
- [65] S. Catani. Higher order QCD corrections in hadron collisions: Soft gluon resummation and exponentiation. *Nucl. Phys. B Proc. Suppl.* 54, (1997) 107–113.
- [66] N. Agarwal, L. Magnea, C. Signorile-Signorile, and A. Tripathi. The Infrared Structure of Perturbative Gauge Theories .
- [67] M. E. Peskin and D. V. Schroeder. An Introduction to quantum field theory. Addison-Wesley, Reading, USA, 1995.
- [68] L. D. Landau. On analytic properties of vertex parts in quantum field theory. *Nucl. Phys.* 13, (1959) 181–192.

- [69] R. J. Eden, P. V. Landshoff, D. I. Olive, and J. C. Polkinghorne. The analytic S-matrix. Cambridge Univ. Press, Cambridge, 1966.
- [70] J. Collins. A new and complete proof of the Landau condition for pinch singularities of Feynman graphs and other integrals .
- [71] T. Dennen, I. Prlina, M. Spradlin, S. Stanojevic, and A. Volovich. Landau Singularities from the Amplituhedron. *JHEP* 06, (2017) 152.
- [72] D. R. Yennie, S. C. Frautschi, and H. Suura. The infrared divergence phenomena and high-energy processes. *Annals Phys.* 13, (1961) 379–452.
- [73] G. Grammer, Jr. and D. R. Yennie. Improved treatment for the infrared divergence problem in quantum electrodynamics. *Phys. Rev. D* 8, (1973) 4332–4344.
- [74] A. H. Mueller. On the Asymptotic Behavior of the Sudakov Form-factor. *Phys. Rev. D* 20, (1979) 2037.
- [75] M. Dasgupta. Power corrections in QCD. *J. Phys. G* 28, (2002) 907–914.
- [76] P. Nason and M. H. Seymour. Infrared renormalons and power suppressed effects in e+ e- jet events. *Nucl. Phys. B* 454, (1995) 291–312.
- [77] N. Agarwal, A. Mukhopadhyay, S. Pal, and A. Tripathi. Power corrections to event shapes using eikonal dressed gluon exponentiation. *JHEP* 03, (2021) 155.
- [78] G. Oderda and G. F. Sterman. Energy and color flow in dijet rapidity gaps. *Phys. Rev. Lett.* 81, (1998) 3591–3594.
- [79] G. Schierholz. On higher order corrections to three-jet cross sections. *AIP Conf. Proc.* 74, (1981) 148–161.
- [80] J. G. M. Gatheral. Exponentiation of Eikonal Cross-sections in Nonabelian Gauge Theories. *Phys. Lett. B* 133, (1983) 90–94.
- [81] J. Frenkel and J. C. Taylor. NONABELIAN EIKONAL EXPONENTIATION. *Nucl. Phys. B* 246, (1984) 231–245.
- [82] A. Mitov, G. Sterman, and I. Sung. Diagrammatic Exponentiation for Products of Wilson Lines. *Phys. Rev. D* 82, (2010) 096,010.
- [83] E. Gardi, E. Laenen, G. Stavenga, and C. D. White. Webs in multiparton scattering using the replica trick. *JHEP* 11, (2010) 155.
- [84] E. Gardi, J. M. Smillie, and C. D. White. On the renormalization of multiparton webs. *JHEP* 09, (2011) 114.
- [85] N. Agarwal, A. Danish, L. Magnea, S. Pal, and A. Tripathi. Multiparton webs beyond three loops. *JHEP* 05, (2020) 128.
- [86] N. Agarwal, S. Pal, A. Srivastav, and A. Tripathi. Building blocks of Cwebs in multiparton scattering amplitudes. *JHEP* 06, (2022) 020.



- [87] S. Catani, G. Turnock, B. R. Webber, and L. Trentadue. Thrust distribution in  $e^+e^-$  annihilation. *Phys. Lett. B* 263, (1991) 491–497.
- [88] S. Chatrchyan et al. Observation of a new boson at a mass of 125 GeV with the CMS experiment at the LHC. *Phys. Lett. B* 716, (2012) 30–61.
- [89] R. P. Kauffman and W. Schaffer. QCD corrections to production of Higgs pseudoscalars. *Phys. Rev. D* 49, (1994) 551–554.
- [90] A. Djouadi, M. Spira, and P. M. Zerwas. Two photon decay widths of Higgs particles. *Phys. Lett. B* 311, (1993) 255–260.
- [91] M. Spira, A. Djouadi, D. Graudenz, and P. M. Zerwas. Higgs boson production at the LHC. *Nucl. Phys. B* 453, (1995) 17–82.
- [92] M. Spira, A. Djouadi, D. Graudenz, and P. M. Zerwas. SUSY Higgs production at proton colliders. *Phys. Lett. B* 318, (1993) 347–353.
- [93] R. V. Harlander and W. B. Kilgore. Next-to-next-to-leading order Higgs production at hadron colliders. *Phys. Rev. Lett.* 88, (2002) 201,801.
- [94] R. V. Harlander and W. B. Kilgore. Production of a pseudoscalar Higgs boson at hadron colliders at next-to-next-to leading order. *JHEP* 10, (2002) 017.
- [95] C. Anastasiou and K. Melnikov. Higgs boson production at hadron colliders in NNLO QCD. *Nucl. Phys. B* 646, (2002) 220–256.
- [96] C. Anastasiou and K. Melnikov. Pseudoscalar Higgs boson production at hadron colliders in NNLO QCD. *Phys. Rev. D* 67, (2003) 037,501.
- [97] V. Ravindran, J. Smith, and W. L. van Neerven. NNLO corrections to the total cross-section for Higgs boson production in hadron hadron collisions. *Nucl. Phys. B* 665, (2003) 325–366.
- [98] C. Anastasiou, C. Duhr, F. Dulat, F. Herzog, and B. Mistlberger. Higgs Boson Gluon-Fusion Production in QCD at Three Loops. *Phys. Rev. Lett.* 114, (2015) 212,001.
- [99] R. V. Harlander and K. J. Ozeren. Top mass effects in Higgs production at next-to-next-to-leading order QCD: Virtual corrections. *Phys. Lett. B* 679, (2009) 467–472.
- [100] R. V. Harlander and K. J. Ozeren. Finite top mass effects for hadronic Higgs production at next-to-next-to-leading order. *JHEP* 11, (2009) 088.
- [101] A. Pak, M. Rogal, and M. Steinhauser. Finite top quark mass effects in NNLO Higgs boson production at LHC. *JHEP* 02, (2010) 025.
- [102] C. Anastasiou, C. Duhr, F. Dulat, E. Furlan, T. Gehrmann, F. Herzog, and B. Mistlberger. Higgs boson gluon fusion production at threshold in  $N^3$ LO QCD. *Phys. Lett. B* 737, (2014) 325–328.
- [103] S. Moch and A. Vogt. Higher-order soft corrections to lepton pair and Higgs boson production. *Phys. Lett. B* 631, (2005) 48–57.

- [104] E. Laenen and L. Magnea. Threshold resummation for electroweak annihilation from DIS data. *Phys. Lett.* B632, (2006) 270–276.
- [105] V. Ravindran. On Sudakov and soft resummations in QCD. *Nucl. Phys.* B746, (2006) 58–76.
- [106] V. Ravindran. Higher-order threshold effects to inclusive processes in QCD. *Nucl. Phys.* B752, (2006) 173–196.
- [107] A. Idilbi, X.-d. Ji, J.-P. Ma, and F. Yuan. Threshold resummation for Higgs production in effective field theory. *Phys. Rev.* D73, (2006) 077,501.
- [108] M. C. Kumar, M. K. Mandal, and V. Ravindran. Associated production of Higgs boson with vector boson at threshold N<sup>3</sup>LO in QCD. *JHEP* 03, (2015) 037.
- [109] T. Ahmed, N. Rana, and V. Ravindran. Higgs boson production through  $b\bar{b}$  annihilation at threshold in N<sup>3</sup>LO QCD. *JHEP* 10, (2014) 139.
- [110] T. Ahmed, M. C. Kumar, P. Mathews, N. Rana, and V. Ravindran. Pseudo-scalar Higgs boson production at threshold N<sup>3</sup> LO and N<sup>3</sup> LL QCD. *Eur. Phys. J.* C76, (2016) 355.
- [111] S. Catani, D. de Florian, M. Grazzini, and P. Nason. Soft gluon resummation for Higgs boson production at hadron colliders. *JHEP* 07, (2003) 028.
- [112] S. Catani, L. Cieri, D. de Florian, G. Ferrera, and M. Grazzini. Threshold resummation at N<sup>3</sup>LL accuracy and soft-virtual cross sections at N<sup>3</sup>LO. *Nucl. Phys.* B888, (2014) 75–91.
- [113] M. Bonvini and S. Marzani. Resummed Higgs cross section at N<sup>3</sup>LL. *JHEP* 09, (2014) 007.
- [114] M. Bonvini, S. Marzani, C. Muselli, and L. Rottoli. On the Higgs cross section at N<sup>3</sup>LO+N<sup>3</sup>LL and its uncertainty. *JHEP* 08, (2016) 105.
- [115] T. Ahmed, G. Das, M. C. Kumar, N. Rana, and V. Ravindran. RG improved Higgs boson production to N<sup>3</sup>LO in QCD .
- [116] T. Schmidt and M. Spira. Higgs Boson Production via Gluon Fusion: Soft-Gluon Resummation including Mass Effects. *Phys. Rev.* D93, (2016) 014,022.
- [117] D. de Florian and J. Zurita. Soft-gluon resummation for pseudoscalar Higgs boson production at hadron colliders. *Phys. Lett.* B659, (2008) 813–820.
- [118] P. Banerjee, G. Das, P. K. Dhani, and V. Ravindran. Threshold resummation of the rapidity distribution for Higgs production at NNLO+NNLL. *Phys. Rev.* D97, (2018) 054,024.
- [119] P. Banerjee, G. Das, P. K. Dhani, and V. Ravindran. Threshold resummation of the rapidity distribution for Drell-Yan production at NNLO+NNLL. *Phys. Rev. D* 98, (2018) 054,018.
- [120] S. Catani and L. Trentadue. Comment on QCD exponentiation at large x. *Nucl. Phys.* B353, (1991) 183–186.
- [121] E. Laenen and G. F. Sterman. Resummation for Drell-Yan differential distributions. In *The Fermilab Meeting DPF 92. Proceedings, 7th Meeting of the American Physical Society, Division of Particles and Fields, Batavia, USA, November 10-14, 1992. Vol. 1, 2.* 1992 987–989.

- [122] G. F. Sterman and W. Vogelsang. Threshold resummation and rapidity dependence. *JHEP* 02, (2001) 016.
- [123] A. Mukherjee and W. Vogelsang. Threshold resummation for W-boson production at RHIC. *Phys. Rev. D* 73, (2006) 074,005.
- [124] P. Bolzoni. Threshold resummation of Drell-Yan rapidity distributions. *Phys. Lett.* B643, (2006) 325–330.
- [125] M. Bonvini, S. Forte, and G. Ridolfi. Soft gluon resummation of Drell-Yan rapidity distributions: Theory and phenomenology. *Nucl. Phys.* B847, (2011) 93–159.
- [126] M. A. Ebert, J. K. L. Michel, and F. J. Tackmann. Resummation Improved Rapidity Spectrum for Gluon Fusion Higgs Production. *JHEP* 05, (2017) 088.
- [127] T. Becher and M. Neubert. Threshold resummation in momentum space from effective field theory. *Phys. Rev. Lett.* 97, (2006) 082,001.
- [128] T. Becher, M. Neubert, and G. Xu. Dynamical Threshold Enhancement and Resummation in Drell-Yan Production. *JHEP* 07, (2008) 030.
- [129] Y. L. Dokshitzer, D. Diakonov, and S. I. Troian. On the Transverse Momentum Distribution of Massive Lepton Pairs. *Phys. Lett.* 79B, (1978) 269–272.
- [130] Y. L. Dokshitzer, D. Diakonov, and S. I. Troian. Hard Processes in Quantum Chromodynamics. *Phys. Rept.* 58, (1980) 269–395.
- [131] G. Parisi and R. Petronzio. Small Transverse Momentum Distributions in Hard Processes. *Nucl. Phys.* B154, (1979) 427–440.
- [132] G. Curci, M. Greco, and Y. Srivastava. QCD Jets From Coherent States. *Nucl. Phys.* B159, (1979) 451–468.
- [133] J. C. Collins and D. E. Soper. Back-To-Back Jets in QCD. *Nucl. Phys.* B193, (1981) 381. [Erratum: *Nucl. Phys.* B213,545(1983)].
- [134] J. Kodaira and L. Trentadue. Summing Soft Emission in QCD. *Phys. Lett.* 112B, (1982) 66.
- [135] J. Kodaira and L. Trentadue. Single Logarithm Effects in electron-Positron Annihilation. *Phys. Lett.* 123B, (1983) 335–338.
- [136] J. C. Collins, D. E. Soper, and G. F. Sterman. Transverse Momentum Distribution in Drell-Yan Pair and W and Z Boson Production. *Nucl. Phys.* B250, (1985) 199–224.
- [137] S. Catani, E. D’Emilio, and L. Trentadue. The Gluon Form-factor to Higher Orders: Gluon Gluon Annihilation at Small  $Q^-$  transverse. *Phys. Lett.* B211, (1988) 335–342.
- [138] D. de Florian and M. Grazzini. Next-to-next-to-leading logarithmic corrections at small transverse momentum in hadronic collisions. *Phys. Rev. Lett.* 85, (2000) 4678–4681.
- [139] S. Catani, D. de Florian, and M. Grazzini. Universality of nonleading logarithmic contributions in transverse momentum distributions. *Nucl. Phys.* B596, (2001) 299–312.

- [140] H. X. Zhu, C. S. Li, H. T. Li, D. Y. Shao, and L. L. Yang. Transverse-momentum resummation for top-quark pairs at hadron colliders. *Phys. Rev. Lett.* 110, (2013) 082,001.
- [141] H. T. Li, C. S. Li, D. Y. Shao, L. L. Yang, and H. X. Zhu. Top quark pair production at small transverse momentum in hadronic collisions. *Phys. Rev.* D88, (2013) 074,004.
- [142] J. C. Collins and D. E. Soper. Back-To-Back Jets: Fourier Transform from B to K-Transverse. *Nucl. Phys.* B197, (1982) 446–476.
- [143] G. Altarelli, R. K. Ellis, M. Greco, and G. Martinelli. Vector Boson Production at Colliders: A Theoretical Reappraisal. *Nucl. Phys.* B246, (1984) 12–44.
- [144] C. W. Bauer, S. Fleming, and M. E. Luke. Summing Sudakov logarithms in  $B \rightarrow X(s \gamma)$  in effective field theory. *Phys. Rev.* D63, (2000) 014,006.
- [145] C. W. Bauer, S. Fleming, D. Pirjol, and I. W. Stewart. An Effective field theory for collinear and soft gluons: Heavy to light decays. *Phys. Rev.* D63, (2001) 114,020.
- [146] C. W. Bauer and I. W. Stewart. Invariant operators in collinear effective theory. *Phys. Lett.* B516, (2001) 134–142.
- [147] C. W. Bauer, D. Pirjol, and I. W. Stewart. Soft collinear factorization in effective field theory. *Phys. Rev.* D65, (2002) 054,022.
- [148] M. Beneke, A. P. Chapovsky, M. Diehl, and T. Feldmann. Soft collinear effective theory and heavy to light currents beyond leading power. *Nucl. Phys.* B643, (2002) 431–476.
- [149] G. Bozzi, S. Catani, D. de Florian, and M. Grazzini. Higgs boson production at the LHC: Transverse-momentum resummation and rapidity dependence. *Nucl. Phys.* B791, (2008) 1–19.
- [150] G. Bozzi, S. Catani, G. Ferrera, D. de Florian, and M. Grazzini. Transverse-momentum resummation: A Perturbative study of Z production at the Tevatron. *Nucl. Phys.* B815, (2009) 174–197.
- [151] S. Catani and M. Grazzini. QCD transverse-momentum resummation in gluon fusion processes. *Nucl. Phys.* B845, (2011) 297–323.
- [152] S. Catani, M. Grazzini, and A. Torre. Soft-gluon resummation for single-particle inclusive hadroproduction at high transverse momentum. *Nucl. Phys.* B874, (2013) 720–745.
- [153] P. F. Monni, E. Re, and P. Torrielli. Higgs Transverse-Momentum Resummation in Direct Space. *Phys. Rev. Lett.* 116, (2016) 242,001.
- [154] M. A. Ebert and F. J. Tackmann. Resummation of Transverse Momentum Distributions in Distribution Space. *JHEP* 02, (2017) 110.
- [155] I. W. Stewart, F. J. Tackmann, J. R. Walsh, and S. Zuberi. Jet  $p_T$  resummation in Higgs production at  $NNLL' + NNLO$ . *Phys. Rev.* D89, (2014) 054,001.
- [156] M. Grazzini, S. Kallweit, D. Rathlev, and M. Wiesemann. Transverse-momentum resummation for vector-boson pair production at NNLL+NNLO. *JHEP* 08, (2015) 154.

- [157] G. Ferrera and J. Pires. Transverse-momentum resummation for Higgs boson pair production at the LHC with top-quark mass effects. *JHEP* 02, (2017) 139.
- [158] A. Belyaev, P. M. Nadolsky, and C. P. Yuan. Transverse momentum resummation for Higgs boson produced via b anti-b fusion at hadron colliders. *JHEP* 04, (2006) 004.
- [159] R. V. Harlander, A. Tripathi, and M. Wiesemann. Higgs production in bottom quark annihilation: Transverse momentum distribution at NNLO+NNLL. *Phys. Rev. D* 90, (2014) 015,017.
- [160] W. Bizon, P. F. Monni, E. Re, L. Rottoli, and P. Torrielli. Momentum-space resummation for transverse observables and the Higgs  $p_{\perp}$  at N<sup>3</sup>LL+NNLO. *JHEP* 02, (2018) 108.
- [161] X. Chen, T. Gehrmann, E. W. N. Glover, A. Huss, Y. Li, D. Neill, M. Schulze, I. W. Stewart, and H. X. Zhu. Precise QCD Description of the Higgs Boson Transverse Momentum Spectrum. *Phys. Lett. B* 788, (2019) 425–430.
- [162] W. Bizoń, X. Chen, A. Gehrmann-De Ridder, T. Gehrmann, N. Glover, A. Huss, P. F. Monni, E. Re, L. Rottoli, and P. Torrielli. Fiducial distributions in Higgs and Drell-Yan production at N<sup>3</sup>LL+NNLO. *JHEP* 12, (2018) 132.
- [163] J. Alwall, R. Frederix, S. Frixione, V. Hirschi, F. Maltoni, O. Mattelaer, H. S. Shao, T. Stelzer, P. Torrielli, and M. Zaro. The automated computation of tree-level and next-to-leading order differential cross sections, and their matching to parton shower simulations. *JHEP* 07, (2014) 079.
- [164] S. Alioli, P. Nason, C. Oleari, and E. Re. A general framework for implementing NLO calculations in shower Monte Carlo programs: the POWHEG BOX. *JHEP* 06, (2010) 043.
- [165] M. Dasgupta, F. A. Dreyer, K. Hamilton, P. F. Monni, and G. P. Salam. Logarithmic accuracy of parton showers: a fixed-order study. *JHEP* 09, (2018) 033. [Erratum: *JHEP* 03, 083 (2020)].
- [166] P. Banerjee, P. K. Dhani, and V. Ravindran. Two loop QCD corrections for the process Pseudo-scalar Higgs  $\rightarrow$  3 partons. *JHEP* 10, (2017) 067.
- [167] K. G. Chetyrkin, B. A. Kniehl, M. Steinhauser, and W. A. Bardeen. Effective QCD interactions of CP odd Higgs bosons at three loops. *Nucl. Phys.* B535, (1998) 3–18.
- [168] C. T. H. Davies, B. R. Webber, and W. J. Stirling. Drell-Yan Cross-Sections at Small Transverse Momentum. *Nucl. Phys.* B256, (1985) 413. [1,I.95(1984)].
- [169] D. de Florian and M. Grazzini. The Structure of large logarithmic corrections at small transverse momentum in hadronic collisions. *Nucl. Phys.* B616, (2001) 247–285.
- [170] T. Becher and M. Neubert. Drell-Yan Production at Small  $q_T$ , Transverse Parton Distributions and the Collinear Anomaly. *Eur. Phys. J.* C71, (2011) 1665.
- [171] C. P. Yuan. Kinematics of the Higgs boson at hadron colliders: NLO QCD gluon resummation. *Phys. Lett.* B283, (1992) 395–402.
- [172] O. V. Tarasov, A. A. Vladimirov, and A. Yu. Zharkov. The Gell-Mann-Low Function of QCD in the Three Loop Approximation. *Phys. Lett.* 93B, (1980) 429–432.

- [173] S. Catani, L. Cieri, D. de Florian, G. Ferrera, and M. Grazzini. Universality of transverse-momentum resummation and hard factors at the NNLO. *Nucl. Phys.* B881, (2014) 414–443.
- [174] L. A. Harland-Lang, A. D. Martin, P. Motylinski, and R. S. Thorne. Parton distributions in the LHC era: MMHT 2014 PDFs. *Eur. Phys. J. C* 75, (2015) 204.
- [175] S. Alekhin, J. Blümlein, S. Moch, and R. Placakyte. Parton distribution functions,  $\alpha_s$ , and heavy-quark masses for LHC Run II. *Phys. Rev.* D96, (2017) 014,011.
- [176] R. D. Ball et al. Parton distributions from high-precision collider data. *Eur. Phys. J. C* 77, (2017) 663.
- [177] J. Butterworth et al. PDF4LHC recommendations for LHC Run II. *J. Phys.* G43, (2016) 023,001.
- [178] I. I. Bigi, M. A. Shifman, N. Uraltsev, and A. Vainshtein. The Pole mass of the heavy quark. Perturbation theory and beyond. *Phys.Rev.* D50, (1994) 2234–2246.
- [179] M. Beneke and V. M. Braun. Heavy quark effective theory beyond perturbation theory: Renormalons, the pole mass and the residual mass term. *Nucl.Phys.* B426, (1994) 301–343.
- [180] B. Webber. Estimation of power corrections to hadronic event shapes. *Phys.Lett.* B339, (1994) 148–150.
- [181] Y. L. Dokshitzer, G. Marchesini, and B. Webber. Dispersive approach to power behaved contributions in QCD hard processes. *Nucl.Phys.* B469, (1996) 93–142.
- [182] M. Dasgupta and G. P. Salam. Event shapes in  $e^+ e^-$  annihilation and deep inelastic scattering. *J.Phys.* G30, (2004) R143.
- [183] C. Lee. Universal nonperturbative effects in event shapes from soft-collinear effective theory. *Mod. Phys. Lett. A* 22, (2007) 835–851.
- [184] E. Gardi. Perturbative and nonperturbative aspects of moments of the thrust distribution in  $e^+ e^-$  annihilation. *JHEP* 04, (2000) 030.
- [185] E. Gardi and J. Rathsman. Renormalon resummation and exponentiation of soft and collinear gluon radiation in the thrust distribution. *Nucl.Phys.* B609, (2001) 123–182.
- [186] E. Gardi and G. Grunberg. Power corrections in the single dressed gluon approximation: The Average thrust as a case study. *JHEP* 11, (1999) 016.
- [187] S. Catani, G. Turnock, and B. Webber. Jet broadening measures in  $e^+e^-$  annihilation. *Phys. Lett. B* 295, (1992) 269–276.
- [188] G. Salam and D. Wicke. Hadron masses and power corrections to event shapes. *JHEP* 05, (2001) 061.
- [189] V. Mateu, I. W. Stewart, and J. Thaler. Power Corrections to Event Shapes with Mass-Dependent Operators. *Phys. Rev. D* 87, (2013) 014,025.
- [190] M. Beneke and V. M. Braun. Renormalons and power corrections 1719–1773.
- [191] M. Beneke. Renormalons. *Phys. Rept.* 317, (1999) 1–142.